Constraining climate and health impacts of atmospheric aerosols using adjoint modeling

by

F. G. Lacey

B.A., Kettering University, 2007

A thesis submitted to the

Faculty of the Graduate School of the

University of Colorado in partial fulfillment

of the requirements for the degree of

Doctor of Philosophy

Department of Mechanical Engineering

2016

This thesis entitled:
Constraining climate and health impacts of atmospheric aerosols using adjoint modeling
written by F. G. Lacey
has been approved for the Department of Mechanical Engineering

Prof. Daven Henze

Prof. Michael Hannigan

Dr. Christine Wiedinmyer

Date _____

The final copy of this thesis has been examined by the signatories, and we find that both the content and the form meet acceptable presentation standards of scholarly work in the above mentioned discipline.

Lacey, F. G. (Ph.D., Mechanical Engineering)

Constraining climate and health impacts of atmospheric aerosols using adjoint modeling

Thesis directed by Prof. Daven Henze

Emissions from anthropogenic activity impact both health and climate. Through the use of adjoint modeling we have developed sensitivities to estimate either the surface temperature change or premature deaths due to an emissions perturbation at the scale of the model resolution. For estimation of ambient climate impacts, this work includes parameterizations of indirect and semi-direct radiative forcing in conjunction with regional radiative forcing scaling factors to estimate a range of temperature impacts, along with a central estimate, for any emissions perturbation. We have combined this with health impact sensitivities that use satellite downscaling in order to calculate human exposure at the 0.1° by 0.1° resolution. As an application of these techniques we have created an emissions inventory of aerosol and greenhouse gas emissions from global solid fuel use for cooking. We have estimated that a linear phased removal of these cookstove emissions leads to cooling of 79 mK (12 mK warming to 169 mK cooling) in 2050 and prevention of 260,000 (137,000 to 268,000) premature deaths per year. This work has also been able to highlight countries that are optimal targets for cookstove interventions based on both overall magnitude of impact and the marginal per-cookstove impacts. The largest impacts for climate and health are realized in China and India, while Ukraine and Azerbaijan have the largest per cookstove impacts. In addition to global impacts, the tools developed here also have been applied on a regional scale to estimate the impacts of clean cookstove implementation scenarios within Mozambique where emissions from solid fuel use is responsible for 278 annual premature deaths and warming of 0.7 mK by 2050. The models and estimates of impacts presented in this work will provide policy makers with improved information that can be used when designing not only cookstove interventions, but any emissions mitigation scenario.

Dedication

This work is dedicated to the ones that I hope it will impact the most, our future generations.

Acknowledgements

The thesis and the work herein would not have been possible without the support of a number of people, which I would like to thank here. First and foremost I would like to thank my family: **Randy**, **Diane**, **Sam**, and his wife **Courtney** who have supported me beyond measure throughout my graduate work. My family is not complete without my fiancé **Dana**, whom I met during my graduate work here, and has given me more love and support than I thought possible.

I would also like to thank my advisor **Dr. Daven Henze** for the knowledge, guidance, and support given to me and my work. Without him being willing to take a risk and guide an industry professional with limited computational background the work here would not have been possible.

In addition, I would like to thank my committee: **Dr. Michael Hannigan**; **Dr. Jana Milford**, Ph.D., J.D.; **Dr. Lupita Montoya**; and **Dr. Christine Wiedinmyer** for the input that they have provided, particularly on this thesis.

The modeling efforts would not have been possible without the **NASA HECC** and **NASA AQAST** groups, along with the **GEOS-Chem** community. Both of these groups were instrumental in model development and operation. Penultimately I would like to thank the **Henze Research Group** for all the work that we have done together, with special thanks to **Dr. Matt Turner** and **Yanko Davila** who have kept our group's computing cluster running and usable despite my best efforts to break it.

Final thanks have to go out to Dana's and my lovely furry companions, **Trace** and **Inca**. These not so little pups have been a constant breath of fresh air outside of academia and provide unconditional, albeit coerced through treats and belly rubs, companionship and love.

Contents

Chapter

Tables

Table

Figures

Figure

Chapter 1

Introduction

Understanding the global impacts of aerosols on climate and health has been a research problem since the mid-twentieth century. Work done through the Global Burden of Disease (GBD) project shows that exposure to ambient $PM_{2.5}$ concentrations was responsible for approximately 2.8 to 3.6 million premature deaths in 2010, in addition to another 2.6 to 4.3 million deaths from indoor air quality (IAQ) [62]. More recent work has shown that in 2013, the predicted number of deaths from ambient air pollution (AAP) outweighs the number of deaths caused by IAQ [18, 31]. Ambient air pollution also impacts climate by perturbing the Earth's energy balance. The latest Intergovernmental Panel on Climate Change (IPCC) report states that -0.9 Wm^{-2} (with a range from -1.9 to -0.1) of the overall anthropogenic radiative forcing of 2.3 Wm^{-2} (with a range of 1.1 to 3.4) is due to aerosols [75, 17]. These estimates of the climate impacts of anthropogenic aerosols have also been rated as medium to low confidence due to gaps in the current scientific understanding and concensus on physical representation of aerosol sources and processes. The combination of the magnitude of these health and climate impacts along with the uncertainties in the present day and future values is the underlying motivation for further research on anthropogenic aerosols.

In order to understand the climate and health impacts of aerosol emissions and quantify the benefits of different mitigation strategies, we need to account for several mechanisms of aerosol formation and processing in the atmosphere. Although aerosol composition varies, this study will focus on anthropogenic emissions and formation of primary carbonaceous aerosols (BC and OC), sulfate, nitrate, and ammonium. These species make up a large portion ($\sim$50%) of fine particulate

mass over land and are the main focus of air quality regulations. In addition to anthropogenic aerosol sources, the global aerosol burden also has contributions from naturally occurring aerosols such as sea salt, mineral dust, and secondary organic aerosol (SOA). The latter two species also have some anthropogenic component as well, but for the purpose of this work, these have either not been included or estimated using a simple parameterization since the level of scientific understanding of their sources is quite nascent and they are thus seldom included in emissions control strategies. Each of the aforementioned anthropogenic species undergoes different processes in the atmosphere, which form two classifications: directly emitted aerosols (BC and OC) and secondary inorganic aerosols (sulfate, nitrate, and ammonium). Atmospheric processing of directly emitted species consists of chemical aging from hydrophobic to hydrophilic states, which controls their deposition rates through wet scavenging [26, 63, 23, 25]. Secondary inorganic aerosols (SIA) are formed through the emission of aerosol precursor species that contain either reactive nitrogen or reactive sulfur [78]. These reactive species then undergo gas-phase oxidation, heterogeneous surface chemistry [28], and phase partitioning. Once in the aerosol form, these SIA species are also subject to various dynamic mechanisms such as coagulation, which will perturb the total aerosol number. In addition, the formation of aerosol affects photolysis rates in the troposphere [69], which is also a feedback on SIA formation rates. All of these chemical and physical processes lead to an atmospheric aerosol mass concentration which in turn impacts human health and climate.

Aerosol concentrations impact health by affecting cardiac and respiratory function, which manifests as a source of premature death. According to the 2015 GBD report on global mortality, the combined IAQ and AAP impacts result in the 4th highest risk factor for premature death globally [31]. The diseases considered to be impacted by air pollution for this study are: ischemic heart disease (IHD), stroke, chronic obstructive pulmonary disease, lower respiratory infections, and lung cancer (the deaths reported in this report only consider deaths for the population above 30 years old and do not account for infant acute lower respiratory infections (ALRI)). The impact of air pollution on each of these diseases is estimated using integrated exposure response (IER) functions which estimate a person's increased risk due to their annual $PM_{2.5}$ exposure [19]. These

IER functions rely on baseline mortality rates [64] at the national-scale along with ambient human exposure estimated as population-weighted $PM_{2.5}$ derived from satellite datasets [18, 116].

Aerosol mass concentrations also affect climate by perturbing the radiative balance at the top of the atmosphere (TOA). In order to calculate this change in radiative flux, we must consider several factors. Species dependent properties, i.e., refractive index and size distribution, of aerosols govern how they interact with incoming radiation in the troposphere. In order to determine the impact on radiative flux, there are several theoretical frameworks for describing aerosol radiative interactions. Mie scattering theory is a good representation for the typical size range of fine particulate matter considered in this work. Mie theory assumes spherical particles and accounts for non-uniform radiation interaction, which includes a reflective component and absorptive component based on species specific optical parameters (phase function, single-scattering albedo and refractive index), to estimate the radiative flux for a given wavelength of incoming radiation. By integrating over a range of wavelengths (315 to 1,667 nm) the total radiative flux for a species can be estimated. Aerosol concentrations in the atmosphere also impact cloud formation and longevity, which in turn impacts the radiative flux at the top of the atmosphere [110]. Based on the results from the IPCC 5th Assessment Report, these aerosol cloud interactions make up approximately 50% of the overall aerosol radiative forcing and are highly uncertain [17]. In our work we treat the species-specific radiative forcing from these effects as being proportional to their direct radiative forcing. This approximation is a source of uncertainty, and therefore applied to calculate not only the central estimate of effective radiative forcing but also the upper and lower bounds.

A valuable tool for understanding the relationship between aerosol sources and their impacts are atmospheric models that attempt to simulate all of these chemical, physical, and radiative aerosol processes. Chemical transport models (CTM) treat these chemical and physical processes in the atmosphere by solving mass balance equations for various species in each grid cell. These mass balance equations account for emissions, chemical reactions within a grid cell, advection to and from the grid cell, dispersion to and from the grid cell, and loss rates owing to both wet and dry deposition. The model used here, GEOS-Chem [7], uses parameterizations for each of these

processes to estimate the global aerosol mass concentrations gridded at the 2° by 2.5° resolution.

In this thesis, the GEOS-Chem model has been modified to examine specific model outputs, hereafter referred to as cost functions, using a number of different modules, inputs, and parameterizations. Human health impacts are estimated by combining the modeled grid-cell aerosol mass concentrations with satellite data and rescaling to the match the annual average $PM_{2.5}$ concentrations from this dataset, along with redistribution from the 2° by 2.5° resolution to the 0.1° by 0.1° resolution that is appropriate for estimating human exposure. These exposure estimates are then combined with IER functions to estimate grid-scale premature deaths from exposure to AAP. For estimation of aerosol radiative forcing, the LIDORT radiative transfer model [107] is used to estimate the grid cell contributions to radiative flux [39] for a baseline pre-industrial state and perturbed case, either present day or future atmospheric condition. A detailed explanation of these models are included in Chapter 7 and Chapter 6 respectively.

In addition to forward models, explained above, adjoint models present several unique opportunities for exploring modeled relationships between aerosol sources and their impacts. In general, adjoint models track the effect of a small perturbation in the model output backward though time in order to generate sensitivities of the model output with respect to all model inputs. Due to the timescales by which aerosols are transported and removed from the atmosphere, aerosol mass concentrations are spatially heterogeneous. This in turn leads to the climate and ambient air quality impacts of aerosols also being spatially heterogenous, although the spatial distribution of the impacts does not directly match the spatial distribution of emissions sources due to formation mechanisms and aerosol lifetime in the atmosphere. Adjoint models are able to capture these source-receptor relationships by taking into account all of the intermediate processes affecting the mass-balance in each grid cell. This means that the adjoint model can calculate the grid-scale sensitivities of the cost function with respect to all inputs (i.e., emissions) while taking into account all of the processes mentioned above. These sensitivities then allow for analysis of the impacts of multiple grid-scale emission perturbations for a limited (approximately an order of magnitude higher) computational cost. The same set of results calculated using finite difference methods requires on

the order of 10^6 model runs. Further details of the adjoint of the GEOS-Chem model are explained in Chapters 6 and 7.

Since an adjoint model output is the sensitivities of the cost function with respect to grid-cell emissions, it is possible to quickly estimate the impacts of a number of different anthropogenic emissions control strategies or sectors. One of the largest contributors to AAP is the global use of solid-fuel for cooking. While previous work [112, 3, 21, 59] has estimated the impacts from various combinations of residential, commercial, and fuel type scenarios, this work focuses on the ranges of impacts from assuming different cookstove emissions factors combined with a baseline aerosol emissions inventory and the percent population using solid fuel at the national and regional level. A full description of the solid fuel cookstove emissions inventory is found in Lacey and Henze, 2015 [55], which is used for the estimation of national-scale climate and health impacts found in Chapter 3 and 6.

This dissertation presents results generated using adjoint methods in conjunction with various emissions scenarios to calculate the impacts of changes in anthropogenic emissions on both human health and climate. In particular, this work focuses on a number of policy-relevant science questions in an effort to further expand our understanding of the link between human activity, health, and climate. The first section of this thesis explores how carbonaceous aerosol emissions from global solid-fuel use impact surface temperature, considering a range of temperature impacts based on the range of stove and fuel specific emissions factors and a range of radiative efficiencies for the different aerosol species, resulting in the range of temperature imapcts from solid-fuel cookstove emissions (Chapter 2). The next chapter expands on this work in a number of ways by considering the role of greenhouse gases on temperature change, calculating transient temperature impacts, and also estimating health impacts from the cookstove emissions. Lastly, these same tools are applied to a single country, in this case Mozambique and are used to estimate the ambient health and climate impacts from a number of different cookstove replacement programs (Chapter 4). While a majority of this thesis focuses on impacts of solid-fuel cookstove use, the models developed throughout can also be used to estimate transient climate and health impacts from other changes in anthropogenic

emissions, therefore providing policy makers with a useful tool for investigating a broad array of emissions mitigation scenarios.

Chapter 2

Climate impacts from country-level solid fuel cookstove carbonaceous aerosol emissions[1]

2.1 Abstract

Cookstove use is globally one of the largest unregulated anthropogenic sources of primary carbonaceous aerosol. While reducing cookstove emissions through national-scale mitigation efforts has clear benefits for improving indoor and ambient air quality, and significant climate benefits from reduced green-house gas emissions, climate impacts associated with reductions to co-emitted black (BC) and organic carbonaceous (OC) aerosol are not well characterized. Here we attribute direct, indirect, semi-direct, and snow/ice albedo radiative forcing (RF) and associated global surface temperature changes to national-scale carbonaceous aerosol cookstove emissions. These results are made possible through the use of adjoint sensitivity modeling to relate direct RF and BC deposition to emissions. Semi- and indirect effects are included via global scaling factors, and bounds on these estimates are drawn from current literature ranges for aerosol RF along with a range of solid fuel emissions characterizations. Absolute regional temperature potentials are used to estimate global surface temperature changes. Bounds are placed on these estimates, drawing from current literature ranges for aerosol RF along with a range of solid fuel emissions characterizations. We estimate a range of 0.16 K warming to 0.28 K cooling with a central estimate of 0.06 K cooling

[1] This chapter is a published article in Environmental Research Letters [55].

from the removal of cookstove aerosol emissions. At the national emissions scale, countries' impacts on global climate range from net warming (e.g., Mexico and Brazil) to net cooling, although the range of estimated impacts for all countries span zero given uncertainties in RF estimates and fuel characterization. We identify similarities and differences in the sets of countries with the highest emissions and largest cookstove temperature impacts (China, India, Nigeria, Pakistan, Bangladesh and Nepal), those with the largest temperature impact per carbon emitted (Kazakhstan, Estonia, and Mongolia), and those that would provide the most efficient cooling from a switch to fuel with a lower BC emission factor (Kazakhstan, Estonia, and Latvia). The results presented here thus provide valuable information for climate impact assessments across a wide range of cookstove initiatives.

2.2 Introduction

Cookstoves and residential sources account for approximately 20% of current black carbonaceous (BC) emissions [14, 56]. Policies targeting reductions to BC aerosol from cookstoves have garnered attention owing to their potential impacts on both climate and human health [118, 34, 27, 3]. Exposure to indoor and ambient fine particulate matter ($PM_{2.5}$) is responsible for approximately 4.3 and 3.2–3.7 million premature deaths per year, respectively [4, 62], with solid fuel use contributing to approximately 0.5 million of the latter [3]. The total pre-industrial to present day effective radiative forcing (RF) of BC from all anthropogenic sources is 1.1 Wm^{-2} with a range of 0.17 to 2.1 Wm^{-2}, which is similar in magnitude to the RF of prominent greenhouse gases [86, 11, 75]. This forcing is a combination of direct, semi-direct, and indirect effects that are in turn a function of chemical and physical processes in the atmosphere. The fraction of this forcing from cookstove BC emissions can not be directly attributed according to the cookstove fraction of global BC emissions owing the regional dependence of BC radiative forcing [39].

Several uncertainties surrounding the net climate impacts of carbonaceous cookstove emissions complicate how mitigation efforts should be accounted for in environmental assessments [35, 101, 57]. Evaluating the climate impacts of actual BC cookstove emission reduction strate-

gies requires accounting for species co-emitted with BC (particularly organic carbon (OC)), the chemical and physical processes affecting these species in the atmosphere, their climate impacts via multiple mechanisms, and the range of uncertainties associated with each of these components [11, 75]. Previous studies have estimated a range of impacts from carbonaceous aerosol cookstove emissions [67, 34, 32] based on the effects of co-emitted aerosol and gaseous precursor species that either have additional warming effects or counteract the effects of BC by reflecting incoming solar radiation. These co-emitted species depend on locally available fuels combined with traditional stoves and cooking methods [15]. A key consideration is the ratio of BC to total carbon emissions, referred to here as Φ. Variations in Φ can also be caused by differences in fuels, stove types, cooking methods and habitation, all of which vary regionally [14, 45, 44]. In addition to carbonaceous aerosol emissions, other species co-emitted from residential cookstove use include trace amounts of aerosol precursors SO_2 and NO_x along with greenhouse gases CO, CH_4, CO_2, and, to a lesser extent, N_2O [102, 8, 88, 44].

In addition to uncertainties related to both the total emissions and characterization of emissions for sectors which emit BC, difficulties in determining the net climate impacts from BC sources arise from the spatial relationships between these emissions and their impact on climate, which is more important for aerosols than for long lived, well-mixed greenhouse gases [98, 39]. BC emitted into regions with a low surface albedo have a smaller direct radiative forcing than BC emitted into regions with a high surface albedo [86, 39]. Another factor that affects the climate impacts of carbonaceous aerosols is their atmospheric lifetime. This is a function of deposition loss rates, which are in turn a function of particle aging from hydrophobic to hydrophilic properties and local meteorology [26, 63, 39, 94]. There are also uncertainties in the absorption of BC particles owing to uncertainties in physical properties and aerosol mixing states [43, 12, 65].

Recent work has explored the global impact of these types of uncertainties (emissions, aerosol properties, etc.) and found the net global temperature impacts of aerosols from all biofuels to be rather ambiguous [52]. Past studies have quantified the radiative forcing and climate impact of individual anthropogenic sectors through modeling studies which perturb the emissions from a

specific species or sector, either globally or from a specific region [33, 112, 6, 66]. Other studies have provided more detailed analysis of radiative forcing specifically from global sources of carbonaceous aerosols [51, 24]. While all of these studies take into account aerosol indirect effects in some form, estimates of aerosol indirect radiative forcing for cookstoves, or carbonaceous aerosol in general, are highly variable [81, 22, 105, 52]. Further, strategies for mitigating cookstove emissions typically depend on local government and cultural factors, highlighting the need for analysis of the climate impacts of cookstove emissions at the national scale.

In this study, we expand on past work by evaluating temperature impacts of carbonaceous aerosol emissions from cookstove use in each country, taking into account co-emitted BC and OC, their emissions ratio as a function of fuel type, the spatial heterogeneity of direct radiative forcing, and the range of temperature responses likely owing to indirect forcing mechanisms. The previously mentioned studies used multiple forward model perturbations for their analysis. In contrast, here we use adjoint modeling to estimate the climate impacts of cookstove emissions simultaneously for all countries. Following Henze et al., 2012 [39], the GEOS-Chem adjoint model is used to estimate changes in direct radiative forcing with respect to carbonaceous aerosol emissions. Here we expand upon this approach to consider multi-model mean estimates and ranges for direct and indirect forcing from Boucher et al., 2013 [17] and Myhre et al., 2013 [75]. Aerosol RF has strong spatial heterogeneity, and climate sensitivities to RF at different latitudes vary by up to an order of magnitude. To account for this, we estimate climate responses using absolute regional temperature potentials (ARTP) for regional surface temperature over land parameterized from a chemistry-climate model [98, 96]. This allows us to estimate temperature responses to radiative forcing within different latitude bands. We also bound the total magnitude of the temperature response from removal of cookstove emissions, changes in cookstove efficiencies, and changes in Φ for each country.

2.3 Methods

2.3.1 GEOS-Chem forward and adjoint modeling

Here we provide a brief overview of the models and methodology used for this paper, which are explained in detail in the Supporting Information. Results were generated using the global $2^\circ \times 2.5^\circ$ GEOS-Chem chemical transport model and its adjoint based on year 2000 historical emissions from Lamarque et al., 2010 [56]. Grid-scale adjoint sensitivities were then multiplied by a grid-scale cookstove emissions inventory constructed from the biofuel emissions inventory from Bond et al., 2007 [14] and the country-level percent solid fuel use from Bonjour et al., 2013 [15], as described in Supporting Information, yielding estimates of the biofuel emissions from the fraction of the population of each country that use solid fuels for cooking with an additional regional correction factor to account for non-cookstove carbonaceous aerosol emissions. This adjoint approach allows us to calculate (at the cost of 12 forward model calculations) grid-cell contributions to changes in the regional direct radiative forcing due to solid fuel cookstove use that would have otherwise required $\sim 10^5$ forward model simulations.

2.3.2 Direct, indirect and semi-direct radiative forcing estimates

Several intermodel comparisons have shown a wide range of estimates for aerosol direct and indirect effects owing to various parameterizations regarding the chemical and physical properties of carbonaceous aerosol and their interaction with the environment [111, 17, 75, 11]. To account for this range, following an approach used in the UNEP Integrated Assessment Report, we rescale the calculated direct radiative forcing to match the species-specific estimated radiative forcing from Myhre et al., 2013 [75], shown in Table 2.1. We also apply additional scaling factors to account for indirect and semi-direct effects, assuming that their magnitudes scale proportionally with direct RF [17]. This simple relationship may not hold on smaller regional scales, where variations in aerosol and cloud microphysics may dominate. However, globally many chemistry-climate models exhibit a relationship between direct and indirect effects that falls within the range encompassed by the

scaling factors applied here [97]. In addition, we use the adjoint model to calculate the contribution of emissions in any grid cell to deposition of BC onto snow and sea ice. These sensitivities are used to spatially distribute the global estimated BC snow albedo effect of 0.15 Wm^{-2} [111, 11] on an emission per grid-cell basis, as shown in Figure A.3.

Table 2.1: Scaling factors for direct radiative forcing ($SF_{k,DRF}$) and various secondary radiative effects ($SF_{k,SI}$) for BC, OC and secondary inorganic aerosol (SIA).

Type	Species	Lower	Central	Upper
$SF_{k,DRF}$	BC	1.840	2.761	3.681
$SF_{k,DRF}$	OC	0.695	1.595	2.394
$SF_{k,DRF}$	SIA	0.256	0.567	1.001
$SF_{k,SI}$	BC	-0.143	1.000	1.471
$SF_{k,SI}$	OC	1.019	1.560	1.740
$SF_{k,SI}$	SIA	1.446	2.214	2.470

These scaling factors and BC snow ice albedo sensitivities are combined for each grid cell, i, and species, k, for a given forcing region, τ (Arctic, NH mid-latitudes, Tropics and SH Extratropics), in Equation 2.1,

$$\hat{\lambda}_{\tau,i,k} = \lambda_{\tau,i,k} SF_{k,DRF} SF_{SI} + \bar{\lambda}_{BC,i,ALB} \cdot \delta(k - BC). \tag{2.1}$$

where $\hat{\lambda}_{\tau,i,k}$ is the rescaled complete radiative forcing sensitivity, $\lambda_{\tau,i,k}$ is the radiative forcing sensitivity calculated by the GEOS-Chem adjoint model and $\bar{\lambda}_{BC,i,ALB}$ is the yearly averaged radiative forcing sensitivity from the BC snow/ice albedo change.

2.3.3 Temperature response estimates

Temperature responses are estimated from the application of ARTP coefficients to regional radiative forcing sensitivities in four different latitude bands calculated with the adjoint model. These ARTP coefficients are developed following the approach of Shine et al., 2005 [100] for global temperature potentials, extended in Shindell and Faluvegi, 2010 [95] and Shindell, 2012 [96] to

regional potentials. These are based on regional climate sensitivities derived from the transient chemistry-climate-ocean GISS model simulations of Shindell et al., 2009 [98] and account for both ocean inertia and the influence of local and remote aerosol direct and indirect forcings. These ARTP coefficients represent the magnification of regional sensitivities relative to the global mean equilibrium climate sensitivity of 1.06 C per W m^{-2} (corresponding to 3.9 C response for a doubling of CO_2). Temperature responses estimated using the ARTP coefficients have been shown [96] to estimate regional climate responses within 20% (at 66-95% confidence intervals) of the response calculated using three independent full chemistry-climate models; the uncertainty is less when considering the global climate response as a combination of area-weighted regional responses. To evaluate the impact of using this method to capture spatially heterogeneous forcings and responses, the temperature response to emissions perturbations is calculated in two different ways. The first method is to calculate the change in global RF for a specific species k (BC and OC in this case) and each grid cell i and multiply it by the global mean sensitivity (GMS) as shown in Equation 2.2,

$$\Delta T_{global,k} = GMS \sum_i \left[\hat{\lambda}_{global,i,k} \sigma_{i,k} \right]. \tag{2.2}$$

where $\sigma_{i,k}$ is the emissions perturbation and $\hat{\lambda}_{global,i,k}$ is the rescaled global radiative forcing sensitivity calculated using the adjoint model as shown in Equation 2.1. The second method is to calculate the temperature response in a region, γ, using absolute regional temperature potential coefficients ($ARTP$) [98, 96]. This method estimates the steady state temperature response from changes in regional RF (forcing regions τ defined in Section A.3) based on the following equation:

$$\Delta T_{\gamma,k} = GMS \sum_\tau \left[ARTP_{\gamma,\tau} \sum_i \left[\hat{\lambda}_{\tau,i,k} \sigma_{i,k} \right] \right]. \tag{2.3}$$

$\Delta T_{\gamma,k}$ is the steady state temperature response in each region, which can then be converted to a global averaged temperature change using the area ratio of each response region,

$$\Delta T_{global,k} = \sum_\gamma \left[\frac{A_\gamma}{A_{global}} \Delta T_{\gamma,k} \right]. \tag{2.4}$$

The contribution of an emission in an individual grid cell to the overall temperature change is thus,

$$\Delta T_{i,k} = GMS \sum_{\gamma} \sum_{\tau} \left[\frac{A_{\gamma}}{A_{global}} ARTP_{\gamma,\tau} \hat{\lambda}_{\tau,i,k} \sigma_{i,k} \right]. \quad (2.5)$$

2.4 Results

2.4.1 Regional versus global climate response

We first evaluate the consequences of using regional rather than global temperature response coefficients. For species where the radiative forcing does not have a strong dependence on latitude, such as OC, the estimated global average temperature response is similar using both methods. For example, the predicted temperature response due to removal of biofuel OC emissions everywhere is 0.10 K using the global method (Equation 2.2) and 0.11 K using the ARTP method (Equation 2.4). In contrast, the removal of BC biofuel emissions yields a global average temperature change of -0.13 K using the global method and -0.22 K using the ARTP method. Figure 2.1 shows each grid cell's contribution to global surface temperature change calculated using the global versus ARTP method, colored by each ARTP response region (γ). The magnitudes are similar for most points in the Tropics, as the climate response in the Tropics follows the global surface temperature response [98]. The largest deviations from the 1:1 line are due to larger ARTP predicted temperature responses in the Arctic and Northern Hemisphere mid-latitudes and smaller ARTP predicted temperature response in the Southern Hemisphere combined with differences in the calculations of $\hat{\lambda}_{\tau,i,k}$ for different regions compared to $\hat{\lambda}_{global,i,k}$. This means that in most regions the ARTP method predicts a larger contribution to the global temperature perturbation than the globally averaged temperature perturbation owing to the higher climate sensitivities as well as higher radiative forcing efficiencies for BC in northern latitudes. These differences in temperature response highlight the value of using the ARTP method for short-lived species that have latitudinally variable radiative forcing sensitivities. Therefore, the rest of this paper will present temperature changes using the ARTP method (Equation 2.4).

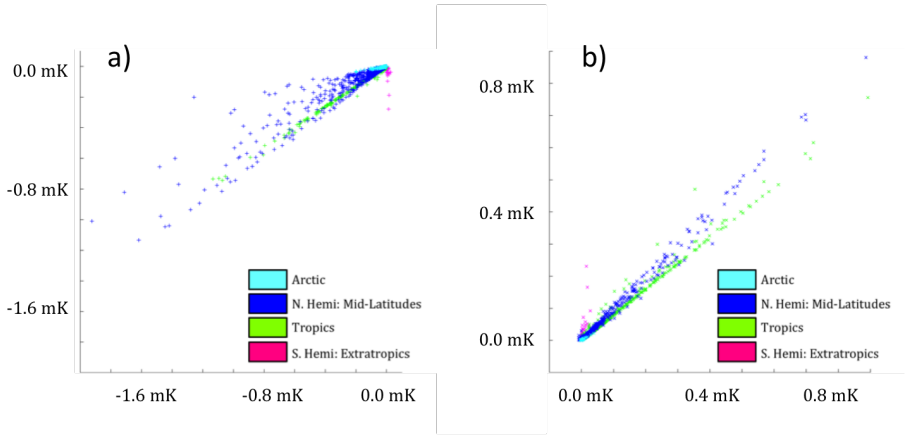

Figure 2.1: Comparison between contributions of $2° \times 2.5°$ grid-cell removal of biofuel emissions to the global mean surface temperature using the ARTP method and the Global Method for (a) BC and (b) OC. Colors represent the location of the grid cells for the emissions inventory.

2.4.2 Temperature response from cookstove emissions

This section explores how uncertainties in emissions, emission characterizations, and radiative forcing mechanisms contribute to temperature change estimates from cookstove emissions reductions. By using the emissions from cookstoves as calculated with Equation A.1, the central estimate for the total temperature change due to removal of all carbonaceous aerosol emissions from residential cookstoves is a cooling of 0.06 K (0.06 K warming from removal of OC and 0.12 K cooling from removal of BC).

Analysis of the BC and OC emission factors shown in Figure A.1 creates a range of Φ of 0.24 +/- 0.09 corresponding to the mean and standard deviation of all emissions factors. We combine this with the upper and lower estimates for radiative forcing scaling factors (Table 2.1) to estimate bounds for the global surface temperature change due to cookstove emissions. Figure 2.2 plots the ranges in surface temperature response to removal of cookstove emissions for a range of uncertainties in the radiative forcing from carbonaceous aerosols (Table 2.1) and the value of Φ for cookstove emissions.

Figure 2.2 shows a large range of uncertainty in the overall temperature impacts due to remove of cookstove emissions based on the effective radiative forcing efficiency of BC and OC along with the characterization of the BC to total carbon emissions ratio for solid fuel use. This plot shows that for low Φ, 0.15, the effects from OC emissions dominate, leading to a central estimate of a net warming of 0.03 K along with higher uncertainties due to the current understanding of OC radiative forcing. The opposite is true for high Φ, 0.33, for which BC dominates the temperature impacts and the potential temperature change due to removal of cookstove emissions is a cooling of as much as 0.28 K. In order to further understand the global climate impacts of cookstove use, the assumptions regarding solid fuel use are further explored below by considering individual national-scale contributions to the overall temperature change.

We next consider the climate impacts of cookstove emissions from each country in which greater than five percent of the population uses solid fuels. Using Equation 2.5, we calculate the

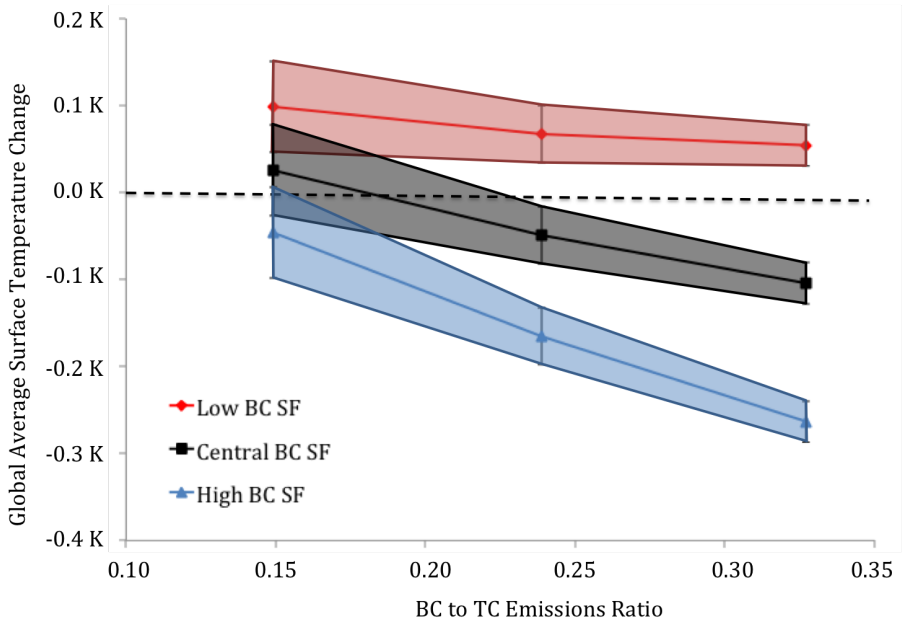

Figure 2.2: Bounds for the global temperature response due to removal of cookstove emissions (y-axis) for a given Φ (x-axis). Lines correspond to the central, high, and low BC radiative forcing scaling factors shown in Table 2.1, and the ranges for each line correspond to the central, high, and low OC radiative forcing scaling factors.

contribution of cookstove aerosol emissions in each grid cell to global surface temperature change. These results are then aggregated by country. Figure 2.3 shows the top 15 countries in terms of the magnitude of the cooling resulting from removal of cookstove removal aerosol emissions, where the temperature change has been separated into species-specific direct and indirect effects. In addition to countries with the largest cooling impact, Brazil and Mexico have been included to show the contrast between countries with cookstove aerosol cooling effects and countries with the largest cookstove aerosol warming effects. The error bars show the range of estimates obtained using the different assumptions regarding radiative forcing scaling factors (shown in Table 2.1) and assumptions for country specific values for Φ. Note that for BC, the semi and indirect effects only contribute to the range but do not perturb the central estimate. In general, the range of estimates in the temperature impact tends to be a function of emissions, where countries with larger emissions mostly have larger uncertainties. Second, the centering of the range of estimates around the central value is a function of Φ. Countries with a Φ around 0.15 (e.g., Ukraine and Kazakhstan, see Figure A.6) will have ranges that are skewed toward a stronger cooling than countries with a Φ greater than 0.2 (e.g., India and China) where the ranges are relatively centered. This is not purely a function of Φ though, as each country's mean radiative forcing sensitivity with respect to BC and OC also plays a role in the range and centering of the ranges. Finally, this plot shows the snow deposition albedo effect and its relative importance for each country; Nepal has an approximately equal impact via the snow-albedo effect as the direct BC effect, while Nigeria has a near-zero snow-albedo effect.

We next consider how individual countries rank in terms of several metrics, using the central estimate for each country in each case. Table 2.2 shows each of the different rankings, which are defined and explained below. We first consider each country's contribution to overall temperature change due to removal of cookstove aerosol emissions (see Figure 2.4(a)) in column two of Table 2.2. With the exception of China, India and Nigeria, the ranking of countries with the largest contribution to total temperature change is not the same as the ranking of countries with the

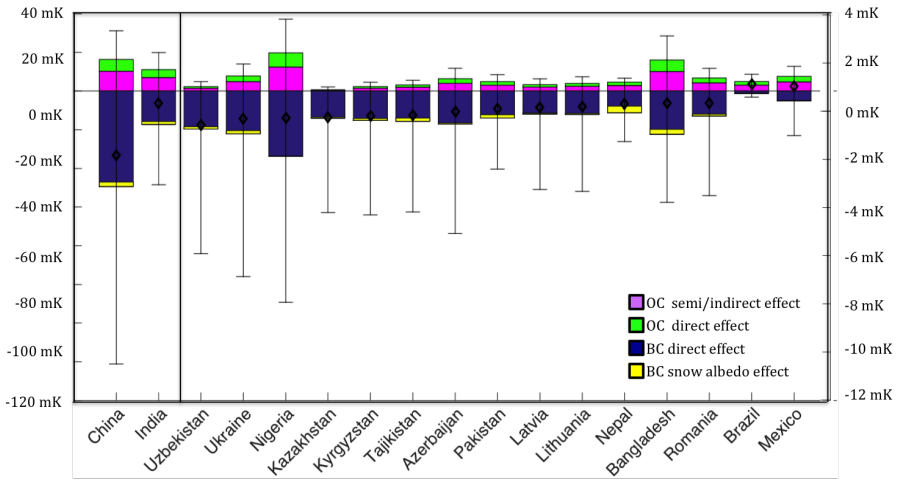

Figure 2.3: Each country's contribution to global surface temperature change broken down into the individual components. The uncertainty ranges are taken from assumptions about the radiative effects shown in Table 2.1 and the reasonable range of Φ shown in Figure 2.2. BC semi-direct and indirect effects perturb only the upper and lower bounds, not the central estimate. China and India are shown on the scale on the left, and all other countries use the scale on the right.

Table 2.2: Rankings of contribution to total temperature change and emissions metrics from the largest annual emissions (Column 1), cooling impact from removal of annual cookstove emissions (Column 2), or efficiency in terms of cooling effect per emission (Column 3 and 4).

Rank	Carbonaceous Aerosol Emissions [Gg C]	Global Temperature Change Contribution [mK]	Cookstove Change Efficiency [mK[kg C]$^{-1}$]	Fuel Switching Efficiency [mK[kg C]$^{-1}$]
1	China	China	Kazakhstan	Kazakhstan
2	India	India	Estonia	Estonia
3	Ethiopia	Uzbekistan	Mongolia	Latvia
4	Bangladesh	Ukraine	Latvia	Lithuania
5	Congo, DRC	Nigeria	Uzbekistan	Ukraine
6	Nigeria	Kazakhstan	Lithuania	Mongolia
7	Kenya	Kyrgyzstan	Kyrgyzstan	Uzbekistan
8	Indonesia	Tajikistan	Georgia	Kyrgyzstan
9	Tanzania	Azerbaijan	Ukraine	Georgia
10	Vietnam	Pakistan	Armenia	Armenia

largest emissions (first column of Table 2.2); instead, the temperature change is a function of the sensitivity of temperature with respect to emissions of BC and OC and the characterization of Φ within that country.

We next consider the results ranked according to the countries that are most efficient in terms of temperature change for a given reduction of emissions. Figure 2.4(b) shows countries colored by their contribution to temperature change per total carbonaceous aerosol emission, and column three of Table 2.2 shows the highest ranked countries according to this efficiency metric. Since many high performance stoves offer a significant reduction in the total carbonaceous aerosol emission factors per fuel used [44], the policy implication of this metric is to show in which countries implementing new stove technologies will result in the largest global cooling per emission reduced. These results also highlight countries where estimates of the total temperature impact (Figure 2.4(a)) are most sensitive to uncertainties in cookstove emission inventories. The countries that rank high in terms of efficiency (blue) differ from countries ranked high in Figure 2.4(a). Since the former have a larger absorptive effect from BC than reflective effect from OC, each stove replaced will have a greater

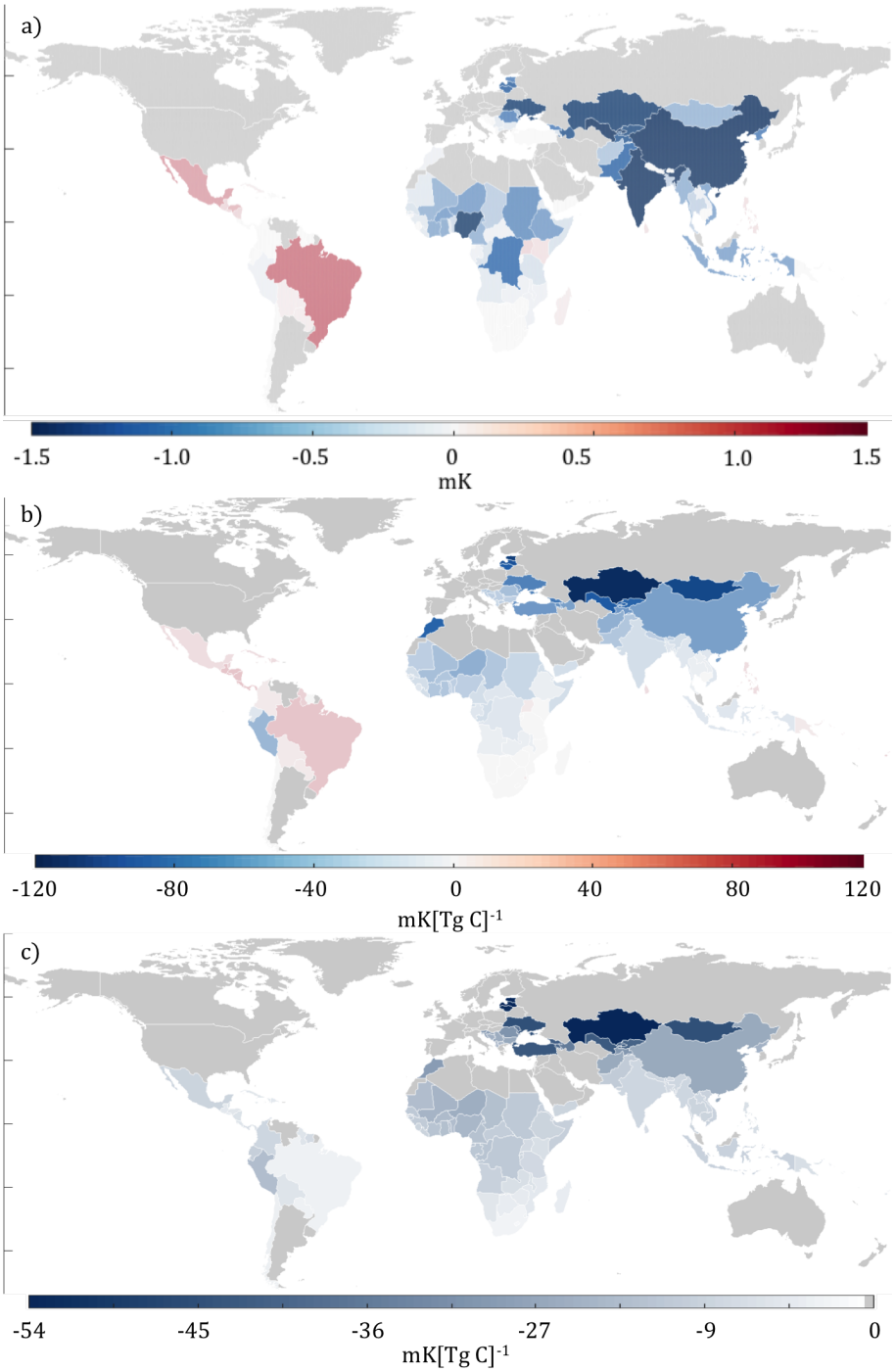

Figure 2.4: Country-level contributions to global temperature change using various metrics: (a) globally averaged surface temperature change from removal of cookstove emissions including direct, semi-direct and indirect effects (total temperature change for India = -6.2 mK and China = -33.1 mK) calculated using Equation 2.4, (b) cookstove mitigation efficiency, i.e., the total temperature effect from removal of cookstove emissions per total cookstove emissions, (c) temperature effect per total biofuel emissions corresponding to a 10% reduction in Φ from cookstove use. Kazakhstan (-86.5), Estonia (-78.9), and Latvia (-62.0) are outside of the scale shown in panel (c). Countries in grey have less than 5% total population using solid fuels for cooking.

climate impact. Conversely, it is inefficient to implement new stoves in countries that rank very low in this metric (red) and in some cases may even result in a net warming through removal of reflective OC.

Another metric which gives important information beyond the total contribution to temperature change is based on characterization of the fuels in a country, i.e., Φ (shown in Figure 2.4(c) and the fourth column of Table 2.2). This metric first calculates the increased cooling effect due to a -0.10 perturbation of Φ owing to a change of fuel type to one with a lower BC to OC ratio, which is optimal for reducing the warming effects of emissions due to biofuel use. This temperature change can then be turned into an efficiency metric by dividing by the total carbonaceous emissions in a country. This metric then gives the temperature response per kilogram of fuel changed for each country. An added benefit of this metric is that it highlights countries that are least robust in terms of estimating temperature impacts owing to uncertainties in Φ.

2.5 Discussion and conclusions

Using the GEOS-Chem adjoint model we have estimated the temperature impacts per amount of carbonaceous aerosol cookstove emissions on a $2^\circ \times 2.5^\circ$ scale. These estimates include parameterizations for indirect and semi-direct aerosol radiative forcing and the contribution of regional radiative forcing to steady-state climate response. Accounting for spatially heterogeneous radiative forcing and climate sensitivities across four zonal bands in our approach is found to double the estimated cooling owing to removal of BC emissions compared to estimates based on global forcing and climate sensitivities. We find the total aerosol climate effect from removal of cookstove emissions (estimated here as the emissions from solid biofuel use from populations that use solid fuel for cooking) ranges from a potential warming of 0.16 K to a cooling of -0.28 K when evaluated for published ranges for both the radiative forcing effects and characterization of the BC to total carbon emission factor. We also develop and apply a new adjoint based method for attributing the global RF of albedo feedback from deposition of BC onto snow and sea ice due to emissions from individual countries. We find this effect is approximately the same order of magnitude as the direct

effect for emissions from Nepal and other high altitude mountainous countries.

By examining the climate impacts of country-specific cookstove emissions, several trends are evident that have importance for policy decisions regarding cookstove interventions and implementation. China and India by far have both the largest carbonaceous cookstove emissions as well as the largest temperature change for national removal of these emissions, which is very likely a net cooling given the current range of estimated forcing magnitudes and emissions factors. In contrast, Nigeria and other countries in Africa with large cookstove emissions have cooling effects that are less certain.

Kazakhstan, Estonia and Mongolia are the most efficient countries for impacting global temperatures by implementing cookstoves, and emissions reductions in former republics of the USSR (e.g., Uzbekistan, Kyrgyzstan, etc.) have the smallest likelihood of warming, relative to the magnitude of their central estimate for cooling. In general, cookstove emissions at higher latitudes have larger climate impacts per kg BC emitted due to radiative forcing and climate sensitivities that are both relatively large in those regions, which results in a difference between BC and OC contributions to climate impact that is greater than one order of magnitude. In contrast, for countries in Central and South America such as Dominica, Brazil, Mexico, and El Salvador, the climate response to cookstove emission reductions is relatively inefficient and may even lead to a net warming due to the larger impacts of OC emissions. This does not mean that cookstove interventions in such countries are not warranted from a climate perspective, as they may have a large climate impact based on co-emitted greenhouse gases or may be potential targets for improved thermal efficiency or fuel switching.

Through the use of scaling factors, the results presented here consider a range of climate impacts due to carbonaceous aerosol emissions from cookstoves owing to uncertainties in radiative forcing and emissions properties. The models used in Myhre et al., 2013 [75] and Boucher et al., 2013 [17] represent a range of parameterizations for various chemical and physical properties including, but not limited to, aerosol mixing state, BC aging, aerosol-cloud interactions, and optical properties; although several additional sources of uncertainty warrant consideration for future work.

First, there is uncertainty in the cookstove emissions inventory itself, which may be biased for reasons discussed in detail in Section A.2. These biases would impact our estimate of absolute temperature impacts from removal of cookstove carbonaceous emissions, although they would not affect our estimates of the efficiency of carbonaceous aerosols emissions reductions or fuel switching on climate (which are linear responses). We have also not considered countries with less than 5% of the population using solid fuel for cooking – thus some high latitude countries with large populations (i.e., Russia and Canada) may have large temperature impacts that have not been considered here – nor have we distinguished between cooking with modern woodstoves versus traditional open-air cookstoves.

In using the ARTP coefficients we are using a climate model parameterization. This parameterization is based off the GISS-ER model, although Shindell, 2012 [96] the calculated regional climate response is within 20% (at a 95% confidence interval) of the response calculated using a suite of full chemistry-climate model, and the uncertainty is less than that when considering the global climate response as a combination of regional responses.

Another source of uncertainty arises from not rigorously treating secondary organic aerosols (SOA) in this analysis owing to the nascent state of understanding of SOA sources and formation mechanisms. We can estimate an upper range of the impact of SOA relative to OC using speciation of biofuel non-methane volatile organic compounds (NMVOC) from Streets et al., 2003 [108] and NMVOC cookstove emissions factors from Grieshop et al., 2011 [34], which are approximately 2:1 relative to OC. Considering both aromatic compounds and other non-speciated compounds to be SOA precursors we estimate the total emissions of SOA precursors to be at most 38% (17% aromatics and 21% other) of total NMVOC emissions from cookstove use. For a 100% upper bound on SOA yield from these emissions, the climate impact from SOA is globally at most 76% of the OC impact. For the high northern latitude countries like Uzbekistan and Kazakhstan, OC impacts are negligible when compared to BC impacts, meaning that the inclusion of SOA would have a very small effect. In contrast, a net warming can not be ruled out for countries like Nigeria and Bangladesh, while the net effect in India and China would still likely be a cooling.

Lastly, with the exception of BC deposition albedo, we have treated aerosol indirect effects as being spatially uniformly proportional to direct effects. While this assumption is used in many models dealing with changes in the global mean impacts [111, 11, 17], other studies have shown that the spatial distribution of these effects can be regionally heterogeneous [81, 10, 52]. Future work should explore these sources of uncertainty to further understand the net impacts of cookstove use and to provide improved information to policymakers, potentially further using adjoint sensitivity analysis to examine spatial heterogeneity in the relationship between aerosol indirect forcing and emissions locations [50, 71].

2.6 Acknowledgement

The research described in the article has been funded wholly or in part by the U.S. Environmental Protection Agency's STAR program through grant 83521101, although it has not been subjected to any EPA review and therefore does not necessarily reflect the views of the Agency, and no official endorsement should be inferred. In addition this work is possible through NASA AQAST (NNH09ZDA001N) and support from the NASA HEC computing facilities.

Chapter 3

Transient climate and ambient health impacts due to solid fuel cookstove use[1]

3.1 Abstract

In addition to drastic impacts on indoor air quality, solid fuel use in residential cookstoves contributes to degraded ambient air quality and may affect global surface temperature. However, the potential for national-scale cookstove intervention programs to mitigate the latter issues are not yet well known; aerosols from cookstoves are spatially and chemically heterogenous and thus have location-dependent impacts on climate and ambient exposure, and they are co-emitted with greenhouse gases that perturb climate on vastly different timescales. Here we employ a combination of atmospheric modeling, remote sensing observations, and adjoint sensitivity analysis to evaluate consequences of a linear phase out of cookstove emissions from the year 2000 - 2020 in the 101 countries with the highest population fraction using solid fuel for cooking. We quantify the global premature deaths from ambient exposure to $PM_{2.5}$ and global mean surface temperature out to the year 2100 owing to each co-emitted species in each country. China, India, and Ethiopia contribute to the largest global surface temperature change in 2050 (combined impact of 37 mK cooling, with a range from 11 mK warming to 85 mK cooling), whereas interventions in Azerbaijan, Ukraine, and Kazakhstan have the largest per cookstove climate benefits. Emissions abatement in China,

[1] This chapter is a document in preparation for submission to Proceedings of the National Academy of Sciences.
Forrest Lacey[1], Daven K. Henze[1], Colin Lee [2], Aaron van Donkelaar[2], Randall V. Martin[2]
[1]University of Colorado, Boulder, CO, USA;[2]Dalhousie University, Dalhousie, NS, Canada.

India, and Bangladesh also contribute to the largest reduction of premature deaths from ambient air pollution, with a combined prevention of 198,000 (102,000 to 204,000) of the 260,000 (137,000 to 268,000) global annual avoided deaths in 2050, while again emissions in Ukraine and Azerbaijan have the largest per cookstove impact, along with Romania. Global cookstove emissions abatement results in an average surface temperature cooling of 77 mK (20 mK warming to 278 mK cooling) in 2050, which increases to a cooling of 118 mK (11 mK to 335 mK cooling) by 2100 due to delayed CO_2 response. Health impacts owing to changes in ambient $PM_{2.5}$ amount to approximately 22.5 million premature deaths prevented between 2000 and 2100.

3.2 Significance Statement

Widespread use of solid fuels for cooking results in a significant source of anthropogenic emissions. Of foremost concern for indoor air quality, reductions to these emissions could also impact both climate and ambient air quality. These potential co-benefits are appealing to efforts aimed at reducing cookstove emissions on national to urban scales, but have yet to be comprehensively evaluated at these scales. We thus estimate the per-cookstove impacts on ambient air quality and global mean surface temperature for every individual country with significant cookstove use, considering reductions to both aerosols and long-lived greenhouse gases over the next century. This provides new information for policy makers evaluating climate and ambient air quality co-benefits of cookstove intervention programs worldwide.

3.3 Introduction

lGobally over three billion people presently use solid fuel for meal preparation [15]. The extent of this activity and the associated air quality pollutant emissions have lead to numerous cookstove intervention studies and programs, such as the Global Alliance for Clean Cookstoves work to implement 80 million clean cookstoves by 2017[1] . A primary goal of these efforts is to improve indoor air quality, estimated to cause approximately 4.3 million premature deaths annually, along

[1] http://cleancookstoves.org/about/news/11-20-2014-market-enabling-roadmap-phase-2-2015-2017.html

with enhancing livelihood of woman and children in the household via repreival from fuel collection and other solid-fuel cooking related tasks [2].

The magnitude of the emissions of aerosols, aerosol precursors, and greenhouse gases from solid fuel use has also motivated studies of the impact of these emissions on climate and ambient air quality. An estimated 370,000 - 500,000 global premature deaths in adults occur annually owing to ambient exposure to fine particulate matter associated with residential cookstoves [62, 3, 21], and there are as many as 1,002,370 global premature deaths of adults and children under that age of 5 annually from combined residential and commercial energy generation (which includes solid fuel use for cooking) [59]. This is a significant fraction of the $\sim$2.9 million premature deaths owing to degraded ambient air quality from all sources [31]. These emission's climate impacts have also been quantified to some extent; for example, Bailis et al. [5] estimates that 1.9 to 2.3% of the global CO_2 emissions are from woodfuel, enough to cause a radiative forcing of 25 to 47 mW m^{-2} [75], while the aerosol radiative forcing ranges from -20 mW m^{-2} to 80 mW m^{-2} [112, 52]. The large range of uncertainty in the aerosol climate impact of cookstoves stems from uncertainties regarding characterization of fuel and the associated emissions of absorbing or reflective co-emitted species, compounded by uncertainties in the interactions of aerosols with clouds [55, 20].

These previous studies have highlighted the potential climate and ambient air quality co-benefits of reducing cookstove emissions globally. However, such findings are limited in terms of their relevance for evaluating domestic-scale mitigation efforts for several reasons. First, the impacts of aerosols on climate and ambient air quality are highly spatially variable owing to several factors, and thus global-scale assessments may not well represent the consequences of national-scale action plans. Unlike long-lived greenhouse gases, which are will mixed in the atmosphere and have a constant impact per ton of emission anywhere in the world, aerosols have atmospheric residences times on the order of a week [92]; their spatial distributions thus contain sharp gradients that lead to order of magnitude regional variances in their health and climate impacts per ton of emission, depending on factors such as their proximity to populated areas [58], their impact on radiative forcing in different regions [39], and the regional climate sensitivity to forcing [98]. Second,

integrated assessment of cookstove interventions must account for both GHG and aerosols, which is a challenge owing to the disparate timescale of the climate impacts of aerosols (decades) compared to that of long-lived GHGs (centuries). Lastly, modeling studies of aerosol health impacts are often detailed yet limited to a single region, or are global yet suffer from errors in exposure estimation at coarse model scales [84, 61].

To address these limitations, here we estimate the transient (present day to 2100) climate and ambient health impacts of national scale co-emissions of aerosols, aerosol precursors, and greenhouse gases resulting from a 20-year phase-out of cookstove emissions in each country with greater than 5% of the population using solid fuels for cooking (101 countries in total). Attribution of these impacts to emissions from individual countries and species is made possible through the use of adjoint sensitivity analysis, building on our earlier work evaluating climate impacts of carbonaceous aerosols [55] and of source attribution of exposure to ambient $PM_{2.5}$ resolved throughout the globe using remote sensing observations [58].

3.4 Methods

Transient climate and health impacts are calculated for a scenario in which emissions of aerosols, aerosol precursors, and GHGs from solid fuel cooking are linearly eliminated over a 20 year horizon. Details of the models and methods summarized here are provided in the Supporting Information. Present day solid fuel cooking emissions are estimated by combining inventories for cabonaceous aerosols [14] and SO_2 [56] with the national-scale population percentage using solid fuels [15]. Emissions of CO_2 and CH_4 are estimated using emissions factors for the carbonaceous aerosol emissions [68, 34], accounting for the spatially variable fraction of non-renewable biomass used as solid fuel [5]. The GEOS-Chem chemical transport model [7] is used to simulate aerosol formation and fate at the $2^\circ \times 2.5^\circ$ global resolution using present day (year 2000) and future anthropogenic emissions following the Representative Concentration Pathway 4.5 (RCP) scenario [104, 73]. All model runs use meteorological data from the Goddard Earth Observing System (GEOS-5) for the year 2009.

Transient climate impacts are estimated as follows. Adjoint model calculations [39] are used to calculate the sensitivities of regional radiative forcing (RF) in four different latitude bands with respect to grid-scale emissions of aerosols and aerosol precursors. Regional RF values are combined with absolute regional temperature potentials [98, 96] to estimate surface temperature response. This approach, introduced in Lacey and Henze, 2015 [55], is expanded here by including greenhouse gases (GHGs) and transient temperature responses. GHG emissions are modeled using transient functions for species-specific radiative impacts [48, 1], which relate the timescale of emissions to the resulting transient RF impacts. These GHG RF impacts are then combined with the aerosol RF to estimate the total RF as a transient function. This net RF is multiplied by the transient global mean sensitivities and integrated for all prior years to estimate the temperature response of an emissions perturbation as a function of time. Uncertainties in climate impacts are derived from ranges of emissions factors based on fuel characterizations [87, 68] combined with ranges of radiative efficiencies of short-lived climate pollutants (SLCPs) [17, 75]. The uncertainties in climate impacts from GHGs are estimated as $\pm 10\%$ of their total impact and are combined with the species-specific SLCP errors in quadrature.

We also estimate global premature mortality due to chronic exposure to ambient concentrations of $PM_{2.5}$. To mitigate uncertainties in exposure estimates owing to model resolution [84, 61], satellite-derived $PM_{2.5}$ concentrations [18, 115] are used to redistribute GEOS-Chem $PM_{2.5}$ concentrations from the $2^\circ \times 2.5^\circ$ to the $0.1^\circ \times 0.1^\circ$ scale following Lee et al., 2015 [58]. Population-weighted $PM_{2.5}$ exposure is calculated using population estimates at the same resolution [30], which have been rescaled to 2050 national scale population based on 2010 United Nations World Population Prospects[1] . The modeled exposure estimates are combined with disease-specific relative risk (RR) parameters for integrated exposure responses (IER) [19] and country-level baseline mortality rates [64] to estimate premature deaths from exposure to ambient $PM_{2.5}$. The adjoint model is used to calculate the sensitivities of global premature deaths with respect to grid-scale speciated emissions perturbations [58]. Transient health impacts are estimated by linear interpolation of sensitivities

[1] https://esa.un.org/unpd/wpp/

calculated for the present day and the year 2050 (using RCP 4.5 emissions). Uncertainties in the health response are calculated following Lee et al., 2015 [58], in which the model was run with perturbed IER responses and baseline mortality rates corresponding to ±1 standard deviation for each impact. These are combined with a comparison of results obtained using different satellite-derived $PM_{2.5}$ surfaces [18, 116] to estimate the range of annual premature deaths that can be attributed to ambient $PM_{2.5}$ exposure from solid fuel cookstove use.

3.5 Results

3.5.1 Transient Global Climate Impacts of National-Scale Emissions

Transient global climate impacts for removal of cookstove emissions, from each species, are shown in Figure 4.2. Panel (a) shows these contributions to the net transient temperature response. SLCP impacts dominate the response for the first half of the century, while the GHG impacts, particularly CO_2, become increasingly important by 2100, consistent with previous studies of other types of mitigation [85, 114, 103, 89]. Cooling caused by removal of the absorptive species (BC, CO_2, and CH_4) outweighs the warming from removal of reflective aerosols (OC and sulfate, the latter from coal), with BC contributing the most to the surface temperature impact.

The use of adjoint sensitivities allows us to identify the contribution of each country's emissions to global climate change. Panel (b) shows countries with the largest contributions of national-scale emissions to the global average surface temperature response in 2050, with the breakdown of each species' contribution to that impact, along with Brazil and Mexico for comparison. Note that countries with large GHG contributions will have relatively larger overall impacts in later decades than are shown in Fig.1(b), as GHG effects increase, consistent with global-scale trends shown in Fig. 1(a); the tabulated transient national-scale contributions for all countries with larger than 5% solid fuel use can be found in the Supporting Information. Considering only carbonaceous aerosols, Lacey and Henze et al. [55] highlighted the value of mitigating BC emissions in high latitude countries, which incur the largest magnitude cooling response per kg of abated BC

emission, while the removal of co-emitted OC in many countries (e.g., Central and South America, parts of Africa) leads to a net warming. Inclusion of GHG emissions shows that in regions wherein residential solid-fuel emissions have a large OC component, the climate impact from CO_2 and CH_4 counteracts the cooling impact of these reflective aerosols. This occurs in African countries that use large amounts of non-renewable solid fuels [5], as shown by the larger percent contribution of CO_2 to the net temperature impact in countries such as Ethiopia and Kenya. This panel also shows the uncertainties in the net global surface temperature response. For several countries (i.e., Ethiopia, Bangladesh, Kenya) the range of temperature impacts spans zero, meaning that the temperature impact from removal of these countries' emissions may have a net warming effect.

3.5.2 Transient Global Health Impacts of National-Scale Emissions

Fig. 3.2(a) shows each species' contribution to cumulative and annual global premature deaths avoided due to changes in ambient $PM_{2.5}$ from the removal of cookstove emissions. The large increase in annual avoided deaths from 2000 to 2020 is due to the phased emissions reduction. The change in annual avoided premature death from 2020 to 2050 is due to the regional increases in population and changes in the formation of sulfate aerosol caused by shifts in anthropogenic emissions. While the sensitivities will continue to change between 2050 to 2100, we have not calculated sensitivities beyond 2050 since the projections of population and baseline mortality have increasingly large uncertainties [113]. Therefore, we have assumed that the population and mortality post-2050 continue to increase following the same rate of change as 2020 to 2050 as a first order estimation in order to compare health and climate on the same horizon.

The health impacts in Fig. 3.2(b) show that throughout all countries OC is the largest contributor to ambient $PM_{2.5}$ exposure from cookstove emissions. This plot also highlights the importance of SO_2 emissions in countries that use a combination of traditional wood and herbaceous fuels along with coal. The countries with the largest contribution to global premature deaths from exposure to ambient $PM_{2.5}$ from cookstoves are not necessarily the countries with the highest solid fuel use or number of cookstoves (i.e., Ethiopia, Nigeria, and Kenya). Large ambient health impacts

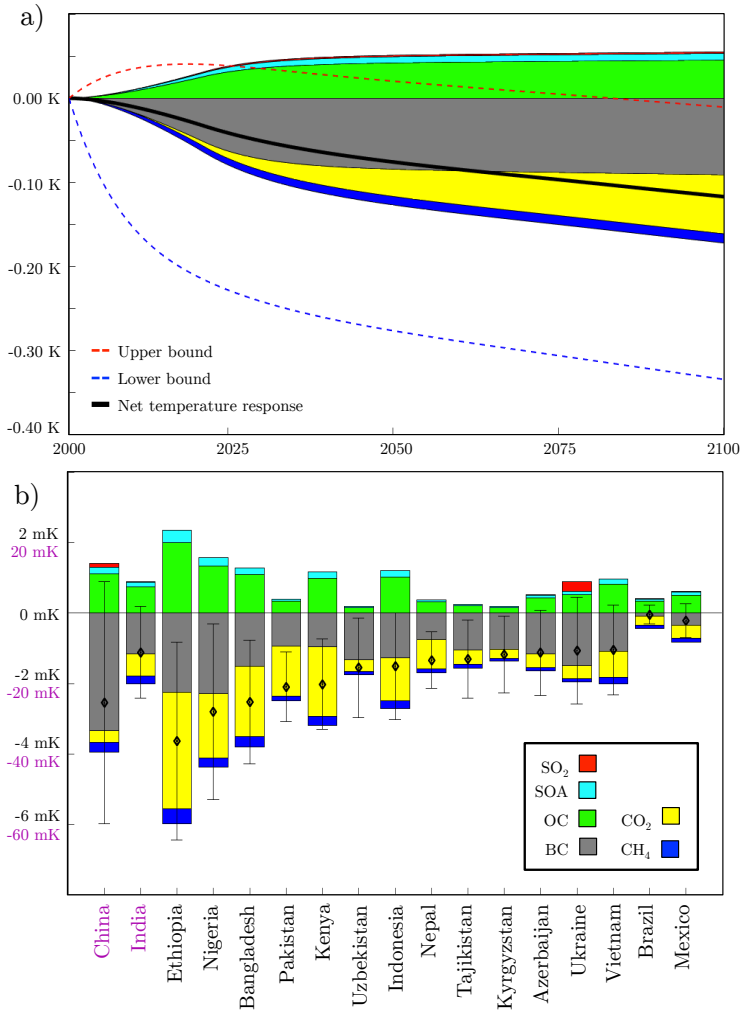

Figure 3.1: The global transient surface temperature response to a phasing out of solid fuel cookstove emissions by 2020. Individual colors represent each species' contribution to the global response. (a) The global mean surface temperature response (net impact shown as solid black line). (b) National contributions to global surface temperature response in 2050 for the countries with the largest contribution, along with Brazil and Mexico for comparison. China and India's contributions are shown in purple on the y-axis.

from emissions in countries such as Nepal, Pakistan, and Vietnam are due to transport of $PM_{2.5}$ over populated regions. In contrast, emissions in countries such as Ukraine and Romania contribute to a large percentage of the global health impact owing to high baseline mortality rates [58].

3.5.3 Climate and Ambient Health Co-Benefits

We next evaluate the combined impacts from national-scale solid fuel cookstove use. In order to directly compare climate and ambient air quality impacts, we have calculated each country's percent contribution to global climate and health impacts, and plotted these in Fig. 3.3 on the x and y axis, respectively. Other studies have compared health and air quality impacts by monetizing both climate and health [76, 99]. In order to avoid confounding the transient estimated global impacts with the changing social costs of emissions and statistical values of life, we present both as equal objectives and recognize that either axis used here could be rescaled or monetized as seen fit in future studies if desired. For simplicity, the impacts plotted here are calculated for 2050, but values for each decade between 2000 and 2100 in the Supporting Information. Countries have been color-coded by continent to highlight differences between regions in terms of the net co-impacts that they exhibit as a response to the phased removal of cookstove emissions. In general, African countries tend to contribute to a larger temperature response due to large amounts of cookstove use and the cooling potential from the removal of the associated GHG emissions. In contrast, the ambient health impacts of emissions from African countries are smaller than in other regions due to the lower population densities. Countries in Southeast Asia tend to contribute to more balanced climate and ambient health impacts in part due to higher population densities and transport of primary aerosol emissions over populated areas, as well as still having significant solid fuel use and high aerosol radiative efficiencies. The large ambient health impacts from Eastern European emissions reductions are a function of higher baseline mortality rates as [58, 64]. Also note that due to the magnitude of solid fuel use in China and India, their impacts lie outside the plot axes.

While the overall magnitude of the impacts is important in understanding the drivers of

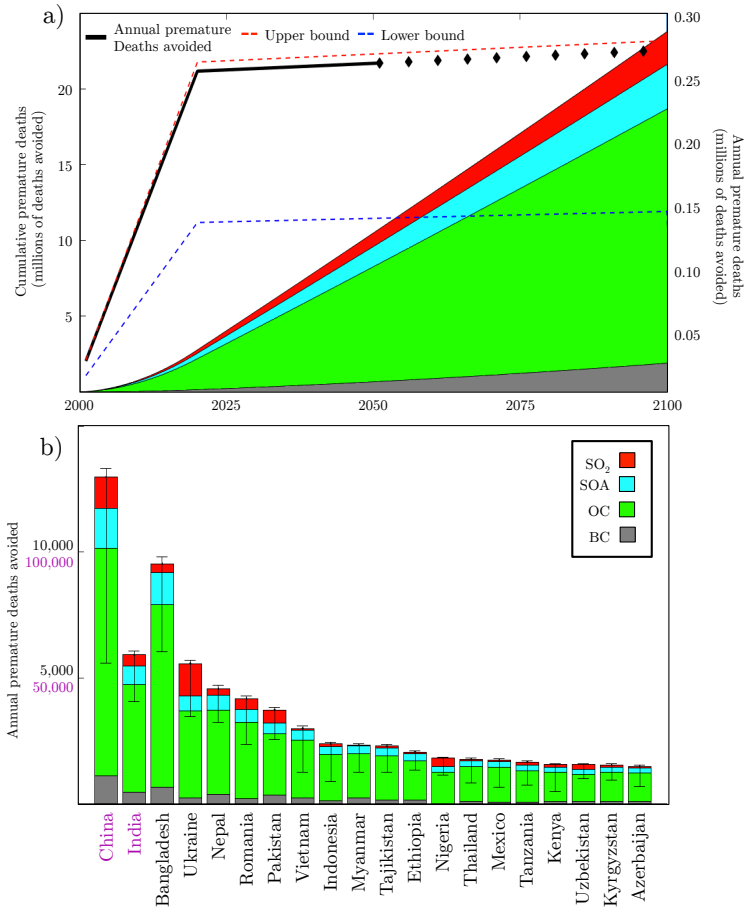

Figure 3.2: The global transient premature deaths avoided due to changes in ambient $PM_{2.5}$ from a phased removal of solid fuel cookstove emissions by 2020. Colors show the species' contributions to the global response. (a) The annual (solid black line) and speciated cumulative response. Points beyond 2050 represent projections further than modeled adjoint sensitivities. (b) National contributions to annual avoided premature deaths in 2050 from changes in ambient $PM_{2.5}$. China and India's impacts are shown in purple on the y-axis.

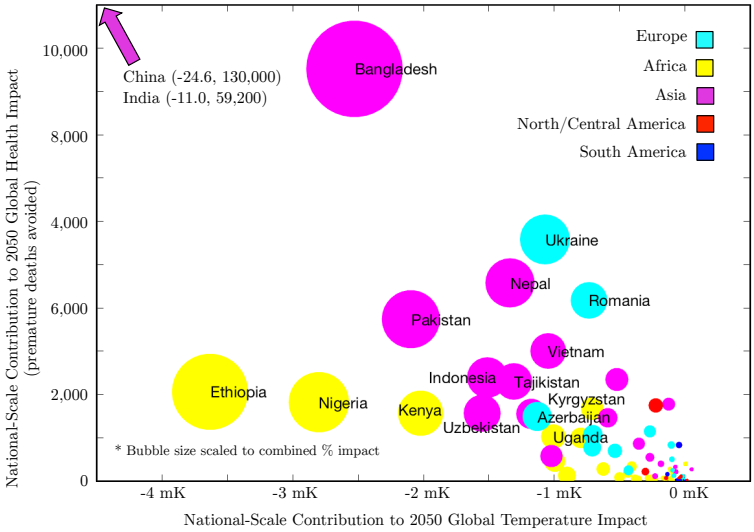

Figure 3.3: National scale contributions to total global climate and health impacts in 2050 for complete phase-out of cookstove emissions by 2020. The x-axis is showing the change in global surface temperature (relative to 2050 following RCP 4.5). The y-axis shows the number of premature deaths from the change in ambient $PM_{2.5}$ concentrations attributed to a country's individual emission reduction. The bubble size of each country is scaled to the combined % contribution of health and climate impacts for that country.

global climate and ambient air quality, of more value with regards to policy, specifically cookstove interventions, are the impacts on a per cookstove basis. We thus next consider (Figure 3.4) the national-scale contributions to global climate and air quality impacts divided by the national-scale number of cookstoves, which is estimated using the number of people using solid fuels in 2010 [15] and the household size from the Global Burden of Disease Institute for Health Metrics and Evaluation[1] . Per cookstove (i.e., marginal) impacts are largest for cookstoves in certain regions not typically targeted for cookstove interventions [114], such as those in Central Asia and Eastern Europe, with emissions from Azerbaijan ranking the highest in terms of climate and second highest in terms of health.

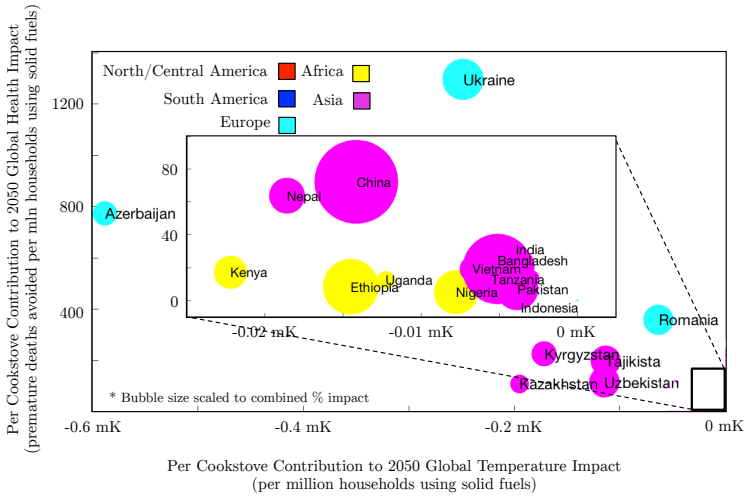

Figure 3.4: National scale per cookstove contributions to climate and health impacts, with inset showing the countries at the lower end of the scale. Individual bubble sizes are colored by continent and scaled to the combined % contribution of health and climate impacts (China and India are scaled by 1/10 due to the overall magnitude of their impacts).

3.6 Conclusions

For the year 2050, the impacts from the phased removal of global solid fuel cookstove emissions is a global average surface temperature cooling of 77 mK (ranging from a 20 mK warming to 278 mK

[1] http://cleancookstoves.org/country-profiles/

cooling) and an avoidance of 260,000 (137,00 - 268,000) annual premature deaths due to ambient $PM_{2.5}$ exposure cumulatively avoiding 10.5 (5.55 - 10.80) million cumulative premature deaths from 2000 to 2050. Aerosols contribute 41% to the central estimate of net global cookstove climate impacts by 2050, and alone may be cooling or warming with large uncertainties based on fuel type and aerosol's climate impacts. However, the net climate impacts of cookstove emissions reductions are very likely cooling, when considering the benefits of curbed GHG emissions, an aspect which becomes increasingly prominent on longer time-horizons. National scale contributions of cookstove emissions to global premature deaths due to ambient $PM_{2.5}$ exposure are driven by primary organic carbonaceous aerosol.

Emissions from cookstoves in China and India are the largest, and they contribute the most to ambient air quality and climate impacts; however, the role of other countries does not in general always correspond to the magnitude of their emissions. Figure 3.5 depicts how ambient air quality and climate benefits of cookstove interventions are modulated by the role of transport of aerosols over populated regions, the combined impacts of absorbing and reflective components of aerosols, the ratio of GHG to aerosol emissions as a function of fuel type, and the magnitude of semi and indirect climate affects of opposite sign. Several countries (Azerbaijan, Kyrgyzstan, Uzbekistan, and Ukraine) rank in the top-20 in terms of their co-impacts without being ranked highly in terms of total population using solid fuels. Despite a smaller amount of cookstove use, intervention programs in these countries are estimated to result in the highest co-benefit per cookstove replaced owing to increased climate impacts of black carbon due to transport to the Arctic and over snow, and the increased number of premature deaths due to high baseline mortality rate in these regions.

While this study addresses a number of factors governing the impacts of emissions from cookstove on climate and ambient air quality, there are several aspects that warrant consideration in future work. First, these estimates use a single emissions dataset and do not explicitly consider the uncertainties in the emissions for our estimate of a country's total contribution (although marginal impacts, to first order, are less sensitive to this type of uncertainty). While we attempt to account for this when estimating health impacts by considering a range of satellite-derived $PM_{2.5}$

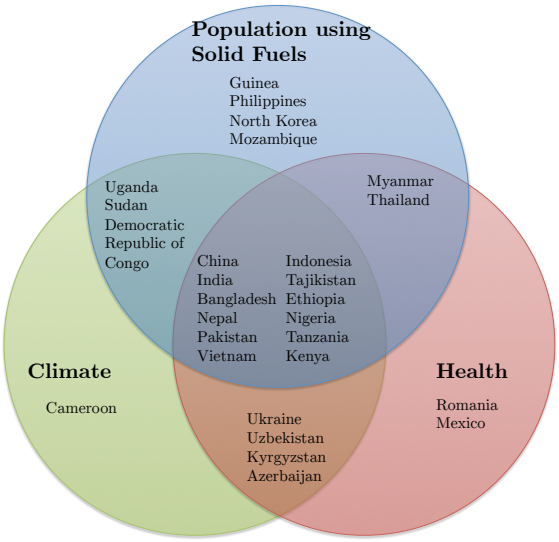

Figure 3.5: The top twenty countries ranked in terms of three variables: population using solid fuels for cooking (blue), contribution to the global surface temperature change from the emissions from cookstove solid fuel emissions (green), and the contribution to to global premature deaths from exposure to ambient $PM_{2.5}$ from cookstove solid fuel emissions (red).

datasets [18, 116], additional assessment of cookstove emissions inventories and resulting $PM_{2.5}$ concentrations would be valuable. Our work only crudely treats SOA formation as 18% of the total OC impact, although based on formation of OC within smoke plumes and the emission factors of non-methane organic compounds will impact this [34, 108]. New understandings in the roles of SO_2 and NO_x emissions on SOA formation [38, 83, 121] may eventually be incorporated into this type of model; neglecting the role of SO_2 and NO_x on SOA formation means our estimates are likely lower bounds. The methods used here also use global estimates of aerosol semi and indirect climate impacts following UNEP and WMO, 2011 [111]. Several studies have shown the regional importance of aerosol and precursor emissions on global climate impacts such as [6, 72]. Future work may be able to extend the source attribution techniques used in our study for direct radiative forcing to indirect effects [49, 90]. Lastly, we have focused on the impact of cookstove emissions under an illustrative yet simplistic scenario. A more comprehensive integrated assessment of life-cycle impacts using realistic cookstove replacement options is warranted.

3.7 Acknowledgements

The research described in the article has been funded wholly or in part by the U.S. Environmental Protection Agency's STAR program through grant 83521101, although it has not been subjected to any EPA review and therefore does not necessarily reflect the views of the Agency, and no official endorsement should be inferred. In addition, this work is possible through NASA AQAST (NNX11AI54G) and support from the NASA HEC computing facilities.

Chapter 4

Air pollution-related health and climate benefits of clean cookstove programs in Mozambique: A scoping analysis

4.1 Executive Summary

Residential solid fuel use for cooking in Mozambique is widespread, imposing a substantial burden on public health and degrading natural landscapes. Approximately 96% of the population in Mozambique uses solid fuels for cooking, with wood typically used in rural areas and charcoal in urban areas. The Global Burden of Disease 2013 study conducted by the Institute for Health Metrics and Evaluation estimated that high household levels of fine particulate matter ($PM_{2.5}$) exposures were associated with 11,750 premature deaths and 501,700 disability-adjusted life years (DALYs) in Mozambique in 2013. In many parts of the world, cookstoves are also a substantial contributor to ambient air pollution, affecting public health on broader spatial scales beyond the household. Cookstoves also emit short-lived climate pollutants and long-lived greenhouse gases, which can exacerbate global and regional climate change over the near-term (decades) and long-term (centuries).

The objective of this study is to provide a first-order estimation of potential air pollution-related health and climate benefits of expanding the use of cleaner stoves and fuels in Mozambique. We use state-of-the-science methods to assess the health and climate benefits of four illustrative scenarios in which traditional cooking fires and stoves are displaced by more efficient wood-burning stoves in rural areas and by cleaner charcoal stoves or LPG stoves in urban areas. These scenarios were designed to use technologies that would be appropriate for local circumstances, including

cooking traditions, typical fuel type used, and economic conditions. These scenarios are feasible with current technologies on the market, though the level of stove penetration and success of program implementation depends on multiple factors beyond the scope of this work. In the absence of Mozambique-specific information on emission and exposure levels, estimated health and climate benefits are based on laboratory-based emissions data and assumptions to convert emissions reductions to exposure reductions.

For rural areas, this analysis suggests that forced draft wood-burning stoves are very cost-effective and could achieve over 2.5 times more health benefits compared to natural draft stoves in the same households, assuming equal usage levels for both cases. Forced draft stoves burn unprocessed biomass and improve combustion efficiency by blowing air into the combustion chamber. Reaching a level of 10% penetration across rural households in Mozambique is estimated to avoid approximately 200 premature deaths and 14,000 DALYs for a 3-year intervention from reduced household air pollution. Approximately 2-3% additional health benefits are likely to result from reduced ambient air pollution. While natural draft stoves achieve fewer health benefits compared with forced draft stoves, they are also very cost-effective. Climate impacts are more uncertain although the central estimate shows that both natural draft and forced draft stoves are estimated to reduce expected climate change-related temperature increases over decadal and longer-term time periods. Concentrating the same number of intervention stoves in a smaller geographical area would not affect the level of household air pollution health benefits but could lead to larger ambient air quality health benefits.

For urban areas, advanced charcoal stoves would achieve approximately 80% of the health benefits of LPG stoves and are estimated to be very cost-effective. LPG stoves are estimated to be very cost-effective in Maputo where charcoal is relatively expensive, cost-effective in Beira, and not cost-effective in Nampula where charcoal is relatively cheap. Switching to LPG is assumed to have a lower usage rate of 0.6 compared with a rate of 0.7 for advanced charcoal stoves. Expanding use of LPG stoves to 10% of households in five major cities, Maputo, Beira, Nampula, Tete, and Pemba, would result in an estimated 160 premature deaths and 11,000 DALYs averted for a 3-

year intervention. Approximately 4-5% additional health benefits are estimated to result from reduced ambient air pollution. The same penetration level of modern charcoal stoves in these five cities would result in an estimated 130 premature deaths and 9,000 DALYs averted and six premature deaths averted annually from reduced ambient air pollution. Although climate impacts are uncertain, the central estimate shows that both modern charcoal stoves and LPG stoves would reduce expected climate change-related temperature increases over decadal and longer-term time periods.

This study demonstrates that substantial health and climate co-benefits can result from expanding the use of cleaner wood and charcoal stoves in Mozambique. Switching to cleaner fuels such as LPG would yield even greater health benefits, but is less cost-effective than modern charcoal stoves. Benefits may be underestimated because they exclude improvements resulting from reduced emissions and forest degradation from fuel production (particularly important for reduced charcoal production).

Health impact and cost-effectiveness results are very uncertain due to lack of information about household adoption of the new technologies, exposure levels, underlying health characteristics, and exposure-response functions specific to Mozambique. Climate impact results are also very uncertain due to lack of information about the mix of short-lived climate forcers reduced by the technologies and limited understanding of their influence on the climate system. The analysis would be improved by obtaining measurements of $PM_{2.5}$ exposures in rural and urban homes in Mozambique, for both the baseline fuels and stoves as well as various improved stove models. As such data become available, sensitivity results presented here for different combinations of baseline and intervention exposure levels can be used to recalculate health benefits and improve program design for potential clean cooking interventions.

4.2 Methods and Results

4.2.1 Ambient air pollution health impacts

4.2.1.1 Model

To estimate the ambient air quality and related health benefits of clean cookstove adoption in Mozambique, we use the GEOS-Chem model (Bey et al. 2001). GEOS-Chem is a chemical transport model that uses input meteorology from the Goddard Earth Observing System along with online calculations of aerosol formation, growth, and deposition at the global 2 by 2.5 degree resolution. While the model can estimate a number of different outputs, the version used for this study to estimate health impacts is fully explained by Lee et al. (2016), and uses disease specific integrated exposure response (IER) functions developed by Burnett et al. (2014) to estimate the number of annual premature deaths due to exposure to ambient concentrations of $PM_{2.5}$. Since the global model spatial resolution is too coarse to estimate exposure impacts, the model uses observations from satellite products to redistribute the aerosol mass concentrations from the model resolution to 0.1 by 0.1 degree resolution (van Donkelaar et al. 2016). This model is used in conjunction with its adjoint, which allows for calculating sensitivities of the model output with respect to all model inputs. The resulting sensitivities are an approximation of the impact of emissions within Mozambique on the total number of global deaths, with an additional model calculation showing impact of emissions on deaths within Mozambique. A full discussion of the model inputs and parameterizations is presented in Annex 2 of this report.

The use of adjoint sensitivities allows for the efficient calculation of the change in annual premature deaths from ambient $PM_{2.5}$ exposure for a given emissions perturbation, as is presented in this report. Here we estimate the impacts as a function of stove emissions reduction efficiency and percent of clean cookstove adoption for emissions from Mozambique alone. From the perspective of premature deaths, ambient air pollution health benefits are theoretically additional to the household air pollution-related health benefits, but since methods used to quantify the two impacts are different, results presented here may not be additive.

4.2.1.2 Data and assumptions

The adjoint model calculations are performed for a given atmospheric condition and disease specific exposure parameters. For this study we have assumed 2005 meteorology and population distribution, combined with year 2000 historical anthropogenic emissions for calculation of the base atmosphere (Lamarque et al. 2010). Additional natural emissions are also included in the model calculations and fully described in Annex 2. While the baseline model calculations are using year 2000 emissions, the estimated $PM_{2.5}$ concentrations are rescaled to 2010 values through the inclusion of satellite biasing at the 2 by 2.5 degree resolution. The satellite data used for the bias calculation is from van Donkelaar et al. (2016) and represents data that most closely matches the in situ measurements in neighboring South Africa (http://www.rbcaa.org.za/, data accessed May 16, 2016) and is an improvement on the GBD 2013 dataset (Brauer et al., 2015) due to the use of geographically weighted regression factors. In addition to satellite biasing, the satellite data is also used for redistributing $PM_{2.5}$ concentrations from the model resolution of 2 by 2.5 degrees to the more appropriate 0.1 by 0.1 resolution. It is at this resolution where the modeled exposure is combined with disease specific IER functions (Burnett et al. 2014) and country specific baseline mortality (Lozano et al., 2012).

Estimation of the health impacts also rely on an emissions perturbation, in this case emissions from solid fuel use in Mozambique. These solid fuel cookstove emissions are estimated by combining the Bond et al. (2007) carbonaceous aerosol emissions inventory for biofuel use with the domestic SO_2 emissions from Lamarque et al. (2010). We then apply country specific solid fuel use from Bonjour et al. (2013). For Mozambique, this is 96% of the total population using solid fuel for cooking. This emissions inventory is at the model resolution so we have also applied a mask to these emissions, which represents the percent population in the grid cell that resides in Mozambique in order to accurately estimate emissions from Mozambique alone. The understanding of the formation of secondary organic aerosol, especially in smoke plumes, is very nascent and therefore a simple parameterization of 18% of the OC impacts are included as impacts from SOA. This percentage is

assuming a 50% formation rate from the aromatic and other compounds emitted as non-methane volatile organic compounds from the biofuel sector (Streets et al., 2003). The regional scenarios, for which impacts are presented in this section, are fully defined in Section 4 of this report, although specific assumptions were made regarding the population distributions for urban and rural regions. For Mozambique we have defined the threshold for urban population density as 100 people per square kilometer, a threshold that captures all of the cities examined in the scenarios described in Section 4 (Figure 4.1). This mask is combined with population at the same scale to disaggregate the urban and rural emissions from the larger model resolution emissions inventory.

Figure 13.

4.2.1.3 Normalized results ambient air pollution health impacts

By multiplying the modeled adjoint sensitivities for premature deaths from exposure to ambient $PM_{2.5}$ by the Mozambique specific solid fuel emissions, we estimate the global annual number of deaths from ambient $PM_{2.5}$ as 278 due to the combined cookstove emissions of carbonaceous aerosols and SO_2. Approximately 38% of these global premature deaths occur within Mozambique. This percentage is relatively low compared with the percentage of $PM_{2.5}$-related premature deaths occurring within the source country versus the rest of the world (e.g. Anenberg et al. 2014), due to meteorological features of Mozambique and neighboring countries. Table 4.1 shows the total potential benefit for a nationwide intervention of cookstoves and Table 4.2 shows the impacts normalized to an implementation of 5000 improved cookstoves.

4.2.2 Ambient air pollution climate impacts

4.2.2.1 Model

The GEOS-Chem adjoint model is also used to estimate the climate impacts from changes in emissions within Mozambique. This version of the model used for this report follows Lacey et

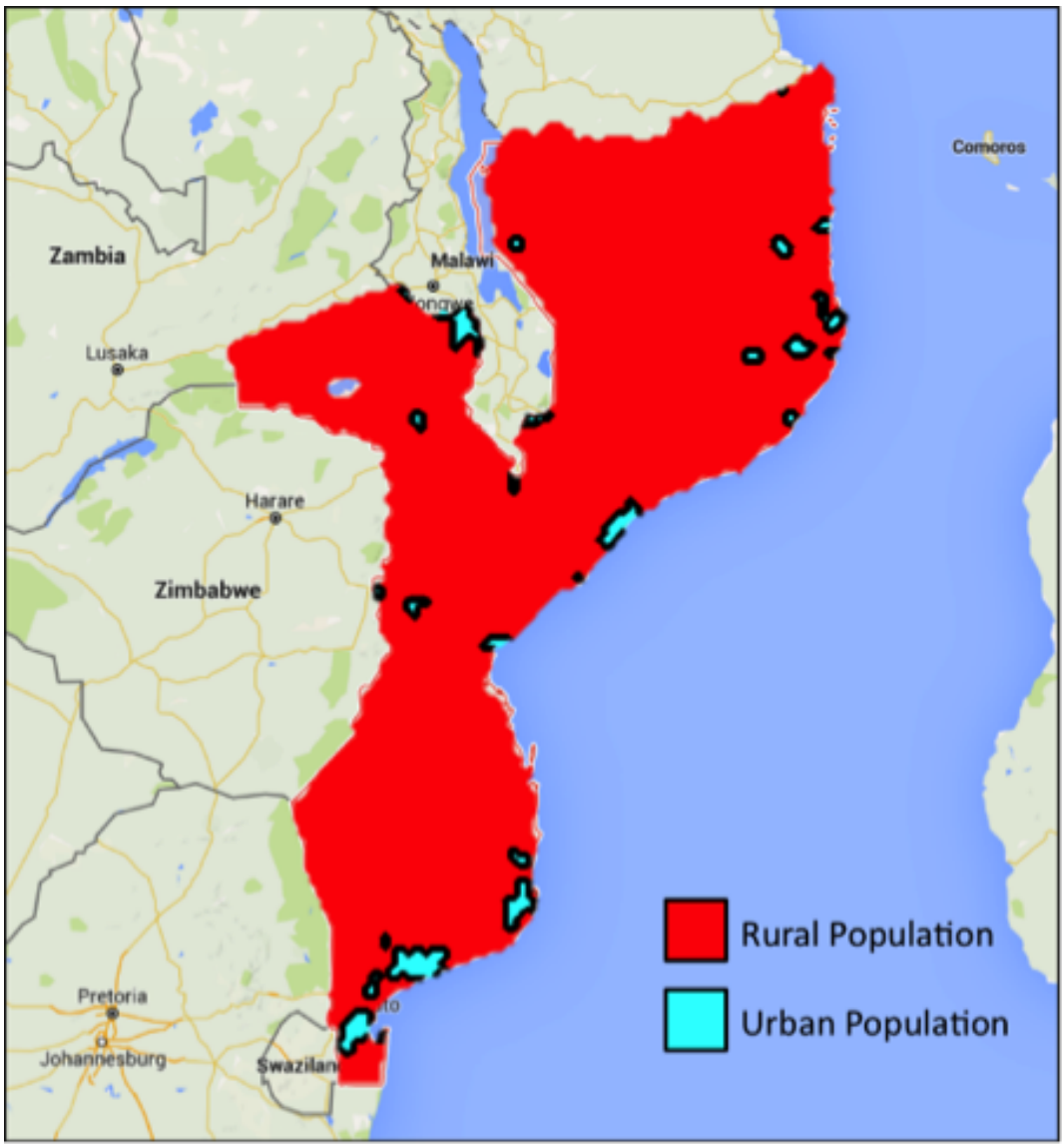

Figure 4.1: Breakdown of urban vs rural gird cells at the 0.1 by 0.1 degree resolution. This data is used to define the regions impacted by rural cookstove mitigation scenarios and urban cookstove mitigation scenarios.

Table 4.1: Annual premature deaths averted due to reduced exposure to ambient $PM_{2.5}$ difference in percent of population using solid fuels and stove efficiency.

% Population Using Improved Cookstoves	Intervention Emission Reduction %						
	0	15	30	45	60	75	90
0	0.0	0.0	0.0	0.0	0.0	0.0	0.0
15	0.0	6.2	12.5	18.7	25.0	31.2	37.5
30	0.0	12.5	25.0	37.5	50.0	62.4	74.9
45	0.0	18.7	37.5	56.2	74.9	93.7	112.4
60	0.0	25.0	50.0	74.9	99.9	124.9	149.9
75	0.0	31.2	62.4	93.7	124.9	156.1	187.3
90	0.0	37.5	74.9	112.4	149.9	187.3	224.8

Table 4.2: Annual premature deaths averted per 5000 households due to reduced exposure to ambient $PM_{2.5}$ as a function of difference in percent of population using solid fuels and stove efficiency.

% Population Using Improved Cookstoves	Intervention Emission Reduction %						
	0	15	30	45	60	75	90
0	0.00	0.00	0.00	0.00	0.00	0.00	0.00
15	0.00	0.01	0.01	0.02	0.02	0.03	0.03
30	0.00	0.01	0.02	0.03	0.05	0.06	0.07
45	0.00	0.02	0.03	0.05	0.07	0.09	0.10
60	0.00	0.02	0.05	0.07	0.09	0.12	0.14
75	0.00	0.03	0.06	0.09	0.12	0.14	0.17
90	0.00	0.03	0.07	0.10	0.14	0.17	0.21

al. (2015), with the addition of sulfur dioxide and greenhouse gas impacts along with transient impact calculations. In summary this model combines modeled aerosol mass concentration with the LIDORT radiative transfer model (Spurr et al., 2001) to estimate the net change in radiative flux from a baseline pre-industrial atmosphere. The adjoint of this model (Henze et al., 2007; Henze et al., 2012) is then used in conjunction with absolute regional temperature potentials to estimate the impact of radiative forcing within a latitude band on global surface temperature change form aerosol and aerosol precursor emissions (Shindell and Faluvegi, 2009; Shindell, 2012).

Impacts from GHGs are calculated using the speciated transient radiative forcing efficiencies from Joos et al. (2012) and Aamaas et al. (2012). These parameterizations estimate the change in radiative forcing as a function of emissions taking into account atmospheric lifetimes and carbon cycle impacts. These well-mixed species are then combined with the transient global mean sensitivity derived from Boucher and Reddy (2008). More detailed explanation of the full methods is described in Annex 2 and can be found in work that is currently in preparation by Lacey et al. to be submitted in the near future.

4.2.2.2 Data and Assumptions

Adjoint modeling techniques are used to develop the sensitivities of regional radiative forcing (i.e., within a latitude band) with respect to changes in global emissions. The base model used, GEOS-Chem, is explained in the previous section and in Annex 2 and uses offline meteorological fields with online calculations of chemical and physical processes related to aerosol formation and fate to estimate grid scale speciated aerosol mass concentrations at the 2 by 2.5 degree resolution (Bey et al., 2001). The model used for the climate impact calculations takes this aerosol mass concentrations and uses offline Mie theory calculations to estimate the optical properties of these mass concentrations which are then passed into the LIDORT radiative transfer model, which in turn estimates the radiative forcing relative to pre-industrial 1850 radiative flux. This assumes species-specific fixed lognormal size distributions and is a calculation of the aerosol direct radiative forcing (DRF). In order to include aerosol indirect and semi direct effects, scaling factors of the DRF

with respect to each other impact is used in a similar manner to prior published works (e.g., UNEP, 2011a). This is an approximation of the indirect effects, but has shown comparable estimates of climate impacts to fully coupled microphysical models looking at similar emissions perturbations (Kodros et al., 2015) and results here are reported on ranges and central estimates of impacts which includes the uncertainties in aerosol radiative efficiencies (Boucher et al., 2013; Myhre et al., 2013). This report also uses estimates of the transient radiative forcing of GHGs through use of time dependent impulse response functions for CO_2, CH_4, and N_2O (Joos et al., 2012; Aamaas et al., 2012). These impulse response functions estimate the time dependent concentrations, which can then be used to estimate the radiative forcing in a given year based on the radiative efficiency of each species, resulting in the temporal calculation of radiative forcing from changes in GHG emissions. In order to accurately estimate impacts of a cookstove intervention on climate from a change in ambient aerosol and GHG concentrations, we must understand the baseline emissions within Mozambique. The aerosol emissions inventory used for the nationwide and scenario level emission is described in Section 3.3.2, while the GHG emissions are derived from a literature review of published emissions factors for GHG emissions relative to aerosol emissions (Turn et al., 1997; Roden et al., 2006; Johnson et al., 2008; Roden et al., 2009; Jetter et al., 2012). While these studies represent a range of stove types, fuels, and test conditions, the baseline emissions inventory only considers the results using traditional stoves and traditional fuels to create an average emissions factor for GHG emissions as a function of aerosol emissions. The range of emissions factors is not considered in this work due to the lack of data for Mozambique specific stoves and fuels but has potential impacts on the central estimate and bounds of the climate estimate. Other studies have shown that the impact of harvesting woodfuels in a renewable manner has a large impact on the net change in CO_2 emissions caused by use of woodfuels for cooking (Bailis et al., 2015). To account for this we have used a Mozambique specific estimate of fraction of non-renewable biomass harvesting of 39.6%, following the estimate from Bailis et al. (2015).

Table 4.3: Central estimate of the reduction in 2050 global temperature (in μK) resulting from solid fuel emissions reductions as a function of difference in percent of population using solid fuels and stove efficiency.

% Population Using Improved Cookstoves	Intervention Emission Reduction Percentage						
	0	15	30	45	60	75	90
0	0.0	0.0	0.0	0.0	0.0	0.0	0.0
15	0.0	19.2	38.4	57.6	76.9	96.1	115.3
30	0.0	38.4	76.9	115.3	153.7	192.2	230.6
45	0.0	57.6	115.3	172.9	230.6	288.2	345.9
60	0.0	76.9	153.7	230.6	307.4	384.3	461.2
75	0.0	96.1	192.2	288.2	384.3	480.4	576.5
90	0.0	115.3	230.6	345.9	461.2	576.5	691.7

4.2.2.3 Normalized results climate change impacts

In addition to HAP and ambient health impacts, emissions of aerosols, aerosol precursors, and greenhouse gases from residential solid fuel use also affect global and regional climate. Here we calculate the impacts by emission species as a transient temperature function as shown in Figure 4.2. This plot shows that central estimate of the short term net impact is negligible due to the balance of reflective carbonaceous aerosol and absorbing black carbon, but later in the century the warming impacts of greenhouse gases outweigh the aerosol impacts, increasing the climate benefit from cookstove interventions. We also see that the bounds of the estimated temperature impact span zero, meaning that there is a potential climate disbenefit due to the removal solid fuel cookstove use in Mozambique. These temperature bounds are dominated by the uncertainties in aerosol radiative impacts, including, but not limited to, their impact on cloud formation and longevity (Boucher et al., 2013). Table 4.3 and Table 4.4 show the reduction in 2050 global temperature resulting from solid fuel emission reductions as a function of percent of the population using improved cookstoves and the intervention emission reduction percentage.

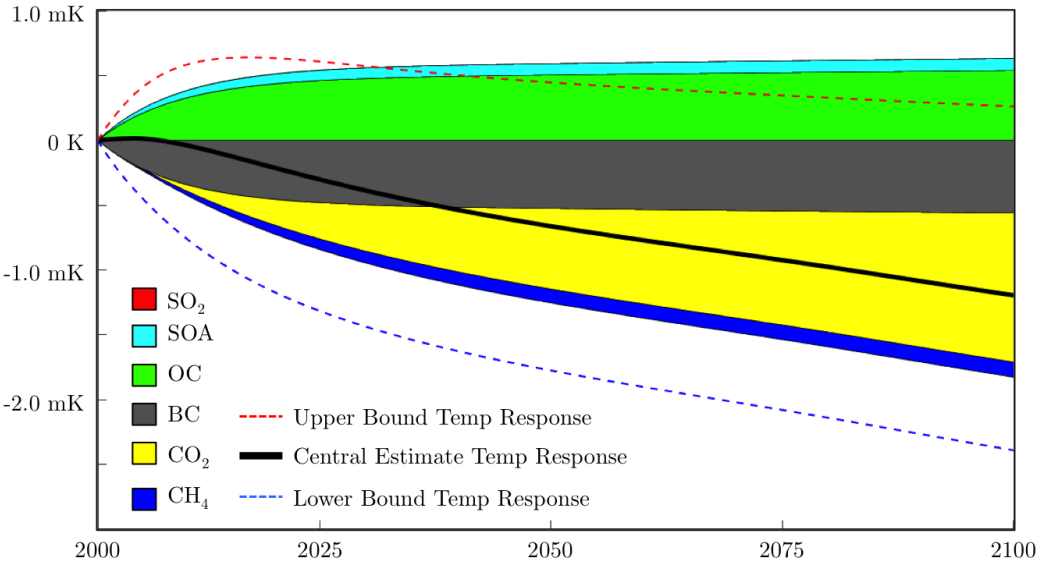

Figure 4.2: Transient central estimate of global temperature change for speciated emissions from 100% removal of cookstove emissions in Mozambique. Upper and lower bounds of the net temperature response are also shown.

Table 4.4: Central estimate of the reduction in 2050 global temperature (in μK) per 5000 cookstoves resulting from solid fuel emissions reductions as a function of difference in percent of population using solid fuels and stove efficiency.

% Population Using Improved Cookstoves	Intervention Emission Reduction Percentage						
	0	15	30	45	60	75	90
0	0.00	0.00	0.00	0.00	0.00	0.00	0.00
15	0.00	0.02	0.04	0.05	0.07	0.09	0.11
30	0.00	0.04	0.07	0.11	0.14	0.18	0.21
45	0.00	0.05	0.11	0.16	0.21	0.27	0.32
60	0.00	0.07	0.14	0.21	0.28	0.36	0.43
75	0.00	0.09	0.18	0.27	0.36	0.44	0.53
90	0.00	0.11	0.21	0.32	0.43	0.53	0.64

4.3 Scenarios

We developed four illustrative scenarios of clean cookstove programs in Mozambique to demonstrate the approximate range of health and climate co-benefits that could be achieved if more households used cleaner stove technologies and fuels. The scenarios were designed to include both rural and urban areas, as these types of areas differ in important aspects such as the types of fuels and stoves used at baseline, the types of fuels and stoves that would continue to meet household energy needs, and accessibility and cost of cleaner fuels and stoves. The scenarios also include both more ambitious, cleaner approaches and more incremental approaches that are perhaps more feasible to implement in the short term. The scenarios are informed by cleaner cooking efforts already underway in Mozambique. EnDev , an energy access partnership financed by several national governments (Netherlands, Germany, Norway, Australia, United Kingdom, Switzerland, and Sweden) has sold through its partners over 15,500 CH2200 Envirofit charcoal stoves and over 5,300 Envirofit Econochar charcoal stoves in one year (personal communication, Rosario Loayza, May 6, 2016). Successful experiences have been recorded in Maputo, Inhambane, Xai-Xai, Beira, and Pemba for charcoal stoves. EnDev is also working with woodstoves in Inhambane, Gaza, Manica, and Sofala, with additional activities beginning in other areas. We develop scenarios that are feasible today based on our understanding of these experiences in Mozambique and in other countries in Africa.

We consider different stove types according to their feasibility for broad dissemination and adoption in Mozambique along with their cleanliness in terms of $PM_{2.5}$ emissions. As a guide for $PM_{2.5}$ emission performance, we consider stove types categorized by the International Workshop Agreements (IWA) Tiers of Performance developed as a first step towards formal International Organization for Standardization (ISO) standards. The IWA framework rates cookstoves on four indicators: efficiency, indoor emissions, total emissions, and safety. Each of these indicators has five tiers, from 0 as the lowest performing to 4 as the highest performing. Tier boundaries were defined by quantitative values determined by laboratory testing. Individual stove models can then

Table 4.5: IWA Tiers of Performance for indoor $PM_{2.5}$ emissions.

	Indoor emissions $PM_{2.5}$ (mg/min)
Tier 0	≥40
Tier 1	≤40
Tier 2	≤17
Tier 3	≤8
Tier 4	≤2

be tested using a consistent protocol to determine its tier of performance for each of the indicators. Sub-tiers for indoor $PM_{2.5}$ emissions are shown in Table 4.5. Since exposure reductions in reality are typically smaller compared with emission reductions taken from laboratory-measurements, we use smaller percentage reductions for each tier for exposure levels. Each percentage reduction in emissions is multiplied by a factor of 0.8 to convert from laboratory-based emissions studies to more realistic changes in exposure levels in households. There were no Mozambique-specific information on which to base this ratio. As new information becomes available as to post-intervention exposure reductions in Mozambique, these estimates can be revised using a more realistic ratio.

The four scenarios are described below and summarized in Table 4.6. We examine two rural scenarios and two urban scenarios. For the rural scenarios, we determined that a switch from unprocessed biomass to a cleaner-burning fuel is unlikely to be feasible. Unprocessed biomass is typically collected rather than purchased, and a market for cleaner burning fuels would likely be restricted to urban and peri-urban areas where fuel for cooking is purchased. We therefore examine two rural scenarios, both using unprocessed biomass as the fuel type. In one scenario, a cheaper but still relatively inefficient natural draft stove is used. In the other scenario, a more expensive and more efficient forced draft stove is used. Forced draft stoves include a mechanism to force air into the fire, raising flame temperature and intensity, thereby enhancing combustion efficiency. For urban areas where purchased charcoal is the main fuel type, we examine one scenario using a modern, more efficient charcoal stove, and one scenario switching to LPG as fuel. LPG stoves are among the cleanest in terms of health-damaging air pollutant emissions, but are more expensive and require a shift from charcoal to LPG. For each of the four scenarios, we examine two

different penetration levels. Penetration levels refer to the percentage of households receiving the intervention. The fraction of households using the intervention is assumed to be 0.6 for the LPG scenarios where fuel switching occurs, and 0.7 for the other three scenarios that do not require fuel switching. These fractions are applied as adjustments to the penetration levels for each scenario. For the rural scenarios, we also examine the impact of implementing the intervention across all of rural Mozambique versus just in four specific provinces. Since the interventions likely reduce not just indoor air pollution for the households receiving the intervention, but ambient pollution as well, this assessment gives an indication as to the magnitude of the ambient air quality improvements and associated health and climate benefits for different types of interventions. The household numbers used for each penetration level are approximations to simplify the analysis and use consistent penetration levels across each scenario. For example, we use 300,000 households for both 10% penetration in rural households across Mozambique and 40% rural penetration in four provinces, though the number of households differ slightly. The results are therefore approximations of 10% and 40% penetration levels in the given geographical area.

To derive baseline exposure levels in both urban and rural areas, we conducted an informal literature review of $PM_{2.5}$ personal exposure monitoring in households in Africa. We found only one personal exposure study in Mozambique, specifically in Maputo, finding that average exposure levels to particles less than about 7 m in diameter were 1200, 540, or 200-380 g/m3 during cooking events for wood, charcoal, and LPG and electricity, respectively (Ellegrd 1996). We were not able to find any studies measuring personal exposure to $PM_{2.5}$ in Mozambique specifically. Further, no studies in Africa of $PM_{2.5}$ personal exposure could be found in the World Health Organization Global Database of Household Air Pollution Measurements, last updated in 2011. For studies in other African countries measuring personal exposure to $PM_{2.5}$, we found only one study of charcoal use in urban areas, which reported a mean exposure level of 130 g/m3 in Ghana (Van Vliet et al. 2013). We found no studies monitoring $PM_{2.5}$ personal exposure levels in rural wood-burning homes in Africa, though a couple studies monitor kitchen concentrations in Malawi (Fullerton et

Table 4.6: Scenarios for clean cookstove programs in Mozambique for which health and climate benefits are calculated (HH=households).

Name	Rural Natural Draft (RND)	Rural Forced Draft (RFD)	Urban Modern Charcoal (UMC)	Urban LPG (ULPG)
Community type	Rural	Rural	Urban	Urban
Baseline fuel	Unprocessed biomass	Unprocessed biomass	Charcoal	Charcoal
Baseline stove	3 stone fire	3 stone fire	Traditional	Traditional
Improved fuel	Unprocessed biomass	Unprocessed biomass	Charcoal	LPG
Improved stove	Natural draft e.g. Envirofit EconoFire	Forced draft e.g. BioLite Homestove or Phillips HD4010	e.g. Envirofit Econochar	e.g. Envirofit Pureflame
IWA Tier (high power indoor PM2.5 emissions)	1	3	3	4
Baseline exposure (μg/m3)	150	150	150	150
% PM2.5 emissions reduced (per HH)	44%	80%	80%	95%
Location	a) Nationwide b) Sofala, Manica, Inhambanee, Gaza provinces	a) Nationwide b) Sofala, Manica, Inhambanee, Gaza provinces	Maputo, Beira, Nampula, Tete, Pemba	Maputo, Beira, Nampula, Tete, Pemba
# households	10%, 40%	10%, 40%	10%, 40%	10%, 40%

al. 2009) and Kenya (Lozier et al. 2016). The Malawi study reported kitchen concentrations of 185 g/m3 in urban homes burning charcoal and 268 g/m3 in rural homes burning wood (Fullerton et al. 2009). Malawi borders Mozambique and is similar to Mozambique in that cooking is typically done outdoors during the dry season and indoors during the wet season. Exposure levels are likely to be lower than kitchen concentrations because during the course of the day, individuals spend time near the stove indoors, but also outdoors where ambient concentrations are lower. For example, one study from Laos found that the ratio of personal exposure levels to kitchen concentrations was 0.33 at baseline and 0.69 with an intervention stove (Hill et al. 2015). With little information to go on, we select a baseline exposure level for both urban and rural areas of 150 g/m3, slightly higher than the one urban charcoal data point from Ghana and slightly less than half the kitchen concentration measurement in rural homes in Malawi. This pre-intervention exposure level may also be roughly consistent with the Ellegrd (1996) PM7 personal exposure measurements during cooking time when converting to 24 hr exposures, assuming all PM7 particles are $PM_{2.5}$ or smaller and that woodfuel household exposures in Mozambique are similar to woodfuel household exposures in rural areas. Since ambient $PM_{2.5}$ levels are considered to be relatively low across Mozambique (values range from approximately 4 g/m3 to 17-18 g/m3 (Figure 4.3), extremely high values during 3 hours of cooking time averaged with ambient $PM_{2.5}$ levels for the remainder of the day result in substantially lower daily exposure estimates. Our pre-intervention exposure estimate are roughly consistent with Ellegard (1996) if urban ambient $PM_{2.5}$ levels are higher than those in Figure 4.3 and may be high if urban concentrations are consistent with those in Figure 4.3. Using what may be a relatively low value for baseline exposure levels in both rural and urban areas means that our results for estimated benefits of clean cooking interventions may be conservative. As additional information on exposure levels in Mozambique and other countries in the same region become available, household air pollution health impacts can be re-estimated using the normalized results in Section 3.2.3.

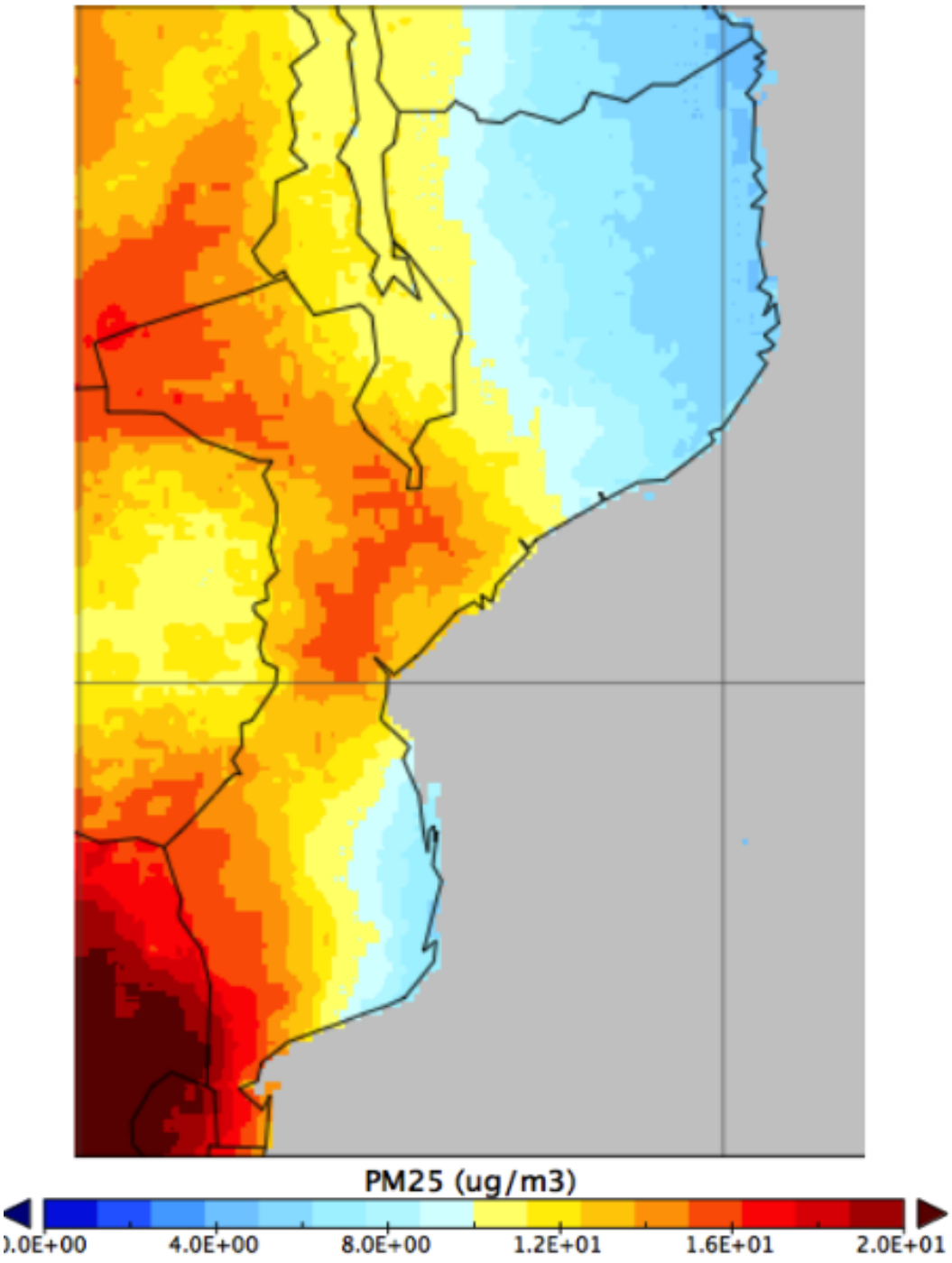

Figure 4.3: Satellite-derived $PM_{2.5}$ concentrations used for ambient $PM_{2.5}$ exposure, from van Donkelaar et al. (2016).

4.3.1 Rural natural draft (RND)

4.3.1.1 Description

The Rural Natural Draft (RND) scenario consists of expanding the use of natural draft stoves burning unprocessed wood and other biomass in rural areas. Natural draft stoves burn more efficiently than three-stone fires and have the advantage of being relatively cheap. They also have no moving parts, and therefore lower risk of breaking or malfunction. Natural draft stoves are typically classified as IWA Tier 1 stoves for indoor $PM_{2.5}$ emissions, with lower emissions than three-stone fires, but higher emissions than more advanced stoves burning unprocessed biomass (e.g. forced draft stoves), and stoves using cleaner burning processed solid fuels (e.g. biomass pellets) or modern fuels (e.g. LPG). An example of a natural draft stove used in Mozambique is the Envirofit Econofire stove (Figure 4.4). We examine the implementation of this scenario in 10% and 40% each of all rural households nationwide and in four provinces: Sofala, Manica, Inhambane, and Gaza. As the number of households is similar between 10% of all rural households and 40% of households in these four provinces, we are able to compare the benefits resulting from achieving a higher percentage penetration in a smaller area versus a lower level of penetration across the entire country. As this scenario does not include a fuel switch, we assume a relatively high rate of adoption of the new technology (0.7).

Laboratory-based measurements have shown that Tier 1 stoves reduce indoor $PM_{2.5}$ emissions by approximately 44% (Jetter et al. 2012). We use this value to scale down ambient emissions for our quantification of ambient air quality health impacts and climate impacts. For household air pollution, we assume that exposure levels are only reduced by 80% as much, or a total of 35% exposure reduction. To analyse cost-effectiveness according to the WHO-CHOICE framework described earlier, we use a stove cost of $13 (personal communication, Rosario Loayza, GIZ, May 18, 2016). A slightly higher cost of was given by Envirofit upon request. We assume fuel costs are minimal as wood is collected and not purchased. We assume there is some maintenance cost, and therefore set the annual cost per household to $2.5. These values are used to estimate the USD() per DALY averted, which we

Figure 4.4: Envirofit Econofire stove (source: Envirofit).

then compare to a GDP per capita of 586.$Where$/DALY averted is less than GDP per-capita, the scenario is considered very cost-effective. Where $/DALY averted is between 1-3x GDP per-capita, the scenario is considered cost-effective. Any scenario in which$/DALY averted is greater than 3x GDP per-capita is considered not cost-effective.

4.3.1.2 Potential benefits/cost-effectiveness

Estimated health and climate benefits of the two rural scenarios are shown in Table 16. We estimate that the rural natural draft stove scenario would avert 200 premature deaths and 14,000 DALYs over the 3-year project lifetime from reduced household air pollution if 10% of rural households nationwide received the cleaner stove. Benefits are four times higher if penetration reached 40% of all rural households in Mozambique. An estimated 5 and 20 annual premature deaths globally would be averted from reduced ambient air pollution for the 10% and 40% penetration levels, respectively. Approximately 37% of the ambient air quality health benefits occur within Mozambique. In terms of climate change, we estimate that the introduction of clean cookstoves would result in a net global cooling in 2050 of 16 and 63 μK respectively for the 10% and 40% penetration level. The cooling impact increases (more climate beneficial) to 28 and 113 μK in the year 2100 due to the increasing effects of GHGs as is shown in Figure 4.5.

For implementation of this scenario in Sofala, Manica, Inhambane, and Gaza provinces only, 10% and 40% penetration levels, respectively, are associated with 50 and 200 premature deaths averted from reduced household air pollution over the 3-year project lifetime and 2 and 8 annual premature deaths averted from reduced ambient air pollution. Approximately 34% of the ambient air quality health benefits occur within Mozambique. The resulting global surface temperature cooling in 2050 from the cookstove intervention at the 10% penetration level is 3 μK and 13 μK at the 40% penetration level in these provinces. The magnitude of the cooling impact again increases for this intervention, to 6 and 26 in 2100 for the 10% and 40% penetration levels, respectively. A slight climate dis-benefit can be seen in the several years following the cookstove intervention scenario implemented in these four provinces, due to the high sensitivity of radiative forcing in

the model gridcells overlaying these provinces with respect to organic carbon emissions. Organic carbon reflects solar radiation and its reduction leads to atmospheric warming, countering cooling effects of reduced black carbon. The dis-benefit is minor and short-lived, as we estimate that the temperature impact trend rapidly turns to cooling and reaches larger and larger cooling magnitudes over the course of the century.

To determine whether benefits are higher for higher penetration levels in smaller geographical areas versus lower penetration levels in larger geographical areas, we compare the 40% penetration level in the four provinces to the 10% penetration level nationwide, which have the same number of households. Health benefits resulting from household air pollution are identical for both cases because the HAPIT model and the underlying inputs for exposures, baseline incidence rates, and others do not differentiate between households located in one area versus another. Contrastingly, the health and climate benefits of reduced ambient air pollution depend on where the emissions are reduced. For 40% penetration in the four provinces compared to 10% penetration nationwide, we find 60% larger ambient air pollution-related health benefits (8 deaths averted versus 5) but 20% and 10% lower climate benefits in 2050 and 2100, respectively (less cooling). Concentrating cleaner stoves in smaller areas results in greater improvements in ambient air quality for that area, whereas dispersing the same number of stoves across a wider area has less of an impact on ambient air quality. Ambient air quality improvements lead to health benefits across a broader population beyond the households receiving the cleaner stove. Climate benefits are larger for the nationwide 10% penetration case versus 40% penetration in the four provinces because OC emissions from gridcells overlaying these four provinces are particularly influential on global radiative forcing. Concentrating the stove intervention in these four provinces therefore results in more warming from OC reductions counterbalancing the cooling from BC reductions, leading to less net climate cooling. While the magnitude of the cooling is less than for nationwide distribution of the cleaner stoves, both cases lead to cooling. In terms of cost-effectiveness, we find that the rural natural draft scenario costs approximately 471 USD per DALY averted (HAPIT result=531 USD, divided by 1.125 to covert from 4 people per household to 4.5), not including ambient air pollution-related

Table 4.7: Estimated health and climate benefits of the rural scenarios. Results are rounded and therefore may not match reported ratios of benefits between scenarios.

Scenario	Rural Natural Draft (RND)				Rural Forced Draft (RFD)			
	Nationwide		4 provinces		Nationwide		4 provinces	
	10%	40%	10%	40%	10%	40%	10%	40%
Household air pollution								
# HHs	300,000	1,200,000	80,000	300,000	300,000	1,200,000	80,000	300,000
Ambient air pollution								
Global deaths averted (annual)	5	20	2	8	10	40	4	20
Temperature								
2050 Global Impact (μK)	-16 (10 to -43)	-63 (41 to -168)	-3 (2 to -8)	-13 (9 to -35)	-29 (19 to -77)	-115 (75 to -307)	-6 (4 to -16)	-23 (15 to -61)
2100 Global Impact (μK)	-28 (6 to -56)	-113 (24 to -226)	-6 (1 to -12)	-26 (6 to -52)	-52 (11 to -104)	-206 (44 to -412)	-12 (3 to -24)	-47 (10 to -94)

health benefits. This scenario is very cost-effective, as it is less than GDP per capita of 586 USD. These cost-effectiveness results do not account for time saved collecting fuel.

4.3.2 Rural forced draft (RFD)

4.3.2.1 Description

The Rural Forced Draft (RFD) scenario mirrors the RND scenario, but uses more efficient forced draft stoves that burn unprocessed biomass. Forced draft stoves have a mechanism such as a fan that blows air into the combustion chamber and improves combustion efficiency. Many forced draft stoves require electricity to operate, but some models have been developed that include the ability to harness energy from the fire to recharge a battery and power the combustion chamber fan. One such model is the BioLite HomeStove (Figure 16), which is being used in a randomized controlled trial in Ghana (Jack et al. 2015). Forced draft stoves have been demonstrated to reduce $PM_{2.5}$ emissions substantially in laboratory settings, yielding approximately 80% reductions (Jetter et al. 2012), and are typically considered Tier 3 stoves for indoor $PM_{2.5}$ emissions. Emission reductions are typically less robust in field settings. However, field studies have also found that

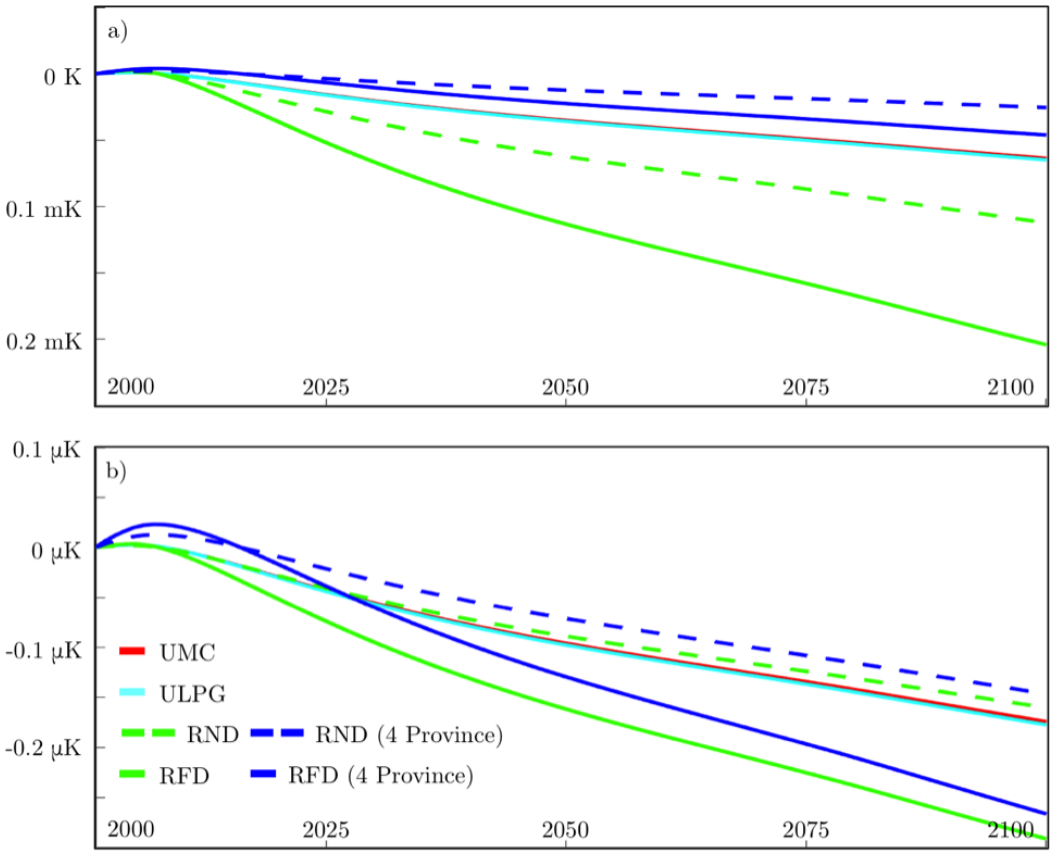

Figure 4.5: Central estimate of the transient climate impact of each cookstove intervention scenario shown as the (a) net impact on global surface temperature, and (b) the global surface temperature response for 5000 cookstove replacements. All impacts are shown at the 40% penetration level; a 10% penetration would reduce the impact by a factor of 4.

forced draft stoves can also achieve substantial emission reductions in the field (Kar et al. 2012, Johnson et al. 2011). We multiply the laboratory based percentage emission reduction by a factor of 0.8 to convert to more realistic exposure changes, for a total of 64% exposure reduction. As for the RND scenario, this scenario does not include a fuel switch, and we assume a relatively high rate of adoption of the new technology (0.7). As this may be high, we also report results using 0.6 adoption rate as a sensitivity. Forced draft stoves are feasible in rural areas of Mozambique because many are designed to use unprocessed biomass and many do not require electricity to run. Unlike natural draft stoves, forced draft stoves have moving parts, and therefore are more susceptible to maintenance issues. We examine the implementation of this scenario in 10% and 40% each of all rural households nationwide and in four provinces: Sofala, Manica, Inhambane, and Gaza. As for the RND scenario, these percentages allow us to compare the benefits resulting from achieving a higher percentage penetration in a smaller area versus a lower level of penetration across the entire country.

Figure 16. BioLite HomeStove forced draft stove (source: Siemens-Stiftung)

Figure 4.6: BioLite HomeStove forced draft stove (source: Siemens-Stiftung).

As we are unaware of forced draft stoves being implemented in Mozambique currently, we use

the cost of the BioLite Home Stove in Ghana of $55 per stove. Costs may be lower given the relatively low cost of natural d
metric used for cost-effectiveness. In other words, our use of the more expensive $55 per forced draft stove is likely to yi
effectiveness, and using a lower value would mean that this scenario is more cost-effective. We use the same assumpt

4.3.2.2 Potential benefits/cost-effectiveness

Health and climate benefits of the rural forced draft scenario are shown in Table 16. We estimate that the rural forced draft stove scenario would avert 500 premature deaths and 38,000 DALYs over the 3-year project lifetime from reduced household air pollution if 10% of rural households nationwide received the cleaner stove. These results are over 2.5 times larger than the results for the rural natural draft scenario. Benefits are four times higher if penetration reached 40% of all rural households in Mozambique. Household air pollution health benefits for the RFD scenario would be reduced by approximately 13% if a lower usage rate of 0.6 is used instead of 0.7, which may be warranted since forced draft stoves are more of a departure from traditional stoves compared with natural draft stoves. An estimated 10 and 40 annual premature deaths globally would also be averted from reduced ambient air pollution for the 10% and 40% penetration levels, respectively. Approximately 37% of the ambient air quality health benefits occur within Mozambique. The ambient air pollution health results are double those estimated for the rural natural draft scenario. In terms of climate change, we estimate that the introduction of clean cookstoves would result in a net global cooling in 2050 of 29 and 115 μK respectively for the 10% and 40% penetration level. The cooling impact increases (larger climate benefits) to 52 and 206 μK in the year 2100 due to the increasing effects of GHGs as is shown in Figure 14.Cooling benefits are approximately double those estimated for the rural natural draft scenario for the same penetration level.

For implementation of this scenario in Sofala, Manica, Inhambane, and Gaza provinces only, 10% and 40% penetration levels are associated with 100 and 500 premature deaths averted from reduced household air pollution over the 3-year project lifetime and 4 and 20 annual premature deaths globally averted from reduced ambient air pollution. Approximately 34% of the ambient air quality health benefits occur within Mozambique. The resulting global surface temperature cooling

in 2050 from the cookstove intervention at the 10% penetration level is 6 and 23 μK at the 40% penetration level in these provinces. The magnitude of the cooling impact again increases for this intervention, to 12 and 47 μK in 2100 for the 10% and 40% penetration levels, respectively. As for the rural natural draft stove scenario, slight climate disbenefits can be seen in the several years following the cookstove intervention scenario implemented in these four provinces, due to the high sensitivity of global radiative forcing to OC emissions in the gridcells overlaying these provinces. The disbenefit is minor and short-lived, as we estimate that the temperature impact trend rapidly turns to cooling and reaches larger and larger cooling magnitudes over the course of the century.

As for the rural natural draft scenario, concentrating the stove intervention in the four provinces rather than dispersing the cleaner stoves nationwide leads to greater ambient air pollution-related health benefits but less climate benefits. However, all cases lead to climate benefits in both 2050 and 2100.

In terms of cost-effectiveness, we find that the rural forced draft scenario costs approximately 497USD per DALY averted (HAPIT result=559USD, divided by 1.125 to covert from 4 people per household to 4.5), not including the ambient air pollution-related health benefits. As for the rural natural draft scenario, this scenario is very cost-effective, as it is less than GDP per capita of 586USD. The USD/DALY value may be overestimated because it is based on what may be a high value for the cost per stove (USD55). These cost-effectiveness values do not account for time saved collecting fuel.

4.3.3 Urban modern charcoal (UMC)

4.3.3.1 Description

The Urban Modern Charcoal (UMC) scenario consists of expanding the use of cleaner charcoal-burning stoves in urban areas in Mozambique. Compared to the typical metal charcoal stove currently used in most cities in Mozambique, modern charcoal stoves burn charcoal more efficiently and substantially reduce emissions. For example, the Envirofit Econochar stove (Figure 17) has

been rated as a Tier 3 stove for indoor $PM_{2.5}$ emissions. Approximately 5,300 Envirofit Econochar charcoal stoves have been disemminated by EnDev in one year, with successful experiences recorded in Maputo, Inhambane, Xai-Xai, Beira, and Pemba (personal communication, Rosario Loayza, May 6, 2016). Since modern charcoal stoves do not require a fuel switch, they may be more likely to be adopted and displace the traditional charcoal stoves. As charcoal is cheap relative to the cleaner fuel LPG, this option also keeps fuel expenditures low, and in fact lowers current charcoal expenditures by reducing the amount of fuel needed to accomplish the same cooking tasks. We examine the implementation of this scenario in 10% and 40% of households in five major cities in Mozambique: Maputo, Beira, Nampula, Tete, and Pemba. As for the RND and RFD scenario, this scenario does not include a fuel switch, and we assume a relatively high rate of adoption of the new technology (0.7).

Figure 4.7: Envirofit Econochar stove (source: Envirofit).

As stoves rated Tier 3 for indoor $PM_{2.5}$ emissions reduce emissions by approximately 80% we use this value to scale down residential emissions in urban areas for quantifying ambient air pollution health benefits and climate benefits. For household air pollution exposure, we scale the 80% emission reduction by a factor of 0.8 to extrapolate from laboratory-based emissions to field exposures (64% exposure reduction). To analyze cost-effectiveness, we use a cost of 15USD per

stove, in line with previous sale price of the Envirofit Econochar stove in Mozambique in recent years (personal communication, Rosario Loayza, GIZ, May 18, 2016). A slightly higher cost of 19.81USD was given by Envirofit upon request. This scenario reduces the amount of charcoal fuel used and therefore household expenditures on fuel, so we set fuel cost for the intervention to 2.5USD to account only for maintenance, consistent with the RND and RFD scenario maintenance costs.

4.3.3.2 Potential benefits/cost-effectiveness

Health and climate benefits of the urban scenarios are shown in Table 17. We estimate that the urban modern charcoal stove scenario would avert 100 premature deaths and 9,000 DALYs over the 3-year project lifetime from reduced household air pollution if 10% of households in the five cities received the cleaner stove. Benefits are four times higher if penetration reached 40% of households (we use rounded numbers of households, approximating the percentage penetration levels, and results are therefore slightly less than four times higher). An estimated 6 and 20 annual premature deaths globally would also be averted from reduced ambient $PM_{2.5}$ for the 10% and 40% penetration levels. Approximately 41% of the ambient air quality health benefits occur within Mozambique. In terms of climate change, we estimate that the introduction of clean cookstoves would result in a net global cooling in 2050 of 9 and 36 μK respectively for the 10% and 40% penetration level. The cooling impact increases (larger climate benefits) to 16 and 64 μK in the year 2100 due to the increasing effects of GHGs as is shown in Figure 14. In terms of cost-effectiveness, we find that the urban modern charcoal stove scenario costs approximately 185USD per DALY averted (HAPIT result=208USD, divided by 1.125 to convert from 4 people per household to 4.5), not including ambient air pollution-related health benefits. As the USD/DALY result is less than GDP per capita (586USD), this scenario is very cost-effective. Intervention costs here do not include program and monitoring and evaluation costs. This scenario is estimated to remain very cost-effective as long as total intervention (stove cost plus program and monitoring and evaluation costs) are below approximately 60USD per stove.

Table 4.8: Estimated health and climate benefits of the urban scenarios. Results are rounded and therefore may not match reported ratios of benefits between scenarios.

Scenario	Urban Modern Charcoal (UMC)		Urban LPG (ULPG)	
	10%	40%	10%	40%
Household air pollution				
# HHs	70,000	275,000	70,000	275,000
Ambient air pollution				
Global deaths averted (annual)	6	23	6	23
Temperature				
2050 Global Impact (μK)	-9 (6 to -24)	-36 (24 to -96)	-9 (6 to -24)	-36 (24 to -96)
2100 Global Temperature Impact (μK)	-16 (10 to -43)	-64 (42 to -171)	-16 (10 to -43)	-65 (43 to -174)

4.3.4 Urban LPG (ULPG)

4.3.4.1 Description

The Urban LPG scenario consists of expanding the use of LPG in place of charcoal in urban areas. Compared with solid fuels, LPG burns much more efficiently and cleanly, reducing indoor $PM_{2.5}$ emissions by approximately 95%. As for the other scenarios, we scale this percentage by a factor of 0.8 to convert to realistic exposure reductions, for a total of a 76% exposure reduction. LPG stoves are considered Tier 4 stoves for indoor $PM_{2.5}$ emissions. An example of an LPG stove that would be appropriate for Mozambique is the Envirofit Pureflame stove (Figure 18). Since this scenario includes a fuel switch from charcoal to LPG, we assume a lower rate of household adoption of the new stove (0.6) relative to the other three scenarios which do not include a fuel switch (0.7). As for the UMC scenario, we examine the implementation of this scenario in 10% and 40% of households in five major cities in Mozambique: Maputo, Beira, Nampula, Tete, and Pemba.

Monthly LPG expenditures ranged from 159USD in Beira to 158USD in Maputo/Matola and 165USD in Nampula. Since this scenario includes a shift from charcoal to LPG, we subtract monthly charcoal costs from monthly LPG costs to derive a fuel cost for each city. These values are 99USD for Nampula, 22USD for Beira, and -30USD for Maputo. The negative value for Maputo results from higher baseline annual expenditures for charcoal versus LPG. We add 5USD to these values to account for maintenance costs, and set the negative value indicating cost savings for Maputo to zero within HAPIT to be able to calculate USD/DALY.

4.3.4.2 Potential benefits/cost-effectiveness

Health and climate benefits of the urban scenarios are shown in Table 17. We estimate that the urban LPG stove scenario would avert 200 premature deaths and 11,000 DALYs over the 3-year project lifetime from reduced household air pollution if 10% of households in the five cities received the cleaner stove. Benefits are four times higher if penetration reached 40% of all rural households in Mozambique (we use rounded numbers of households, approximating the percentage penetration

Figure 4.8: Envirofit Pureflame LPG stove (source: Envirofit)

levels, and results are therefore slightly less than four times higher). These results would be 16% higher if a usage rate of 0.7 was used, as for the other three scenarios. An estimated 6 and 20 annual premature deaths globally would also be averted from reduced ambient air pollution for the 10% and 40% penetration levels, respectively, the same as for the urban modern charcoal scenario. Approximately 41% of the ambient air quality health benefits occur within Mozambique. In terms of climate change, we estimate that the introduction of clean cookstoves would result in a net global cooling in 2050 of 9 and 36 μK respectively for the 10% and 40% penetration level, slightly more climate beneficial compared with the urban modern charcoal scenario. The cooling impact increases (larger climate benefits) to 16 and 65 μK in the year 2100 due to the increasing effects of GHGs as is shown in Figure 14. In terms of cost-effectiveness, we find that the urban LPG stove scenario costs approximately $125 in Maputo, 634 USD in Beira, and 2080$ in Nampula. The difference between the cities is due to the highly variable household expenditures on charcoal, which is offset by the switch to LPG. In Maputo, this scenario leads to a cost savings since baseline household expenditures are higher for charcoal versus LPG. Using the WHO-CHOICE cost-effectiveness framework, this scenario is very cost-effective in Maputo, cost-effective in Beira, and not cost-effective in Nampula. We have not included intervention costs (e.g. program cost and monitoring and evaluation cost) other than stove costs. Total intervention cost per stove would need to be approximately 200USD for Beira and 275USD for Maputo before the urban LPG scenario in these cities stops being cost effective.

4.4 Conclusion

4.4.1 Health and climate benefits of the scenarios

We used state-of-the-science air pollution health and climate impact models to estimate the air pollution-related health and climate benefits of four scenarios in which clean cooking programs are implemented in rural and urban areas of Mozambique. This study demonstrates that substantial health and climate co-benefits can result from expanding the use of cleaner wood and charcoal

or LPG stoves in Mozambique. For rural areas, forced draft wood-burning stoves are estimated to be very cost-effective and achieve over 2.5 times more health benefits compared to natural draft stoves in the same households, assuming equal usage rates. Reaching a level of 10% penetration across rural households in Mozambique is estimated to avoid approximately 200 premature deaths and 14,000 DALYs for a 3-year intervention from reduced household air pollution. The same level of penetration of 10% of households in the four Provinces Sofala, Manica, Inhambane, and Gaza, can avoid an estimated 50 premature deaths and 3,700 DALYs from household air pollution. Approximately 2-3% additional health benefits are estimated to result from reduced ambient air pollution. While natural draft stoves achieve fewer health benefits compared with forced draft stoves, they are also very cost-effective. Both natural draft and forced draft stoves reduce expected climate change-related temperature increases over short- and long-term time periods. Larger ambient air quality health benefits can be achieved by concentrating the same number of intervention stoves in a smaller geographical area, though the household air quality health benefits, which are the dominant contributor to total health benefits, would be the same for both cases. For urban areas, advanced charcoal stoves would achieve approximately 80% of the health benefits of LPG stoves and are estimated to be very cost-effective. LPG stoves are estimated to be very cost-effective in Maputo where charcoal is relatively expensive, cost-effective in Beira, and not cost-effective in Nampula, where charcoal is relatively cheap. Expanding use of LPG stoves to 10% of households in five major cities, Maputo, Beira, Nampula, Tete, and Pemba, would result in an estimated 200 premature deaths and 11,000 DALYs averted for a 3-year intervention. The same penetration level of modern charcoal stoves in these five cities would result in an estimated 100 premature deaths and 9,000 DALYs averted. Approximately 2-3% additional health benefits are estimated to result from reduced ambient air pollution. Both urban scenarios would be climate beneficial in both the short-term and long-term.

Estimated health benefits from reduced household air pollution and ambient air pollution are based on different methods and are therefore not directly additive. The health impacts of household air pollution are inclusive of child acute lower respiratory infections and chronic disease incidence

for all ages, while ambient air pollution health impacts are calculated for the chronic diseases for the population age 30 years and older only. HAPIT, the model used to quantify household air pollution health benefits, applies an approach in which health benefits from reduced exposure are distributed over a 20 year period, and results are calculated for each year of the project until the end of the user-specified project lifetime, after which attenuated health benefits accrue for two additional years. HAPIT also assumes that for the three year project lifetime assumed here, the total number of stoves within the intervention are distributed equally over each year of the project (i.e. 1/3 of stoves distributed in each of the three years). The ambient air pollution health benefits assume all stoves are distributed at the start of the project, are not distributed over time, and are calculated as an annual benefit estimate. For these reasons, the health benefits from reduced household and ambient air pollution are not necessarily additive. However, they may be close to comparable because HAPITs cumulative benefits of 1/3 stove deployment over three years may be similar to 1-year benefits of 100% stove deployment at the start of the intervention, the assumption made for the ambient health benefit calculations.

Each step of the analysis carries uncertainties, particularly given that in many cases there is a lack of data specific to conditions in Mozambique. This section describes uncertainties in both data inputs and methods used to translate the input information to impacts, and considers several important limitations to the analysis. It is unknown whether these uncertainties lead our results to be underestimates or overestimates. The models used here to estimate health and climate impacts require input information about baseline and intervention emission and exposure levels. Very little information exists that is specific to Mozambique, or even nearby countries in Eastern Africa. Information about baseline and intervention emissions is important to calculate ambient air quality and resulting health and climate impacts. This analysis drew information about emissions from laboratory studies of various traditional and improved cooking stoves, matching the stove models examined in the scenarios here to PM2.5 emission reductions expected for similar stoves, as categorized by IWA stove tiers. Laboratory studies often do not indicate levels of emission reductions that would be achieved in the field, and field measurements in Mozambique were not

available. There was also a lack of information about potential usage rates for different technology types and the degree to which stacking (use of the new technology alongside the old technology) would occur. Both of these variables would influence post-intervention exposure levels.

Similarly, no field measurements in Mozambique of baseline PM2.5 exposure levels or exposure levels in homes using cleaner and more efficient cookstoves were available. We therefore used information from studies in other African countries to derive conservative baseline exposure levels. For intervention exposure levels, we started with the emission reductions from laboratory-based studies expected for each type of stove and used slightly lower percentage reductions since exposure is typically not reduced as much as emissions. Both baseline and intervention exposure levels applied here could be higher or lower in reality. Using the default methods built into the HAPIT tool, we assume that all adults in the household have the same exposure levels, though exposure levels for non-cook adults are likely to be lower than for the cook, who spends more time near the stove. For children, HAPIT adjusts exposure levels based on mother to child ratios of carbon monoxide exposures from a study in Guatemala. It is unlikely that these ratios would be applicable to Mozambique given differences in household characteristics, cultural norms, and cooking practices. As field measurements of emissions and exposure levels become available, the normalized results presented here can be used to recalculate benefits. The impact assessment models used to translate input information to health and climate impacts also carry with them some uncertainties. We apply exposure-response curves that draw from studies on ambient air pollution, second-hand smoke, and cigarette smoking in addition to household air pollution. These relationships assume that all PM2.5 mixtures have the same effects on human health, though the mixture of pollution varies significantly between emission sectors, and within the residential sector between stove and fuel types (e.g., Jetter et al. 2012, Anenberg et al. 2013). We assume disease incidence rates estimated by IHME apply, but in reality these are uncertain due to data limitations (e.g. accurate coding of cause of death, accounting for all pneumonia cases, etc.). We also do not consider subnational variability in disease incidence rates, number of people per household, exposure levels, or any other factor affecting susceptibility to household air pollution health effects. We also limit the analysis only to

PM2.5, the dominant contributor to the global health impacts of air pollution, but other pollutants may also contribute to household air pollution health impacts, such as carbon monoxide, volatile organic compounds, and others (e.g. Guarnieri et al. 2014, Pope et al. 2015). Climate impacts of short-lived climate pollutants are also highly uncertain due to limited data on the ratio of black carbon and organic carbon emitted from different stove types and fuels, the degree to which emissions of each are reduced from the baseline for different intervention stoves, and their influence on the climate system (e.g. Anenberg et al. 2013, Bond et al. 2013, Soneja et al. 2016, Wang et al. 2016).

For the cost-effectiveness calculations, consistent with Pillarisetti et al. (2015), we do not include dissemination or monitoring and evaluation costs, the household costs associated with reduced medical expenditures, and time spent collecting fuel. For the urban LPG scenario, we assume that fuel costs beyond baseline expenditures on charcoal are covered by the program. Including additional costs would lower our USD/DALY values used for cost-effectiveness determinations, while considering time spent collecting fuel and other health, environmental, and social benefits would make the scenarios more cost-effective.

As described in Section 3.4, several important impacts were excluded from this analysis due to lack of data that precluded quantification. Reducing charcoal production could slow forest degradation and deforestation in Mozambique, preserving ecosystems, habitats, and biodiversity. The health impact assessment considered only five diseases (ischemic heart disease, stroke, chronic obstructive pulmonary disease, lung cancer, and child acute lower respiratory infection), but household air pollution is likely to impact other health outcomes, such as premature birth, low birth weight, ocular disorders, and burns. Not enough information about the connection between household air pollution and these health outcomes was available to enable their inclusion in the quantified analysis. In addition, reduced household fuel needs is likely to have economic and social benefits, as it would lead to lower household expenses and more time available (particularly for women) to pursue other activities such as education, income-generating activities, and leisure.

4.5 Future analyses

This analysis is intended to be a first-order approximation of the level of health and climate benefits that could be achieved through implementing different types of clean cooking programs in Mozambique. To enable more specific analysis for conditions in Mozambique, more information is needed, particularly related to emission and exposure levels. More specific scenarios for policies and stove dissemination methods can also be developed by engaging further with the Mozambique government and other stakeholders. This type of analysis can also be undertaken for other countries and additional scenarios. Future analyses should utilize emerging measurements of emissions and exposure levels for the baseline and intervention scenarios examined here. Ideally, these measurements would be taken in the field in Mozambique using normal cooking practices. Exposure levels should be measured both in the wet and dry seasons, for both the baseline and intervention scenarios, to determine different exposure levels for outdoor versus indoor cooking. Field measurements taken in nearby countries may also be helpful to estimate emissions and exposure levels in Mozambique, considering similarities and differences in cultural norms and cooking practices. Household surveys in both rural and urban areas would also be helpful in understanding typical cooking practices, activity patterns, and exposure from other pollution sources, such as smoking, trash burning, and industrial plants. Such improved information specific to Mozambique would reduce uncertainties associated with this type of analysis. As new information on exposure levels becomes available, the normalized results presented here can be used to re-estimate benefits and improve program design for potential clean cooking interventions. This type of analysis can also be undertaken for other situations, in other countries or examining additional scenarios, to highlight the air pollution-related health and climate benefits that could be achieved through cleaner cooking programs. The methods used here can be applied in any country to generate screening-level approximations of the benefits of various types of clean cookstove programs. Higher confidence in results is possible for analysis in countries where more specific information exists on emission and exposure levels.

4.6 Methods: Annex 2

Detailed explanations of the methods for quantifying ambient air pollution health impacts and climate change impacts are soon to be submitted for peer-reviewed publication. This annex briefly summarizes key methods and data inputs. Both the ambient air quality health impacts and the climate impacts are calculated using different versions of the GEOS-Chem adjoint model. GEOS-Chem is a chemical transport model that runs at the global scale of 2 by 2.5 degrees (Bey et al., 2001). This model is run using historical anthropogenic emissions (Lamarque et al., 2010) and natural emissions including lightning NOX (Murray et al., 2012), soil emissions (Hudman et al., 2012) and biogenic emissions (Guenther et al., 2012). The model also included aerosol chemical processes such as; heterogeneous chemistry (Evans and Jacob, 2005) phase partitioning (Binkowski and Roselle, 2003), formation rate feedbacks (Martin et al., 2003), hygroscopic growth (Martin et al., 2003) among other transport and deposition processes driven by the Goddard Earth Observing System (GEOS5) offline calculated meteorological fields.

The adjoint of the GEOS-Chem model is also used to estimate species and spatial variant impacts of emissions on the model output (Henze et al., 2007). The adjoint model uses estimated model sensitivities to calculate a model output perturbation, which is then propagated backward through the model in order to calculate the partial derivative of model output with respect to all model inputs, taking into account the various chemical and physical model processes. For small perturbations, these partial derivatives can be estimates of the change in model output with respect to grid-cell changes in emissions.

Ambient PM2.5 health impacts are calculated using a modified version of the base model fully described in Lee et al. (2015). This model uses the modeled aerosol mass concentrations at the model resolution of 2 by 2.5 degrees and uses satellite biasing and satellite downscaling to estimate human exposure at the 0.1 by 0.1 degree resolution. In order to do this satellite data from van Donkelaar et al (2016) is used. These sub-grid scale PM2.5 mass concentrations are then compared to disease specific integrated exposure response (Burnett et al., 2014) curves in

conjunction with country level baseline mortality rates (Lozano et al., 2012) in order to estimate the premature deaths due to concentration of ambient PM2.5. The adjoint model then takes the predicted deaths and calculates spatial and species variant sensitivities of premature deaths with respect to aerosol and aerosol precursor emissions. This calculation is done at both the global scale and for Mozambique alone to give the contribution of emissions to deaths within Mozambique and globally.

The climate impacts are calculated following Lacey and Henze (2015), which uses the GEOS-Chem adjoint model to calculate the direct radiative forcing and then uses scaling factors and climate parameterizations to in turn estimate the global surface temperature response. The adjoint sensitivities are calculated by combining the GEOS-Chem aerosol mass concentrations with the LIDORT radiative transfer model and offline Mie calculations to get speciated aerosol direct radiative forcing sensitivities. The direct radiative forcing is then scaled to include indirect and semi-direct effects following the methods used in the UNEP/WMO (2011) report on short-lived climate forcers to give the net effective radiative forcing impacts. This work expands on the prior studies by also including estimation of RF impacts from greenhouse gases in addition to aerosol RF. This is done by using concentration impulse response functions with radiative forcing efficiencies (Aamaas et al., 2013; Joos et al., 2013) to estimate the net radiative forcing for a given year following future RCP 4.5 emissions (Smith and Wigley, 2006). This radiative forcing is combined with the transient SLCF forcing and a transient global mean sensitivity calculation (Boucher and Reddy, 2008) to estimate the radiative forcing as a function of time from the emissions perturbation. These radiative forcing values are then combined with absolute regional temperature potentials (Shindell and Faluvegi, 2009; Shindell ,2012) to estimate the surface temperature response as detailed in Lacey and Henze (2015).

Chapter 5

Conclusions

The work presented here includes development of new methods for using adjoint sensitivities in the GEOS-Chem model, which are then applied to a range of science questions. We have shown that the methods developed can be used for global impacts studies (Chapter 2 and Chapter 3), where estimated impacts from a global removal of solid fuel cooking emissions results in the avoidance of 22.5 (11.9 to 23.2) million premature deaths through the 21st century and a climate impact of 118 mK cooling (11 mK to 335 mK cooling) by the year 2100. These estimates are calculated as transient functions following future emissions from the Representative Concentration Pathways (RCP) [73, 104] and future national-scale population trends. These estimates include aerosol indirect and semi-direct climate impacts and utilize the latest available satellite $PM_{2.5}$ datasets [18, 116] for human exposure estimates as an input into integrated exposure response functions [19]. In order to provide improved information to policy makers, the use of adjoint sensitivity analysis enables us to dis-aggregate the global impacts to national-scale contributions, which allows for targeting specific countries with clean cookstove and fuel-switching implementation projects. This highlights areas where there are discrepancies between the amount of solid fuel used and the resulting impacts, as is shown in Figure 3.5. We have also shown that the approach developed can be used to estimate impacts of a range of specific mitigation scenarios at the national scale, in this case Mozambique (Chapter 4). The estimated impacts from solid fuel cookstove use in Mozambique are 277 annual premature deaths and a warming of 0.69 mK (cooling of 0.48 mK to warming of 1.76 mK) due to ambient $PM_{2.5}$ concentrations.

This work treats a more comprehensive set of climate-relevant processes than previous studies wut hthe GEOS-Chem adjoint model [39], particularly in terms of short lived species. Since the GEOS-Chem model, combined with LIDORT, calculates only the aerosol direct radiative forcing, scaling factors derived from the IPCC model estimates of radiative forcing are used to treat aerosol indirect and semi-direct effects [17, 75]. These scaling factors are important since they apply to not only the central estimate of aerosol climate impacts, but also perturb the upper and lower bounds of the estimated impacts, in turn leading to a range of estimates that does not preclude climate dis-benefits from removal of carbonaceous aerosol emissions from cookstove solid fuel use in some countries [55]. In addition to the variability in aerosol radiative efficiency, we have also treated the fact that aerosols are short-lived and do not impact global radiative forcing in the same manner as greenhouse gases. This is done by calculating the impacts of emissions on radiative forcing within a latitude band and utilizing the varied impacts of regional radiative forcing on surface temperature response following the absolute regional temperature potentials from Shindell et al., 2009 [98] and Shindell, 2012 [96]. This method is novel since it allows for the estimation of surface temperature response, taking into account the regional impacts of aerosol transport, formation, and radiative efficiency, without the additional steps and computational requirements of running a fully-coupled chemistry climate model. In order to estimate net climate impacts, including both short-lived climate forcers and well-mixed greenhouse gases (GHG), we have combined the transient aerosol radiative forcing with the transient GHG impacts following Joos et al., 2013 [48] and Aamaas et al., 2013 [1] by calculating the future concentrations of GHGs from an impulse in emissions, then estimating the difference in radiative forcing from a baseline to this perturbed state. The net RF in a given year then uses the transient global mean climate sensitivity derived from Boucher et al., 2013 [16] to estimate the surface temperature response from a change in emissions. The combination of all of these effects results in a novel and efficient approach to calculating the net bounded climate impacts as a function of time from a given change in sectoral emissions of aerosols, aerosol precursors, and GHGs.

We have also used adjoint sensitivities to estimate the transient health impacts from a change

in sectoral emissions. Expanding on prior work from Lee et al., 2015 [58], we have separated the use of satellite data for downscaling to exposure relevant scales from the use of satellite data for both downscaling and bias correction to estimate annual average concentrations. This is important since future concentrations of $PM_{2.5}$ will be different in overall magnitude and should not be tied to present day levels. We have also used two of the most recently available satellite datasets [18, 116] in order to further bound our estimates of premature deaths from changes in ambient $PM_{2.5}$ concentrations. Transient health estimates also take into account future population following estimates from the 2010 United Nations World Population Prospects . This yields improved estimates of premature deaths from ambient $PM_{2.5}$, especially in regions that are projected to experience large shifts in population over the next several decades (i.e., regions of Africa that see a projected 300% population growth). This is an important factor that must be accounted for when proposing regional emissions mitigation strategies that take a number of years to be fully realized.

While this work takes into account a number of parameters that are not commonly included in global climate and health models, there are additional sources of error and uncertainty that may need to be accounted for in future work. For the estimate of impacts from solid fuel use for cooking, we have here created an emissions inventory based on available information, but other studies have shown that the emissions from cookstoves is both regional and uncertain with emissions varying based on stove type, fuel use, and cooking method [44, 45, 87, 120]. Therefore, improved emissions factors would aid in increasing the accuracy of these modeled impacts from solid fuel use. Another source of uncertainty is the parameterization used to treat the central estimate of impacts from secondary organic aerosol (SOA) as 18% of the total OC impact for solid fuel use. This is based on the emissions of non-methane volatile organic compounds (VOC) and proposed 50% formation rate of SOA from these species [108]. Recently. there have been a number of advances in not only the characterization of VOCs from solid fuel combustion [34], but also the formation mechanisms of SOA [37, 46, 79] that should be accounted for when estimating the SOA impacts on climate and health. The work done here also found a large discrepancy in the estimated number

https://esa.un.org/unpd/wpp/

of global premature deaths depending on which satellite reanalysis product is used for the satellite downscaling and exposure estimation. According to personal communication with Michael Brauer, there is a new satellite product being released in late-2016 that will improve on the current datasets. This new dataset should be used for estimation of future health impact sensitivities. This work also uses scaling factor parameterizations to estimate the indirect aerosol climate effects, which cannot accurately capture some of the regional impacts of aerosol emissions on the formation and lifetime of clouds shown in prior work [49, 90, 52]. Also, while the focus of this work has been on ambient health impacts, the indoor air quality impacts far outweigh these impacts in some areas with low population density and relatively clean ambient air, so the use of indoor health impacts models such as HAPIT [82] would be a useful addition towards understanding the net impacts of cookstove interventions. The inclusion of each of these different aspects in future work will serve to improve the model estimates of both surface temperature change and premature deaths from ambient $PM_{2.5}$.

Understanding impacts of ambient aerosol concentrations on climate and health is currently a focus of policy-makers worldwide. The latest GBD report on global death statistics [31] has shown that the number of premature deaths from ambient concentrations is starting to outweigh the deaths due to indoor air quality. Also, a number of studies have highlighted SLCFs as the target pathway for reducing the global anthropogenic impacts on climate by the end of the century [27, 99, 114]. The work presented throughout this thesis show an improvement in the level of understanding of both climate and health impacts from ambient aerosol concentrations, and more importantly provides policy makers with information on the net impacts of a change in anthropogenic activity. While the detailed impacts focus on the removal of solid fuel use for cooking, the scope of these calculated adjoint sensitivities is not limited to this sector and are also being used for analysis of other sectors and species including diesel transportation emissions. By utilizing the tools and models developed here we can quickly provide accurate and policy-relevant information regarding the impacts of a wide range of proposed mitigation scenarios.

Bibliography

[1] B. Aamaas, G. P. Peters, and J. S. Fuglestvedt. Simple emission metrics for climate impacts. Earth Syst. Dynam., 4(1):145–170, June 2013.

[2] Heather Adair-Rohani, Jessica Lewis, Johnathan Mingle, Sophie Gumy, Maria Neira, Carlos Dora, Vera Brinkman, Nigel Bruce, Marie-Noel Brune Drisse, Ariel Charney, Joy Clancy, Dan Dorner, Rachael Freeth, Carsten Hellpap, Marlis Kees, Vanesse Lopes Janik, Helen Patech, Marit Viktoria Pettersen, Annette Prüss-Ustün, Elisa Puzzolo, Jennifer Rasanathan, Ivan Vera, Joanna Vogel, Adrian Whiteman, Blake Zachary, and Tony Zhang. Burning Opportunity: Clean Household Energy for Health, Sustainable Development, and Wellbeing of Women and Children. Technical report, World Health Organization, Geneva, Switzerland, February 2016.

[3] Susan C. Anenberg, Kalpana Balakrishnan, James Jetter, Omar Masera, Sumi Mehta, Jacob Moss, and Veerabhadran Ramanathan. Cleaner Cooking Solutions to Achieve Health, Climate, and Economic Cobenefits. Environmental Science & Technology, 47(9):3944–3952, May 2013.

[4] Susan C Anenberg, Larry W Horowitz, Daniel Q Tong, and J Jason West. An estimate of the global burden of anthropogenic ozone and fine particulate matter on premature human mortality using atmospheric modeling. Environ Health Perspect, 118(9):1189–1195, Sep 2010.

[5] Robert Bailis, Rudi Drigo, Adrian Ghilardi, and Omar Masera. The carbon footprint of traditional woodfuels. Nature Climate Change, 5(3):266–272, March 2015.

[6] Susanne E. Bauer and Surabi Menon. Aerosol direct, indirect, semidirect, and surface albedo effects from sector contributions based on the IPCC AR5 emissions for preindustrial and present-day conditions. Journal of Geophysical Research: Atmospheres, 117(D1):D01206, January 2012.

[7] Isabelle Bey, Daniel J. Jacob, Robert M. Yantosca, Jennifer A. Logan, Brendan D. Field, Arlene M. Fiore, Qinbin Li, Honguy Y. Liu, Loretta J. Mickley, and Martin G. Schultz. Global modeling of tropospheric chemistry with assimilated meteorology: Model description and evaluation. Journal of Geophysical Research, 106(D19):PP. 23,073–23,095, 2001.

[8] S. C. Bhattacharya, D. O. Albina, and P. Abdul Salam. Emission factors of wood and charcoal-fired cookstoves. Biomass and Bioenergy, 23(6):453–469, 2002.

[9] Francis S. Binkowski and Shawn J. Roselle. Models-3 Community Multiscale Air Quality (CMAQ) model aerosol component 1. Model description. Journal of Geophysical Research: Atmospheres, 108(D6):4183, March 2003.

[10] M. A. Bollasina, Y. Ming, and V. Ramaswamy. Anthropogenic Aerosols and the Weakening of the South Asian Summer Monsoon. Science, 334(6055):502–505, September 2011.

[11] T. C. Bond, S. J. Doherty, D. W. Fahey, P. M. Forster, T. Berntsen, B. J. DeAngelo, M. G. Flanner, S. Ghan, B. Kärcher, D. Koch, S. Kinne, Y. Kondo, P. K. Quinn, M. C. Sarofim, M. G. Schultz, M. Schulz, C. Venkataraman, H. Zhang, S. Zhang, N. Bellouin, S. K. Guttikunda, P. K. Hopke, M. Z. Jacobson, J. W. Kaiser, Z. Klimont, U. Lohmann, J. P. Schwarz, D. Shindell, T. Storelvmo, S. G. Warren, and C. S. Zender. Bounding the role of black carbon in the climate system: A scientific assessment. Journal of Geophysical Research: Atmospheres, 118(11):5380–5552, June 2013.

[12] Tami Bond, Chandra Venkataraman, and Omar Masera. Global atmospheric impacts of residential fuels. Energy for Sustainable Development, 8(3):20–32, September 2004.

[13] Tami C. Bond and Robert W. Bergstrom. Light absorption by carbonaceous particles: An investigative review. Aerosol Science and Technology, 40(1):27–67, January 2006.

[14] Tami C. Bond, Ekta Bhardwaj, Rong Dong, Rahil Jogani, Soonkyu Jung, Christoph Roden, David G. Streets, and Nina M. Trautmann. Historical emissions of black and organic carbon aerosol from energy-related combustion, 1850-2000: HISTORICAL BC/OC EMISSIONS. Global Biogeochemical Cycles, 21(2):n/a–n/a, June 2007.

[15] Sophie Bonjour, Heather Adair-Rohani, Jennyfer Wolf, Nigel G. Bruce, Sumi Mehta, Annette Prüss-Ustün, Maureen Lahiff, Eva A. Rehfuess, Vinod Mishra, and Kirk R. Smith. Solid fuel use for household cooking: Country and regional estimates for 1980–2010. Environmental Health Perspectives, 121(7):784–790, May 2013.

[16] O. Boucher and M. S. Reddy. Climate trade-off between black carbon and carbon dioxide emissions. Energy Policy, 36(1):193–200, January 2008.

[17] Olivier Boucher, David Randall, Paulo Artaxo, Christopher Bretherton, Graham Feingold, Piers Forster, Veli-Matti Kerminen, Yutaka Kondo, Hong Liao, Ulrike Lohmann, Philip Rasch, S.K. Satheesh, Steven Sherwood, Bjorn Stevens, and Xiao-Ye Zhang. Clouds and aerosols. In Climate Change 2013: The Physical Science Basis. Contribution of Working Group I to the Fifth Assessment Report of the Intergovernmental Panel on Climate Change. Cambridge University Press, 2013.

[18] Michael Brauer, Greg Freedman, Joseph Frostad, Aaron van Donkelaar, Randall V. Martin, Frank Dentener, Rita van Dingenen, Kara Estep, Heresh Amini, Joshua S. Apte, Kalpana Balakrishnan, Lars Barregard, David Broday, Valery Feigin, Santu Ghosh, Philip K. Hopke, Luke D. Knibbs, Yoshihiro Kokubo, Yang Liu, Stefan Ma, Lidia Morawska, José Luis Texcalac Sangrador, Gavin Shaddick, H. Ross Anderson, Theo Vos, Mohammad H. Forouzanfar, Richard T. Burnett, and Aaron Cohen. Ambient Air Pollution Exposure Estimation for the Global Burden of Disease 2013. Environmental Science & Technology, 50(1):79–88, January 2015.

[19] Richard T. Burnett, C. Arden Pope, III, Majid Ezzati, Casey Olives, Stephen S. Lim, Sumi Mehta, Hwashin H. Shin, Gitanjali Singh, Bryan Hubbell, Michael Brauer, H Ross Anderson, Kirk R. Smith, John R. Balmes, Nigel G. Bruce, Haidong Kan, Francine Laden, Annette Prüss-Ustün, Michelle C. Turner, Susan M. Gapstur, W. Ryan Diver, and Aaron Cohen. An Integrated Risk Function for Estimating the Global Burden of Disease Attributable to Ambient Fine Particulate Matter Exposure. Environmental Health Perspectives, February 2014.

[20] E. W. Butt, A. Rap, A. Schmidt, C. E. Scott, K. J. Pringle, C. L. Reddington, N. A. D. Richards, M. T. Woodhouse, J. Ramirez-Villegas, H. Yang, V. Vakkari, E. A. Stone, M. Rupakheti, P. S. Praveen, P. G. van Zyl, J. P. Beukes, M. Josipovic, E. J. S. Mitchell, S. M. Sallu, P. M. Forster, and D. V. Spracklen. The impact of residential combustion emissions on atmospheric aerosol, human health and climate. Atmos. Chem. Phys. Discuss., 15(14):20449–20520, July 2015.

[21] Zoë A. Chafe, Michael Brauer, Zbigniew Klimont, Rita Van Dingenen, Sumi Mehta, Shilpa Rao, Keywan Riahi, Frank Dentener, and Kirk R. Smith. Household cooking with solid fuels contributes to ambient PM2.5 air pollution and the burden of disease. Environmental Health Perspectives, September 2014.

[22] W.-T. Chen, Y. H. Lee, P. J. Adams, A. Nenes, and J. H. Seinfeld. Will black carbon mitigation dampen aerosol indirect forcing?: BLACK CARBON MITIGATION. Geophysical Research Letters, 37(9):n/a–n/a, May 2010.

[23] Mian Chin, Paul Ginoux, Stefan Kinne, Omar Torres, Brent N. Holben, Bryan N. Duncan, Randall V. Martin, Jennifer A. Logan, Akiko Higurashi, and Teruyuki Nakajima. Tropospheric Aerosol Optical Thickness from the GOCART Model and Comparisons with Satellite and Sun Photometer Measurements. Journal of the Atmospheric Sciences, 59(3):461–483, February 2002.

[24] C. E. Chung, V. Ramanathan, and D. Decremer. Observationally constrained estimates of carbonaceous aerosol radiative forcing. Proceedings of the National Academy of Sciences, 109(29):11624–11629, July 2012.

[25] Serena H. Chung and John H. Seinfeld. Global distribution and climate forcing of carbonaceous aerosols. Journal of Geophysical Research: Atmospheres, 107(D19):4407, October 2002.

[26] W.F. Cooke, C. Jiousse, H. Cachier, and J. Feichter. Construction of a 1 ° x 1 ° fossil fuel emission data set for carbonaceous aerosol and implementation and radiative impact in the ECHAM-4 model. Journal of Geophysical Research, 104(D18):22,137–22162, September 1999.

[27] Department of State. The climate and clean air coalition to reduce short-lived climate pollutants, February 2012. The Climate and Clean Air Coalition to Reduce Short-Lived Climate Pollutants.

[28] M. J. Evans and D. J. Jacob. Impact of new laboratory studies of N2o5 hydrolysis on global model budgets of tropospheric nitrogen oxides, ozone, and OH. Geophysical Research Letters, 32(9):L09813, May 2005.

[29] Suneeta D. Fernandes, Nina M. Trautmann, David G. Streets, Christoph A. Roden, and Tami C. Bond. Global biofuel use, 1850–2000. Global Biogeochemical Cycles, 21(2):GB2019, June 2007.

[30] Center for International Earth Science Information Network CIESIN Columbia University, United Nations Food, Agriculture Programme FAO, and Centro Internacional de Agricultura Tropical CIAT. Gridded population of the world, version 3 (gpwv3): Population count grid, future estimates. 20160329 2005.

[31] Mohammad H Forouzanfar, Lily Alexander, H Ross Anderson, Victoria F Bachman, Stan Biryukov, Michael Brauer, Richard Burnett, Daniel Casey, Matthew M Coates, Aaron Cohen, Kristen Delwiche, Kara Estep, Joseph J Frostad, Astha Kc, Hmwe H Kyu, Maziar Moradi-Lakeh, Marie Ng, Erica Leigh Slepak, Bernadette A Thomas, Joseph Wagner, Gunn Marit Aasvang, Cristiana Abbafati, Ayse Abbasoglu Ozgoren, Foad Abd-Allah, Semaw F Abera, Victor Aboyans, Biju Abraham, Jerry Puthenpurakal Abraham, Ibrahim Abubakar, Niveen M E Abu-Rmeileh, Tania C Aburto, Tom Achoki, Ademola Adelekan, Koranteng Adofo, Arsène K Adou, José C Adsuar, Ashkan Afshin, Emilie E Agardh, Mazin J Al Khabouri, Faris H Al Lami, Sayed Saidul Alam, Deena Alasfoor, Mohammed I Albittar, Miguel A Alegretti, Alicia V Aleman, Zewdie A Alemu, Rafael Alfonso-Cristancho, Samia Alhabib, Raghib Ali, Mohammed K Ali, François Alla, Peter Allebeck, Peter J Allen, Ubai Alsharif, Elena Alvarez, Nelson Alvis-Guzman, Adansi A Amankwaa, Azmeraw T Amare, Emmanuel A Ameh, Omid Ameli, Heresh Amini, Walid Ammar, Benjamin O Anderson, Carl Abelardo T Antonio, Palwasha Anwari, Solveig Argeseanu Cunningham, Johan Arnlöv, Valentina S Arsic Arsenijevic, Al Artaman, Rana J Asghar, Reza Assadi, Lydia S Atkins, Charles Atkinson, Marco A Avila, Baffour Awuah, Alaa Badawi, Maria C Bahit, Talal Bakfalouni, Kalpana Balakrishnan, Shivanthi Balalla, Ravi Kumar Balu, Amitava Banerjee, Ryan M Barber, Suzanne L Barker-Collo, Simon Barquera, Lars Barregard, Lope H Barrero, Tonatiuh Barrientos-Gutierrez, Ana C Basto-Abreu, Arindam Basu, Sanjay Basu, Mohammed O Basulaiman, Carolina Batis Ruvalcaba, Justin Beardsley, Neeraj Bedi, Tolesa Bekele, Michelle L Bell, Corina Benjet, Derrick A Bennett, Habib Benzian, Eduardo Bernabé, Tariku J Beyene, Neeraj Bhala, Ashish Bhalla, Zulfiqar A Bhutta, Boris Bikbov, Aref A Bin Abdulhak, Jed D Blore, Fiona M Blyth, Megan A Bohensky, Berrak Bora Başara, Guilherme Borges, Natan M Bornstein, Dipan Bose, Soufiane Boufous, Rupert R Bourne, Michael Brainin, Alexandra Brazinova, Nicholas J Breitborde, Hermann Brenner, Adam D M Briggs, David M Broday, Peter M Brooks, Nigel G Bruce, Traolach S Brugha, Bert Brunekreef, Rachelle Buchbinder, Linh N Bui, Gene Bukhman, Andrew G Bulloch, Michael Burch, Peter G J Burney, Ismael R Campos-Nonato, Julio C Campuzano, Alejandra J Cantoral, Jack Caravanos, Rosario Cárdenas, Elisabeth Cardis, David O Carpenter, Valeria Caso, Carlos A Castañeda-Orjuela, Ruben E Castro, Ferrán Catalá-López, Fiorella Cavalleri, Alanur Çavlin, Vineet K Chadha, Jung-chen Chang, Fiona J Charlson, Honglei Chen, Wanqing Chen, Zhengming Chen, Peggy P Chiang, Odgerel Chimed-Ochir, Rajiv Chowdhury, Costas A Christophi, Ting-Wu Chuang, Sumeet S Chugh, Massimo Cirillo, Thomas KD Claßen, Valentina Colistro, Mercedes Colomar, Samantha M Colquhoun, Alejandra G Contreras, Cyrus Cooper, Kimberly Cooperrider, Leslie T Cooper, Josef Coresh, Karen J Courville, Michael H Criqui, Lucia Cuevas-Nasu, James Damsere-Derry, Hadi Danawi, Lalit Dandona, Rakhi Dandona, Paul I Dargan, Adrian Davis, Dragos V Davitoiu, Anand Dayama, E Filipa de Castro, Vanessa De la Cruz-Góngora, Diego De Leo, Graça de Lima, Louisa Degenhardt, Borja del Pozo-Cruz, Robert P Dellavalle, Kebede Deribe, Sarah Derrett, Don C Des Jarlais, Muluken Dessalegn, Gabrielle A deVeber, Karen M De-

vries, Samath D Dharmaratne, Mukesh K Dherani, Daniel Dicker, Eric L Ding, Klara Dokova, E Ray Dorsey, Tim R Driscoll, Leilei Duan, Adnan M Durrani, Beth E Ebel, Richard G Ellenbogen, Yousef M Elshrek, Matthias Endres, Sergey P Ermakov, Holly E Erskine, Babak Eshrati, Alireza Esteghamati, Saman Fahimi, Emerito Jose A Faraon, Farshad Farzadfar, Derek F J Fay, Valery L Feigin, Andrea B Feigl, Seyed-Mohammad Fereshtehnejad, Alize J Ferrari, Cleusa P Ferri, Abraham D Flaxman, Thomas D Fleming, Nataliya Foigt, Kyle J Foreman, Urbano Fra Paleo, Richard C Franklin, Belinda Gabbe, Lynne Gaffikin, Emmanuela Gakidou, Amiran Gamkrelidze, Fortuné G Gankpé, Ron T Gansevoort, Francisco A García-Guerra, Evariste Gasana, Johanna M Geleijnse, Bradford D Gessner, Pete Gething, Katherine B Gibney, Richard F Gillum, Ibrahim A M Ginawi, Maurice Giroud, Giorgia Giussani, Shifalika Goenka, Ketevan Goginashvili, Hector Gomez Dantes, Philimon Gona, Teresita Gonzalez de Cosio, Dinorah González-Castell, Carolyn C Gotay, Atsushi Goto, Hebe N Gouda, Richard L Guerrant, Harish C Gugnani, Francis Guillemin, David Gunnell, Rahul Gupta, Rajeev Gupta, Reyna A Gutiérrez, Nima Hafezi-Nejad, Holly Hagan, Maria Hagstromer, Yara A Halasa, Randah R Hamadeh, Mouhanad Hammami, Graeme J Hankey, Yuantao Hao, Hilda L Harb, Tilahun Nigatu Haregu, Josep Maria Haro, Rasmus Havmoeller, Simon I Hay, Mohammad T Hedayati, Ileana B Heredia-Pi, Lucia Hernandez, Kyle R Heuton, Pouria Heydarpour, Martha Hijar, Hans W Hoek, Howard J Hoffman, John C Hornberger, H Dean Hosgood, Damian G Hoy, Mohamed Hsairi, Guoqing Hu, Howard Hu, Cheng Huang, John J Huang, Bryan J Hubbell, Laetitia Huiart, Abdullatif Husseini, Marissa L Iannarone, Kim M Iburg, Bulat T Idrisov, Nayu Ikeda, Kaire Innos, Manami Inoue, Farhad Islami, Samaya Ismayilova, Kathryn H Jacobsen, Henrica A Jansen, Deborah L Jarvis, Simerjot K Jassal, Alejandra Jauregui, Sudha Jayaraman, Panniyammakal Jeemon, Paul N Jensen, Vivekanand Jha, Fan Jiang, Guohong Jiang, Ying Jiang, Jost B Jonas, Knud Juel, Haidong Kan, Sidibe S Kany Roseline, Nadim E Karam, André Karch, Corine K Karema, Ganesan Karthikeyan, Anil Kaul, Norito Kawakami, Dhruv S Kazi, Andrew H Kemp, Andre P Kengne, Andre Keren, Yousef S Khader, Shams Eldin Ali Hassan Khalifa, Ejaz A Khan, Young-Ho Khang, Shahab Khatibzadeh, Irma Khonelidze, Christian Kieling, Daniel Kim, Sungroul Kim, Yunjin Kim, Ruth W Kimokoti, Yohannes Kinfu, Jonas M Kinge, Brett M Kissela, Miia Kivipelto, Luke D Knibbs, Ann Kristin Knudsen, Yoshihiro Kokubo, M Rifat Kose, Soewarta Kosen, Alexander Kraemer, Michael Kravchenko, Sanjay Krishnaswami, Hans Kromhout, Tiffany Ku, Barthelemy Kuate Defo, Burcu Kucuk Bicer, Ernst J Kuipers, Chanda Kulkarni, Veena S Kulkarni, G Anil Kumar, Gene F Kwan, Taavi Lai, Arjun Lakshmana Balaji, Ratilal Lalloo, Tea Lallukka, Hilton Lam, Qing Lan, Van C Lansingh, Heidi J Larson, Anders Larsson, Dennis O Laryea, Pablo M Lavados, Alicia E Lawrynowicz, Janet L Leasher, Jong-Tae Lee, James Leigh, Ricky Leung, Miriam Levi, Yichong Li, Yongmei Li, Juan Liang, Xiaofeng Liang, Stephen S Lim, M Patrice Lindsay, Steven E Lipshultz, Shiwei Liu, Yang Liu, Belinda K Lloyd, Giancarlo Logroscino, Stephanie J London, Nancy Lopez, Joannie Lortet-Tieulent, Paulo A Lotufo, Rafael Lozano, Raimundas Lunevicius, Jixiang Ma, Stefan Ma, Vasco M P Machado, Michael F MacIntyre, Carlos Magis-Rodriguez, Abbas A Mahdi, Marek Majdan, Reza Malekzadeh, Srikanth Mangalam, Christopher C Mapoma, Marape Marape, Wagner Marcenes, David J Margolis, Christopher Margono, Guy B Marks, Randall V Martin, Melvin B Marzan, Mohammad T Mashal, Felix Masiye, Amanda J Mason-Jones, Kunihiro Matsushita, Richard Matzopoulos, Bongani M Mayosi, Tasara T Mazorodze, Abigail C McKay, Martin McKee, Abigail McLain, Peter A Meaney, Catalina Medina, Man Mohan Mehndiratta, Fabiola Mejia-Rodriguez, Wubegzier Mekonnen, Yohannes A Melaku, Michele Meltzer, Ziad A Memish, Walter Mendoza, George A Mensah, Atte Meretoja, Francis Apoli-

nary Mhimbira, Renata Micha, Ted R Miller, Edward J Mills, Awoke Misganaw, Santosh Mishra, Norlinah Mohamed Ibrahim, Karzan A Mohammad, Ali H Mokdad, Glen L Mola, Lorenzo Monasta, Julio C Montañez Hernandez, Marcella Montico, Ami R Moore, Lidia Morawska, Rintaro Mori, Joanna Moschandreas, Wilkister N Moturi, Dariush Mozaffarian, Ulrich O Mueller, Mitsuru Mukaigawara, Erin C Mullany, Kinnari S Murthy, Mohsen Naghavi, Ziad Nahas, Aliya Naheed, Kovin S Naidoo, Luigi Naldi, Devina Nand, Vinay Nangia, KM Venkat Narayan, Denis Nash, Bruce Neal, Chakib Nejjari, Sudan P Neupane, Charles R Newton, Frida N Ngalesoni, Jean de Dieu Ngirabega, Grant Nguyen, Nhung T Nguyen, Mark J Nieuwenhuijsen, Muhammad I Nisar, José R Nogueira, Joan M Nolla, Sandra Nolte, Ole F Norheim, Rosana E Norman, Bo Norrving, Luke Nyakarahuka, In-Hwan Oh, Takayoshi Ohkubo, Bolajoko O Olusanya, Saad B Omer, John Nelson Opio, Ricardo Orozco, Rodolfo S Pagcatipunan, Amanda W Pain, Jeyaraj D Pandian, Carlo Irwin A Panelo, Christina Papachristou, Eun-Kee Park, Charles D Parry, Angel J Paternina Caicedo, Scott B Patten, Vinod K Paul, Boris I Pavlin, Neil Pearce, Lilia S Pedraza, Andrea Pedroza, Ljiljana Pejin Stokic, Ayfer Pekericli, David M Pereira, Rogelio Perez-Padilla, Fernando Perez-Ruiz, Norberto Perico, Samuel A L Perry, Aslam Pervaiz, Konrad Pesudovs, Carrie B Peterson, Max Petzold, Michael R Phillips, Hwee Pin Phua, Dietrich Plass, Dan Poenaru, Guilherme V Polanczyk, Suzanne Polinder, Constance D Pond, C Arden Pope, Daniel Pope, Svetlana Popova, Farshad Pourmalek, John Powles, Dorairaj Prabhakaran, Noela M Prasad, Dima M Qato, Amado D Quezada, D Alex A Quistberg, Lionel Racapé, Anwar Rafay, Kazem Rahimi, Vafa Rahimi-Movaghar, Sajjad Ur Rahman, Murugesan Raju, Ivo Rakovac, Saleem M Rana, Mayuree Rao, Homie Razavi, K Srinath Reddy, Amany H Refaat, Jürgen Rehm, Giuseppe Remuzzi, Antonio L Ribeiro, Patricia M Riccio, Lee Richardson, Anne Riederer, Margaret Robinson, Anna Roca, Alina Rodriguez, David Rojas-Rueda, Isabelle Romieu, Luca Ronfani, Robin Room, Nobhojit Roy, George M Ruhago, Lesley Rushton, Nsanzimana Sabin, Ralph L Sacco, Sukanta Saha, Ramesh Sahathevan, Mohammad Ali Sahraian, Joshua A Salomon, Deborah Salvo, Uchechukwu K Sampson, Juan R Sanabria, Luz Maria Sanchez, Tania G Sánchez-Pimienta, Lidia Sanchez-Riera, Logan Sandar, Itamar S Santos, Amir Sapkota, Maheswar Satpathy, James E Saunders, Monika Sawhney, Mete I Saylan, Peter Scarborough, Jürgen C Schmidt, Ione J C Schneider, Ben Schöttker, David C Schwebel, James G Scott, Soraya Seedat, Sadaf G Sepanlou, Berrin Serdar, Edson E Servan-Mori, Gavin Shaddick, Saeid Shahraz, Teresa Shamah Levy, Siyi Shangguan, Jun She, Sara Sheikhbahaei, Kenji Shibuya, Hwashin H Shin, Yukito Shinohara, Rahman Shiri, Kawkab Shishani, Ivy Shiue, Inga D Sigfusdottir, Donald H Silberberg, Edgar P Simard, Shireen Sindi, Abhishek Singh, Gitanjali M Singh, Jasvinder A Singh, Vegard Skirbekk, Karen Sliwa, Michael Soljak, Samir Soneji, Kjetil Søreide, Sergey Soshnikov, Luciano A Sposato, Chandrashekhar T Sreeramareddy, Nicolas J C Stapelberg, Vasiliki Stathopoulou, Nadine Steckling, Dan J Stein, Murray B Stein, Natalie Stephens, Heidi Stöckl, Kurt Straif, Konstantinos Stroumpoulis, Lela Sturua, Bruno F Sunguya, Soumya Swaminathan, Mamta Swaroop, Bryan L Sykes, Karen M Tabb, Ken Takahashi, Roberto T Talongwa, Nikhil Tandon, David Tanne, Marcel Tanner, Mohammad Tavakkoli, Braden J Te Ao, Carolina M Teixeira, Martha M Téllez Rojo, Abdullah S Terkawi, José Luis Texcalac-Sangrador, Sarah V Thackway, Blake Thomson, Andrew L Thorne-Lyman, Amanda G Thrift, George D Thurston, Taavi Tillmann, Myriam Tobollik, Marcello Tonelli, Fotis Topouzis, Jeffrey A Towbin, Hideaki Toyoshima, Jefferson Traebert, Bach X Tran, Leonardo Trasande, Matias Trillini, Ulises Trujillo, Zacharie Tsala Dimbuene, Miltiadis Tsilimbaris, Emin Murat Tuzcu, Uche S Uchendu, Kingsley N Ukwaja, Selen B Uzun, Steven van de Vijver, Rita Van Dingenen, Coen H van

Gool, Jim van Os, Yuri Y Varakin, Tommi J Vasankari, Ana Maria N Vasconcelos, Monica S Vavilala, Lennert J Veerman, Gustavo Velasquez-Melendez, N Venketasubramanian, Lakshmi Vijayakumar, Salvador Villalpando, Francesco S Violante, Vasiliy Victorovich Vlassov, Stein Emil Vollset, Gregory R Wagner, Stephen G Waller, Mitchell T Wallin, Xia Wan, Haidong Wang, JianLi Wang, Linhong Wang, Wenzhi Wang, Yanping Wang, Tati S Warouw, Charlotte H Watts, Scott Weichenthal, Elisabete Weiderpass, Robert G Weintraub, Andrea Werdecker, K Ryan Wessells, Ronny Westerman, Harvey A Whiteford, James D Wilkinson, Hywel C Williams, Thomas N Williams, Solomon M Woldeyohannes, Charles D A Wolfe, John Q Wong, Anthony D Woolf, Jonathan L Wright, Brittany Wurtz, Gelin Xu, Lijing L Yan, Gonghuan Yang, Yuichiro Yano, Pengpeng Ye, Muluken Yenesew, Gökalp K Yentür, Paul Yip, Naohiro Yonemoto, Seok-Jun Yoon, Mustafa Z Younis, Zourkaleini Younoussi, Chuanhua Yu, Maysaa E Zaki, Yong Zhao, Yingfeng Zheng, Maigeng Zhou, Jun Zhu, Shankuan Zhu, Xiaonong Zou, Joseph R Zunt, Alan D Lopez, Theo Vos, and Christopher J Murray. Global, regional, and national comparative risk assessment of 79 behavioural, environmental and occupational, and metabolic risks or clusters of risks in 188 countries, 1990–2013: a systematic analysis for the Global Burden of Disease Study 2013. The Lancet, 386(10010):2287–2323, December 2015.

[32] Olivia E. Freeman and Hisham Zerriffi. How You Count Carbon Matters: Implications of Differing Cookstove Carbon Credit Methodologies for Climate and Development Cobenefits. Environmental Science & Technology, 48(24):14112–14120, December 2014.

[33] J. Fuglestvedt, T. Berntsen, G. Myhre, K. Rypdal, and R. B Skeie. Climate forcing from the transport sectors. Proceedings of the National Academy of Sciences, 105(2):454, 2008.

[34] Andrew P. Grieshop, Julian D. Marshall, and Milind Kandlikar. Health and climate benefits of cookstove replacement options. Energy Policy, 39(12):7530–7542, December 2011.

[35] Andrew P. Grieshop, Conor CO Reynolds, Milind Kandlikar, and Hadi Dowlatabadi. A black-carbon mitigation wedge. Nature Geoscience, 2(8):533–534, 2009.

[36] A. B. Guenther, X. Jiang, C. L. Heald, T. Sakulyanontvittaya, T. Duhl, L. K. Emmons, and X. Wang. The model of emissions of gases and aerosols from nature version 2.1 (MEGAN2.1): an extended and updated framework for modeling biogenic emissions. Geoscientific Model Development, 5(6):1471–1492, November 2012.

[37] M. Hallquist, J. C. Wenger, U. Baltensperger, Y. Rudich, D. Simpson, M. Claeys, J. Dommen, N. M. Donahue, C. George, A. H. Goldstein, J. F. Hamilton, H. Herrmann, T. Hoffmann, Y. Iinuma, M. Jang, M. E. Jenkin, J. L. Jimenez, A. Kiendler-Scharr, W. Maenhaut, G. McFiggans, Th. F. Mentel, A. Monod, A. S. H. Prévôt, J. H. Seinfeld, J. D. Surratt, R. Szmigielski, and J. Wildt. The formation, properties and impact of secondary organic aerosol: current and emerging issues. Atmos. Chem. Phys., 9(14):5155–5236, July 2009.

[38] D. K. Henze, J. H. Seinfeld, N. L. Ng, J. H. Kroll, T.-M. Fu, D. J. Jacob, and C. L. Heald. Global modeling of secondary organic aerosol formation from aromatic hydrocarbons: high-vs. low-yield pathways. Atmos. Chem. Phys., 8(9):2405–2420, May 2008.

[39] D. K. Henze, D. T. Shindell, F. Akhtar, R. J. D. Spurr, R. W. Pinder, D. Loughlin, M. Kopacz, K. Singh, and C. Shim. Spatially refined aerosol direct radiative forcing efficiencies. Environmental Science & Technology, 2012.

[40] DK Henze and JH Seinfeld. Development of the adjoint of GEOS-Chem. Atmospheric Chemistry and Physics Discussions, 6(5):10591–10648, 2007.

[41] R. C. Hudman, N. E. Moore, A. K. Mebust, R. V. Martin, A. R. Russell, L. C. Valin, and R. C. Cohen. Steps towards a mechanistic model of global soil nitric oxide emissions: implementation and space based-constraints. Atmospheric Chemistry and Physics, 12(16):7779–7795, August 2012.

[42] D. J. Jacob, H. Lui, C. Mari, and R.M. Yantosca. Harvard wet deposition scheme for GMI. Technical report, February 2000.

[43] Mark Z. Jacobson. Strong radiative heating due to the mixing state of black carbon in atmospheric aerosols. Nature, 409(6821):695–697, February 2001.

[44] James Jetter, Yongxin Zhao, Kirk R. Smith, Bernine Khan, Tiffany Yelverton, Peter DeCarlo, and Michael D. Hays. Pollutant emissions and energy efficiency under controlled conditions for household biomass cookstoves and implications for metrics useful in setting international test standards. Environmental Science & Technology, 46(19):10827–10834, October 2012.

[45] James J. Jetter and Peter Kariher. Solid-fuel household cook stoves: Characterization of performance and emissions. Biomass and Bioenergy, 33(2):294–305, February 2009.

[46] J. L. Jimenez, M. R. Canagaratna, N. M. Donahue, A. S. H. Prevot, Q. Zhang, J. H. Kroll, P. F. DeCarlo, J. D. Allan, H. Coe, N. L. Ng, A. C. Aiken, K. S. Docherty, I. M. Ulbrich, A. P. Grieshop, A. L. Robinson, J. Duplissy, J. D. Smith, K. R. Wilson, V. A. Lanz, C. Hueglin, Y. L. Sun, J. Tian, A. Laaksonen, T. Raatikainen, J. Rautiainen, P. Vaattovaara, M. Ehn, M. Kulmala, J. M. Tomlinson, D. R. Collins, M. J. Cubison, E, J. Dunlea, J. A. Huffman, T. B. Onasch, M. R. Alfarra, P. I. Williams, K. Bower, Y. Kondo, J. Schneider, F. Drewnick, S. Borrmann, S. Weimer, K. Demerjian, D. Salcedo, L. Cottrell, R. Griffin, A. Takami, T. Miyoshi, S. Hatakeyama, A. Shimono, J. Y. Sun, Y. M. Zhang, K. Dzepina, J. R. Kimmel, D. Sueper, J. T. Jayne, S. C. Herndon, A. M. Trimborn, L. R. Williams, E. C. Wood, A. M. Middlebrook, C. E. Kolb, U. Baltensperger, and D. R. Worsnop. Evolution of Organic Aerosols in the Atmosphere. Science, 326(5959):1525–1529, December 2009.

[47] Michael Johnson, Rufus Edwards, Claudio Alatorre Frenk, and Omar Masera. In-field greenhouse gas emissions from cookstoves in rural mexican households. Atmospheric Environment, 42(6):1206 – 1222, 2008.

[48] F. Joos, R. Roth, J. S. Fuglestvedt, G. P. Peters, I. G. Enting, W. von Bloh, V. Brovkin, E. J. Burke, M. Eby, N. R. Edwards, T. Friedrich, T. L. Frölicher, P. R. Halloran, P. B. Holden, C. Jones, T. Kleinen, F. T. Mackenzie, K. Matsumoto, M. Meinshausen, G.-K. Plattner, A. Reisinger, J. Segschneider, G. Shaffer, M. Steinacher, K. Strassmann, K. Tanaka, A. Timmermann, and A. J. Weaver. Carbon dioxide and climate impulse response functions for the computation of greenhouse gas metrics: a multi-model analysis. Atmos. Chem. Phys., 13(5):2793–2825, March 2013.

[49] V. A. Karydis, S. L. Capps, R. H. Moore, A. G. Russell, D. K. Henze, and A. Nenes. Using a global aerosol model adjoint to unravel the footprint of spatially-distributed emissions on cloud droplet number and cloud albedo: EMISSIONS FOOTPRINT ON CLOUD PROPERTIES. Geophysical Research Letters, 39(24):n/a–n/a, December 2012.

[50] V. A. Karydis, S. L. Capps, A. G. Russell, and A. Nenes. Adjoint sensitivity of global cloud droplet number to aerosol and dynamical parameters. Atmospheric Chemistry and Physics, 12(19):9041–9055, October 2012.

[51] D. Koch and A. D. Del Genio. Black carbon semi-direct effects on cloud cover: review and synthesis. Atmos. Chem. Phys., 10(16):7685–7696, August 2010.

[52] J. K. Kodros, C. E. Scott, S. C. Farina, Y. H. Lee, C. L'Orange, J. Volckens, and J. R. Pierce. Uncertainties in global aerosols and climate effects due to biofuel emissions. Atmos. Chem. Phys. Discuss., 15(7):10199–10256, April 2015.

[53] R. B. A. Koelemeijer, J. F. de Haan, and P. Stammes. A database of spectral surface reflectivity in the range 335–772 nm derived from 5.5 years of GOME observations. Journal of Geophysical Research: Atmospheres, 108(D2):4070, January 2003.

[54] P. Koepke, M. (Muenchen Univ (Germany) Meteorologisches Inst) Hess, I. (Max-Planck-Institut fuer Meteorologie Schult, and E. P. (Naval Research Lab Shettle. Global aerosol data set, 1997.

[55] Forrest Lacey and Daven Henze. Global climate impacts of country-level primary carbonaceous aerosol from solid-fuel cookstove emissions. Environmental Research Letters, 10(11):114003, 2015.

[56] J.-F. Lamarque, T. C. Bond, V. Eyring, C. Granier, A. Heil, Z. Klimont, D. Lee, C. Liousse, A. Mieville, B. Owen, M. G. Schultz, D. Shindell, S. J. Smith, E. Stehfest, J. Van Aardenne, O. R. Cooper, M. Kainuma, N. Mahowald, J. R. McConnell, V. Naik, K. Riahi, and D. P. van Vuuren. Historical (1850–2000) gridded anthropogenic and biomass burning emissions of reactive gases and aerosols: methodology and application. Atmospheric Chemistry and Physics, 10(15):7017–7039, August 2010.

[57] Carrie M. Lee, Chelsea Chandler, Michael Lazarus, and Francis X. Johnson. Assessing the Climate Impacts of Cookstove Projects: Issues in Emissions Accounting. Technical Report 53-71, September 2013.

[58] Colin Lee, Randall Martin, Daven K. Henze, Michael Brauer, Aaron Cohen, and Aaron van Donkelaar. Response of global particulate-matter-related mortality to changes in local precursor emissions. Environmental Science & Technology, March 2015.

[59] J. Lelieveld, J. S. Evans, M. Fnais, D. Giannadaki, and A. Pozzer. The contribution of outdoor air pollution sources to premature mortality on a global scale. Nature, 525(7569):367–371, September 2015.

[60] Xinghua Li, Shuxiao Wang, Lei Duan, Jiming Hao, and Yongfeng Nie. Carbonaceous aerosol emissions from household biofuel combustion in china. Environmental Science & Technology, 43(15):6076–6081, August 2009.

[61] Ying Li, Daven K. Henze, Darby Jack, and Patrick L. Kinney. The influence of air quality model resolution on health impact assessment for fine particulate matter and its components. Air Quality, Atmosphere & Health, pages 1–18, February 2015.

[62] Stephen S Lim, Theo Vos, Abraham D Flaxman, Goodarz Danaei, Kenji Shibuya, Heather Adair-Rohani, Mohammad A AlMazroa, Markus Amann, H Ross Anderson, Kathryn G Andrews, Martin Aryee, Charles Atkinson, Loraine J Bacchus, Adil N Bahalim, Kalpana Balakrishnan, John Balmes, Suzanne Barker-Collo, Amanda Baxter, Michelle L Bell, Jed D Blore, Fiona Blyth, Carissa Bonner, Guilherme Borges, Rupert Bourne, Michel Boussinesq, Michael Brauer, Peter Brooks, Nigel G Bruce, Bert Brunekreef, Claire Bryan-Hancock, Chiara Bucello, Rachelle Buchbinder, Fiona Bull, Richard T Burnett, Tim E Byers, Bianca Calabria, Jonathan Carapetis, Emily Carnahan, Zoe Chafe, Fiona Charlson, Honglei Chen, Jian Shen Chen, Andrew Tai-Ann Cheng, Jennifer Christine Child, Aaron Cohen, K Ellicott Colson, Benjamin C Cowie, Sarah Darby, Susan Darling, Adrian Davis, Louisa Degenhardt, Frank Dentener, Don C Des Jarlais, Karen Devries, Mukesh Dherani, Eric L Ding, E Ray Dorsey, Tim Driscoll, Karen Edmond, Suad Eltahir Ali, Rebecca E Engell, Patricia J Erwin, Saman Fahimi, Gail Falder, Farshad Farzadfar, Alize Ferrari, Mariel M Finucane, Seth Flaxman, Francis Gerry R Fowkes, Greg Freedman, Michael K Freeman, Emmanuela Gakidou, Santu Ghosh, Edward Giovannucci, Gerhard Gmel, Kathryn Graham, Rebecca Grainger, Bridget Grant, David Gunnell, Hialy R Gutierrez, Wayne Hall, Hans W Hoek, Anthony Hogan, H Dean Hosgood, Damian Hoy, Howard Hu, Bryan J Hubbell, Sally J Hutchings, Sydney E Ibeanusi, Gemma L Jacklyn, Rashmi Jasrasaria, Jost B Jonas, Haidong Kan, John A Kanis, Nicholas Kassebaum, Norito Kawakami, Young-Ho Khang, Shahab Khatibzadeh, Jon-Paul Khoo, Cindy Kok, Francine Laden, Ratilal Lalloo, Qing Lan, Tim Lathlean, Janet L Leasher, James Leigh, Yang Li, John Kent Lin, Steven E Lipshultz, Stephanie London, Rafael Lozano, Yuan Lu, Joelle Mak, Reza Malekzadeh, Leslie Mallinger, Wagner Marcenes, Lyn March, Robin Marks, Randall Martin, Paul McGale, John McGrath, Sumi Mehta, Ziad A Memish, George A Mensah, Tony R Merriman, Renata Micha, Catherine Michaud, Vinod Mishra, Khayriyyah Mohd Hanafiah, Ali A Mokdad, Lidia Morawska, Dariush Mozaffarian, Tasha Murphy, Mohsen Naghavi, Bruce Neal, Paul K Nelson, Joan Miquel Nolla, Rosana Norman, Casey Olives, Saad B Omer, Jessica Orchard, Richard Osborne, Bart Ostro, Andrew Page, Kiran D Pandey, Charles DH Parry, Erin Passmore, Jayadeep Patra, Neil Pearce, Pamela M Pelizzari, Max Petzold, Michael R Phillips, Dan Pope, C Arden Pope, John Powles, Mayuree Rao, Homie Razavi, Eva A Rehfuess, Jürgen T Rehm, Beate Ritz, Frederick P Rivara, Thomas Roberts, Carolyn Robinson, Jose A Rodriguez-Portales, Isabelle Romieu, Robin Room, Lisa C Rosenfeld, Ananya Roy, Lesley Rushton, Joshua A Salomon, Uchechukwu Sampson, Lidia Sanchez-Riera, Ella Sanman, Amir Sapkota, Soraya Seedat, Peilin Shi, Kevin Shield, Rupak Shivakoti, Gitanjali M Singh, David A Sleet, Emma Smith, Kirk R Smith, Nicolas JC Stapelberg, Kyle Steenland, Heidi Stöckl, Lars Jacob Stovner, Kurt Straif, Lahn Straney, George D Thurston, Jimmy H Tran, Rita Van Dingenen, Aaron van Donkelaar, J Lennert Veerman, Lakshmi Vijayakumar, Robert Weintraub, Myrna M Weissman, Richard A White, Harvey Whiteford, Steven T Wiersma, James D Wilkinson, Hywel C Williams, Warwick Williams, Nicholas Wilson, Anthony D Woolf, Paul Yip, Jan M Zielinski, Alan D Lopez, Christopher JL Murray, and Majid Ezzati. A comparative risk assessment of burden of disease and injury attributable to 67 risk factors and risk factor clusters in 21 regions, 1990–2010: a systematic analysis for the Global Burden of Disease Study 2010. The Lancet, 380(9859):2224–2260, December 2012.

[63] Hongyu Y. Liu, Daniel Jacob, Isabelle Bey, and Robert M. Yantosca. Constraints from 210Pb and 7Be on wet deposition and transport in a global three-dimensional chemical tracer model driven by assimilated meteorological fields. Journal of Geophysical Research,

106(D11):12,109–12,128, June 2001.

[64] Rafael Lozano, Mohsen Naghavi, Kyle Foreman, Stephen Lim, Kenji Shibuya, Victor Aboyans, Jerry Abraham, Timothy Adair, Rakesh Aggarwal, Stephanie Y Ahn, Mohammad A AlMazroa, Miriam Alvarado, H Ross Anderson, Laurie M Anderson, Kathryn G Andrews, Charles Atkinson, Larry M Baddour, Suzanne Barker-Collo, David H Bartels, Michelle L Bell, Emelia J Benjamin, Derrick Bennett, Kavi Bhalla, Boris Bikbov, Aref Bin Abdulhak, Gretchen Birbeck, Fiona Blyth, Ian Bolliger, Soufiane Boufous, Chiara Bucello, Michael Burch, Peter Burney, Jonathan Carapetis, Honglei Chen, David Chou, Sumeet S Chugh, Luc E Coffeng, Steven D Colan, Samantha Colquhoun, K Ellicott Colson, John Condon, Myles D Connor, Leslie T Cooper, Matthew Corriere, Monica Cortinovis, Karen Courville de Vaccaro, William Couser, Benjamin C Cowie, Michael H Criqui, Marita Cross, Kaustubh C Dabhadkar, Nabila Dahodwala, Diego De Leo, Louisa Degenhardt, Allyne Delossantos, Julie Denenberg, Don C Des Jarlais, Samath D Dharmaratne, E Ray Dorsey, Tim Driscoll, Herbert Duber, Beth Ebel, Patricia J Erwin, Patricia Espindola, Majid Ezzati, Valery Feigin, Abraham D Flaxman, Mohammad H Forouzanfar, Francis Gerry R Fowkes, Richard Franklin, Marlene Fransen, Michael K Freeman, Sherine E Gabriel, Emmanuela Gakidou, Flavio Gaspari, Richard F Gillum, Diego Gonzalez-Medina, Yara A Halasa, Diana Haring, James E Harrison, Rasmus Havmoeller, Roderick J Hay, Bruno Hoen, Peter J Hotez, Damian Hoy, Kathryn H Jacobsen, Spencer L James, Rashmi Jasrasaria, Sudha Jayaraman, Nicole Johns, Ganesan Karthikeyan, Nicholas Kassebaum, Andre Keren, Jon-Paul Khoo, Lisa Marie Knowlton, Olive Kobusingye, Adofo Koranteng, Rita Krishnamurthi, Michael Lipnick, Steven E Lipshultz, Summer Lockett Ohno, Jacqueline Mabweijano, Michael F MacIntyre, Leslie Mallinger, Lyn March, Guy B Marks, Robin Marks, Akira Matsumori, Richard Matzopoulos, Bongani M Mayosi, John H McAnulty, Mary M McDermott, John McGrath, Ziad A Memish, George A Mensah, Tony R Merriman, Catherine Michaud, Matthew Miller, Ted R Miller, Charles Mock, Ana Olga Mocumbi, Ali A Mokdad, Andrew Moran, Kim Mulholland, M Nathan Nair, Luigi Naldi, K M Venkat Narayan, Kiumarss Nasseri, Paul Norman, Martin O'Donnell, Saad B Omer, Katrina Ortblad, Richard Osborne, Doruk Ozgediz, Bishnu Pahari, Jeyaraj Durai Pandian, Andrea Panozo Rivero, Rogelio Perez Padilla, Fernando Perez-Ruiz, Norberto Perico, David Phillips, Kelsey Pierce, C Arden Pope III, Esteban Porrini, Farshad Pourmalek, Murugesan Raju, Dharani Ranganathan, Jürgen T Rehm, David B Rein, Guiseppe Remuzzi, Frederick P Rivara, Thomas Roberts, Felipe Rodriguez De León, Lisa C Rosenfeld, Lesley Rushton, Ralph L Sacco, Joshua A Salomon, Uchechukwu Sampson, Ella Sanman, David C Schwebel, Maria Segui-Gomez, Donald S Shepard, David Singh, Jessica Singleton, Karen Sliwa, Emma Smith, Andrew Steer, Jennifer A Taylor, Bernadette Thomas, Imad M Tleyjeh, Jeffrey A Towbin, Thomas Truelsen, Eduardo A Undurraga, N Venketasubramanian, Lakshmi Vijayakumar, Theo Vos, Gregory R Wagner, Mengru Wang, Wenzhi Wang, Kerrianne Watt, Martin A Weinstock, Robert Weintraub, James D Wilkinson, Anthony D Woolf, Sarah Wulf, Pon-Hsiu Yeh, Paul Yip, Azadeh Zabetian, Zhi-Jie Zheng, Alan D Lopez, and Christopher JL Murray. Global and regional mortality from 235 causes of death for 20 age groups in 1990 and 2010: a systematic analysis for the Global Burden of Disease Study 2010. The Lancet, 380(9859):2095–2128, December 2012.

[65] Zifeng Lu, David G. Streets, Ekbordin Winijkul, Fang Yan, Yanju Chen, Tami C. Bond, Yan Feng, Manvendra K. Dubey, Shang Liu, Joseph P. Pinto, and Gregory R. Carmichael. Light Absorption Properties and Radiative Effects of Primary Organic Aerosol Emissions. Environmental Science & Technology, 49(8):4868–4877, April 2015.

[66] Marianne T. Lund, Terje K. Berntsen, Chris Heyes, Zbigniew Klimont, and Bjørn H. Samset. Global and regional climate impacts of black carbon and co-emitted species from the on-road diesel sector. Atmospheric Environment, 98:50–58, December 2014.

[67] Nordica MacCarty, Damon Ogle, Dean Still, Tami Bond, and Christoph Roden. A laboratory comparison of the global warming impact of five major types of biomass cooking stoves. Energy for Sustainable Development, 12(2):56–65, June 2008.

[68] Nordica MacCarty, Dean Still, and Damon Ogle. Fuel use and emissions performance of fifty cooking stoves in the laboratory and related benchmarks of performance. Energy for Sustainable Development, 14(3):161–171, September 2010.

[69] Randall V. Martin, Daniel J. Jacob, Robert M. Yantosca, Mian Chin, and Paul Ginoux. Global and regional decreases in tropospheric oxidants from photochemical effects of aerosols. Journal of Geophysical Research: Atmospheres, 108(D3):4097, February 2003.

[70] S. T. Martin, H.-M. Hung, R. J. Park, D. J. Jacob, R. J. D. Spurr, K. V. Chance, and M. Chin. Effects of the physical state of tropospheric ammonium-sulfate-nitrate particles on global aerosol direct radiative forcing. Atmospheric Chemistry and Physics, 4(1):183–214, 2004.

[71] R. H. Moore, V. A. Karydis, S. L. Capps, T. L. Lathem, and A. Nenes. Droplet number uncertainties associated with CCN: an assessment using observations and a global model adjoint. Atmospheric Chemistry and Physics, 13(8):4235–4251, April 2013.

[72] R. Morales Betancourt and A. Nenes. Understanding the contributions of aerosol properties and parameterization discrepancies to droplet number variability in a global climate model. Atmos. Chem. Phys., 14(9):4809–4826, May 2014.

[73] Richard H. Moss, Jae A. Edmonds, Kathy A. Hibbard, Martin R. Manning, Steven K. Rose, Detlef P. van Vuuren, Timothy R. Carter, Seita Emori, Mikiko Kainuma, Tom Kram, Gerald A. Meehl, John F. B. Mitchell, Nebojsa Nakicenovic, Keywan Riahi, Steven J. Smith, Ronald J. Stouffer, Allison M. Thomson, John P. Weyant, and Thomas J. Wilbanks. The next generation of scenarios for climate change research and assessment. Nature, 463(7282):747–756, February 2010.

[74] Lee T. Murray, Daniel J. Jacob, Jennifer A. Logan, Rynda C. Hudman, and William J. Koshak. Optimized regional and interannual variability of lightning in a global chemical transport model constrained by LIS/OTD satellite data: IAV OF LIGHTNING CONSTRAINED BY LIS/OTD. Journal of Geophysical Research: Atmospheres, 117(D20):n/a–n/a, October 2012.

[75] Gunnar Myhre, Drew Shindell, François-Marie Bréon, William Collins, Jan Fuglestvedt, Jianping Huang, Dorothy Koch, Jean-François Lamarque, David Lee, Blanca Mendoza, Teruyuki Nakakima, Alan Robock, Graeme Stephens, Toshihiko Takemura, and Hua Zhang. Anthropogenic and natural radiative forcing. In Climate Change 2013: The Physical Science Basis. Contribution of Working Group I to the Fifth Assessment Report of the Intergovernmental Panel on Climate Change. Cambridge University Press, 2013.

[76] G. F. Nemet, T. Holloway, and P. Meier. Implications of incorporating air-quality co-benefits into climate change policymaking. Environmental Research Letters, 5(1):014007, 2010.

[77] R.J. Park, D.J. Jacob, M. Chin, and R.V. Martin. Sources of carbonaceous aerosols over the united states and implications for natural visibility. J. Geophys. Res, 108(12):4355, 2003.

[78] R.J. Park, D.J. Jacob, B.D. Field, R.M. Yantosca, and M. Chin. Natural and transboundary pollution influences on sulfate-nitrate-ammonium aerosols in the united states: Implications for policy. J. Geophys. Res, 109:15, 2004.

[79] Véronique Perraud, Emily A. Bruns, Michael J. Ezell, Stanley N. Johnson, Yong Yu, M. Lizabeth Alexander, Alla Zelenyuk, Dan Imre, Wayne L. Chang, Donald Dabdub, James F. Pankow, and Barbara J. Finlayson-Pitts. Nonequilibrium atmospheric secondary organic aerosol formation and growth. Proceedings of the National Academy of Sciences, 109(8):2836–2841, February 2012.

[80] S. Philip, R. V. Martin, J. R. Pierce, J. L. Jimenez, Q. Zhang, M. R. Canagaratna, D. V. Spracklen, C. R. Nowlan, L. N. Lamsal, M. J. Cooper, and N. A. Krotkov. Spatially and seasonally resolved estimate of the ratio of organic mass to organic carbon. Atmospheric Environment, 87:34–40, April 2014.

[81] J. R. Pierce, K. Chen, and P. J. Adams. Contribution of primary carbonaceous aerosol to cloud condensation nuclei: processes and uncertainties evaluated with a global aerosol microphysics model. Atmos. Chem. Phys., 7(20):5447–5466, October 2007.

[82] Ajay Pillarisetti, Sumi Mehta, and Kirk R. Smith. HAPIT, the Household Air Pollution Intervention Tool, to Evaluate the Health Benefits and Cost-Effectiveness of Clean Cooking Interventions. In Evan A. Thomas, editor, Broken Pumps and Promises, pages 147–169. Springer International Publishing, 2016. DOI: 10.1007/978-3-319-28643-3_10.

[83] Albert A. Presto, Marissa A. Miracolo, Neil M. Donahue, and Allen L. Robinson. Secondary Organic Aerosol Formation from High-NOx Photo-Oxidation of Low Volatility Precursors: n-Alkanes. Environmental Science & Technology, 44(6):2029–2034, March 2010.

[84] Elizabeth M. Punger and J. Jason West. The effect of grid resolution on estimates of the burden of ozone and fine particulate matter on premature mortality in the USA. Air Quality, Atmosphere & Health, 6(3):563–573, May 2013.

[85] V. Ramanathan and Y. Xu. The Copenhagen Accord for limiting global warming: Criteria, constraints, and available avenues. Proceedings of the National Academy of Sciences, 107:8055–8062, May 2010.

[86] Veerabhadran Ramanathan and Gregory Carmichael. Global and regional climate changes due to black carbon. Nature geoscience, 1(4):221–227, 2008.

[87] Christoph A. Roden, Tami C. Bond, Stuart Conway, Anibal Benjamin Osorto Pinel, Nordica MacCarty, and Dean Still. Laboratory and field investigations of particulate and carbon monoxide emissions from traditional and improved cookstoves. Atmospheric Environment, 43(6):1170–1181, February 2009.

[88] Christoph A. Roden, Tami C. Bond, Stuart Conway, and Anibal Benjamin Osorto Pinel. Emission factors and real-time optical properties of particles emitted from traditional wood burning cookstoves. Environmental Science & Technology, 40(21):6750–6757, November 2006.

[89] Joeri Rogelj, Michiel Schaeffer, Malte Meinshausen, Drew T. Shindell, William Hare, Zbigniew Klimont, Guus J. M. Velders, Markus Amann, and Hans Joachim Schellnhuber. Disentangling the effects of CO2 and short-lived climate forcer mitigation. Proceedings of the National Academy of Sciences, 111(46):16325–16330, November 2014.

[90] Daniel Rosenfeld, Meinrat O. Andreae, Ari Asmi, Mian Chin, Gerrit de Leeuw, David P. Donovan, Ralph Kahn, Stefan Kinne, Niku Kivekäs, Markku Kulmala, William Lau, K. Sebastian Schmidt, Tanja Suni, Thomas Wagner, Martin Wild, and Johannes Quaas. Global observations of aerosol-cloud-precipitation-climate interactions. Reviews of Geophysics, 52(4):2013RG000441, December 2014.

[91] B. Sauvage, R. V. Martin, A. van Donkelaar, X. Liu, K. Chance, L. Jaeglé, P. I. Palmer, S. Wu, and T.-M. Fu. Remote sensed and in situ constraints on processes affecting tropical tropospheric ozone. Atmospheric Chemistry and Physics, 7(3):815–838, 2007.

[92] John H. Seinfeld and Spyros N. Pandis. Atmospheric Chemistry and Physics: From Air Pollution to Climate Change. Wiley-Interscience, 2 edition, August 2006.

[93] Rebecca J. Sheesley, James J. Schauer, Zohir Chowdhury, Glen R. Cass, and Bernd R. T. Simoneit. Characterization of organic aerosols emitted from the combustion of biomass indigenous to South Asia. Journal of Geophysical Research: Atmospheres, 108(D9):4285, May 2003.

[94] Z. Shen, J. Liu, L. W. Horowitz, D. K. Henze, S. Fan, H. Levy, II, D. L. Mauzerall, J.-T. Lin, and S. Tao. Analysis of transpacific transport of black carbon during HIPPO-3: implications for black carbon aging. Atmospheric Chemistry & Physics Discussions, 14:505–540, January 2014.

[95] D. Shindell and G. Faluvegi. The net climate impact of coal-fired power plant emissions. Atmospheric Chemistry and Physics, 10(7):3247–3260, 2010.

[96] D. T. Shindell. Evaluation of the absolute regional temperature potential. Atmospheric Chemistry and Physics, 12(17):7955–7960, September 2012.

[97] D. T. Shindell, J.-F. Lamarque, M. Schulz, M. Flanner, C. Jiao, M. Chin, P. J. Young, Y. H. Lee, L. Rotstayn, N. Mahowald, G. Milly, G. Faluvegi, Y. Balkanski, W. J. Collins, A. J. Conley, S. Dalsoren, R. Easter, S. Ghan, L. Horowitz, X. Liu, G. Myhre, T. Nagashima, V. Naik, S. T. Rumbold, R. Skeie, K. Sudo, S. Szopa, T. Takemura, A. Voulgarakis, J.-H. Yoon, and F. Lo. Radiative forcing in the ACCMIP historical and future climate simulations. Atmos. Chem. Phys., 13(6):2939–2974, March 2013.

[98] Drew Shindell and Greg Faluvegi. Climate response to regional radiative forcing during the twentieth century. Nature Geoscience, 2(4):294–300, March 2009.

[99] Drew T. Shindell, Yunha Lee, and Greg Faluvegi. Climate and health impacts of us emissions reductions consistent with 2c. Nature Climate Change, 6(5):503–507, May 2016.

[100] Keith P. Shine, Jan S. Fuglestvedt, Kinfe Hailemariam, and Nicola Stuber. Alternatives to the Global Warming Potential for Comparing Climate Impacts of Emissions of Greenhouse Gases. Climatic Change, 68(3):281–302, February 2005.

[101] Gregory L. Simon, Adam G. Bumpus, and Philip Mann. Win-win scenarios at the climate–development interface: Challenges and opportunities for stove replacement programs through carbon finance. Global Environmental Change, 22(1):275–287, February 2012.

[102] Kirk R. Smith, R. Uma, V. V. N. Kishore, Junfeng Zhang, V. Joshi, and M. A. K. Khalil. Greenhouse implications of household stoves: an analysis for India. Annual Review of Energy and the Environment, 25(1):741–763, 2000.

[103] S. J. Smith and A. Mizrahi. Near-term climate mitigation by short-lived forcers. Proceedings of the National Academy of Sciences, 110(35):14202–14206, August 2013.

[104] Steven J. Smith and T. M. L. Wigley. Multi-gas forcing stabilization with the MiniCAM. Energy Journal, 3(Special Issue):373–391, 2006.

[105] D. V. Spracklen, K. S. Carslaw, U. Pöschl, A. Rap, and P. M. Forster. Global cloud condensation nuclei influenced by carbonaceous combustion aerosol. Atmos. Chem. Phys., 11(17):9067–9087, September 2011.

[106] R. J. D. Spurr. Simultaneous derivation of intensities and weighting functionsvin a general pseudo-spherical discrete ordinate radiative transfer treatment. Journal of Quantitative Spectroscopy & Radiative Transfer, 75:129–175, March 2001.

[107] R. J. D. Spurr, T. P. Kurosu, and K. V. Chance. A linearized discrete ordinate radiative transfer model for atmospheric remote-sensing retrieval. Journal of Quantitative Spectroscopy and Radiative Transfer, 68(6):689–735, 2001.

[108] D. G. Streets, T. C. Bond, G. R. Carmichael, S. D. Fernandes, Q. Fu, D. He, Z. Klimont, S. M. Nelson, N. Y. Tsai, M. Q. Wang, J.-H. Woo, and K. F. Yarber. An inventory of gaseous and primary aerosol emissions in Asia in the year 2000. Journal of Geophysical Research: Atmospheres, 108(D21):8809, November 2003.

[109] S. Q. Turn, B. M. Jenkins, J. C. Chow, L. C. Pritchett, D. Campbell, T. Cahill, and S. A. Whalen. Elemental characterization of particulate matter emitted from biomass burning: Wind tunnel derived source profiles for herbaceous and wood fuels. Journal of Geophysical Research: Atmospheres, 102(D3):3683–3699, February 1997.

[110] S. Twomey. The Influence of Pollution on the Shortwave Albedo of Clouds. Journal of the Atmospheric Sciences, 34(7):1149–1152, July 1977.

[111] UNEP and WMO. Integrated assessment of black carbon and tropospheric ozone. Technical report, United Nations Environment Programme, 2011.

[112] N. Unger, T. C Bond, J. S Wang, D. M Koch, S. Menon, D. T Shindell, and S. Bauer. Attribution of climate forcing to economic sectors. Proceedings of the National Academy of Sciences, 107(8):3382–3387, 2010.

[113] United Nations, Department of Social and Economic Affairs, Population Division. World Population Prospects: The 2015 Revision, Key Findings and Advance Tables., 2015.

[114] United Nations Environment Programme. Near-term climate protection and clean air benefits actions for controlling short-lived climate forcers: a UNEP synthesis report., 2011.

[115] Aaron van Donkelaar, Randall V. Martin, Michael Brauer, and Brian L. Boys. Use of Satellite Observations for Long-Term Exposure Assessment of Global Concentrations of Fine Particulate Matter. Environmental Health Perspectives, October 2015.

[116] Aaron van Donkelaar, Randall V. Martin, Michael Brauer, N. Christina Hsu, Ralph A. Kahn, Robert C. Levy, Alexei Lyapustin, Andrew M. Sayer, and David M. Winker. Global Estimates of Fine Particulate Matter using a Combined Geophysical-Statistical Method with Information from Satellites, Models, and Monitors. Environmental Science & Technology, 50(7):3762–3772, April 2016.

[117] C. Venkataraman. Residential biofuels in south asia: Carbonaceous aerosol emissions and climate impacts. Science, 307(5714):1454–1456, March 2005.

[118] C. Venkataraman, A. D. Sagar, G. Habib, N. Lam, and K. R. Smith. The indian national initiative for advanced biomass cookstoves: The benefits of clean combustion. Energy for Sustainable Development, 14(2):63–72, June 2010.

[119] M. L. Wesely. Parameterization of surface resistances to gaseous dry deposition in regional-scale numerical models. Atmospheric Environment (1967), 23(6):1293–1304, 1989.

[120] Ekbordin Winijkul, Laura Fierce, and Tami C. Bond. Emissions from Residential Combustion Considering End-Uses and Spatial Constraints: Part I, Methods and Spatial Distribution. Atmospheric Environment, 2015.

[121] Lu Xu, Hongyu Guo, Christopher M. Boyd, Mitchel Klein, Aikaterini Bougiatioti, Kate M. Cerully, James R. Hite, Gabriel Isaacman-VanWertz, Nathan M. Kreisberg, Christoph Knote, Kevin Olson, Abigail Koss, Allen H. Goldstein, Susanne V. Hering, Joost de Gouw, Karsten Baumann, Shan-Hu Lee, Athanasios Nenes, Rodney J. Weber, and Nga Lee Ng. Effects of anthropogenic emissions on aerosol formation from isoprene and monoterpenes in the southeastern United States. Proceedings of the National Academy of Sciences, 112(1):37–42, January 2015.

Appendix A

Supporting Information: Climate impacts from country-level solid fuel cookstove carbonaceous aerosol emissions

A.1 Forward model

The chemical transport model used in this study is GEOS-Chem. This model uses meteorological data from the Goddard Earth Observing System (GEOS) that has been regridded to the $2^\circ \times 2.5^\circ$ resolution [7]. Anthropogenic emissions for the simulations are taken from the RCP Database [73] hosted by the International Institute for Applied System's Analysis (http://www.iiasa.ac.at/). For this particular analysis, historical year 2000 emissions are considered [56]. Anthropogenic emissions are separated into the following sectors: energy, domestic, industry, transportation, landfill waste, agriculture, waste burning, solvents, shipping, grassfires and forest fires. Carbonaceous aerosol emissions from biofuel sources in the domestic sector are from Fernandes et al., 2007 [29] and Bond et al., 2007 [14]. Natural emissions of aerosols and aerosol precursors in GEOS-Chem include volcanoes, lightning NO_x [91, 74], ocean dimethyl sulfide, soil emissions [41], and biogenic species (isoprene, terpenes) from MEGAN v2.1 [36]. A fraction (20%) of the total biomass burning emissions from the inventory are also considered natural emissions.

GEOS-Chem tracks the formation and transport of the following aerosol species: sulfate, nitrate, ammonium, carbonaceous aerosol (organic and BC), sea salt and mineral dust [77, 78]. GEOS-Chem includes heterogeneous chemistry on the surface of aerosols [28], aerosol phase partitioning using RPMARES [9], and aerosol effects on photolysis rates in the troposphere [69]. Aerosol removal from the atmosphere includes both dry and wet deposition [119, 42, 63]. Aerosols are con-

sidered to be formed or emitted with a fixed log-normal size distribution, while hygroscopic growth is calculated offline using relative humidity retrieved from the GEOS-5 meteorology in each grid cell [69]. This offline calculation is used when considering surface area for heterogeneous chemistry along with aerosol optical properties. BC is emitted in a 4:1 ratio of hydrophobic to hydrophilic particles, while OC is considered to have a 1:1 ratio of hydrophobic to hydrophilic components. Both of these species have an e-folding time of 1.15 days for their conversion from being hydrophobic to hydrophilic [26, 23, 25].

Optical properties for aerosols in the model use refractive indices and size distributions retrieved from the Global Aerosol Data Set (GADS) [54]. These optical properties are then applied to the GEOS-Chem aerosol mass concentrations in order to calculate aerosol optical depths, single-scattering albedos (SSA) and phase functions (ϕ) using Mie scattering theory [70]. For these calculations aerosols are assumed to be an external mixture, which results in underestimating total aerosol absorption [43]. In order to accommodate for this we increase the absorption of BC aerosol by a factor of 1.5 following recommendations in Bond et al., 2006 [13] such that the aerosol absorption matches published values. These optical parameters are inputs for the LIDORT radiative transfer model [107] which is used to calculate the top of atmosphere (TOA) radiative flux over wavelengths from 315 to 1,667 nm [13, 107, 106]. Radiative flux calculations use surface albedos from remote sensing measurements [53] and cloud fractions from the NASA Global Modeling and Assimilation Office (GMAO).

A.2 Cookstove emissions

The Bond et al., 2007 [14] carbonaceous aerosol emissions inventory contains all biofuel emissions, which not only includes cookstoves, but other residential emissions sources and additional non-residential biofuel sectors [29, 14]. The total biofuel emissions within a country, c, are thus $\sigma_{biofuel,c}$

$$\sigma_{biofuel,c} = \sigma_{cs,c} + \sigma_{ncs,c}, \tag{A.1}$$

where $\sigma_{cs,c}$ is the carbonaceous aerosol emission from cookstoves and $\sigma_{ncs,c}$ is the carbonaceous aerosol emission from non-cookstove sectors. In order to isolate the amount of biofuel aerosol emissions owing to cookstove use, $\sigma_{cs,c}$, we must first determine the amount of carbonaceous emissions from other sources, $\sigma_{ncs,c}$. We start by considering the percent of the year 2000 population in country c using solid fuels (SF_c) for cooking from Bonjour et al., 2013 [15]. A number of countries have less than 5% of their population using solid fuel for cooking, or are assumed so in Bonjour et al., 2013 [15] based on per-capita income greater than US$12,276. We can use these countries to calculate a non-cookstove use emissions fraction (Θ_r) for each region (Africa, Asia, Europe, N. America, Oceanic Pacific, S. America and Central America),

$$\Theta_r = \left(\sum_{c \in r} \sigma_{biofuel,c} \cdot (1 - u(SF_c - 0.05)) \right) \left(\sum_{c \in r} P_c \cdot (1 - u(SF_c - 0.05)) \right)^{-1} \tag{A.2}$$

where P_c is year 2000 the population within a country and u is the Heaviside step function. The numerator therefore represents the sum of biofuel emissions for all countries in the region (r) that have less than 5% of the population using solid fuel for cooking and the denominator represents the sum of population across those same countries. This gives Θ_r in the units of kilograms of non-cookstove biofuel carbonaceous emissions per capita. This equation assumes that $\sigma_{biofuel,c}$ is approximately $\sigma_{ncs,c}$ for countries with less than 5% of the population using solid fuel for cooking. With this regional emissions factor calculated we can now calculate $\sigma_{cs,c}$ based on the following equation,

$$\sigma_{cs,c} = \sigma_{biofuel,c} - P_c \left[1 - SF_c\right] \Theta_r \tag{A.3}$$

The inventory of carbonaceous aerosol emission from residential cookstove use per country calculated using this approach is shown in Figure A.5. We note that this inventory does not distinguish between solid fuels used for cooking with modern wood-burning stoves versus more traditional cookstoves. Non-cooking solid fuel used by the fraction of the population that also uses solid fuel for cooking will be ascribed to $\sigma_{cs,c}$ by this approach, which will thus may be biased high compared

to the emissions from cooking alone. The inventory could also be biased low owing to exclusion of fossil-fuel coal used for cookstoves, which is considered as a solid fuel for cooking in Bonjour et al., 2013 [15] but not the biofuel inventory of Bond et al., 2007 [14]. Based on national-scale surveys that have been compiled and made available by the World Health Organization (WHO) this source contributes less than 10% of solid fuel use for cooking in most countries, although values in China are notably higher (34%) (http://www.who.int).

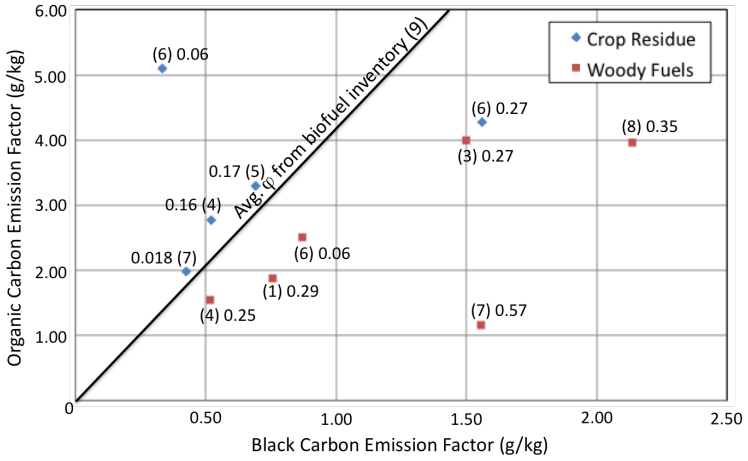

Figure A.1: BC and OC emissions factors reported in various biofuel characterization studies: (1) Turn et al., 1997 [109], (2) Sheesley et al., 2003 [93], (3) Streets et al., 2003 [108], (4) Venkataraman et al., 2005 [117], (5) Roden et al., 2006 [88], (6) Johnson et al., 2008 [47], (7) Li et al., 2009 [60], (8) Roden et al., 2009 [87] and the average Φ limits are calculated from the Bond et al., 2007 [14] biofuel emissions inventory.

These cookstove emissions can be further refined in terms of BC (σ_{BC}) and OC (σ_{OC}) emissions using emissions factors for different types of stoves and fuels. A summary of emissions factors used for both OC and BC is shown in Figure A.1. These studies are based on a variety of different fuels, stoves, and measurement techniques. Crop residue fuels tend to have a statistically significant lower BC to total carbon ratio, Φ, compared to woody fuels. While Φ is different between woody fuels and crop residue, the total carbonaceous emission factors are not statistically different for different fuel types, although some studies [87] have shown that differences between different measurement techniques [87] can lead to differences in characterizations of both the total carbonaceous

emissions and Φ.

A.3 Adjoint model calculations

The GEOS-Chem adjoint model is used in combination with the analytical Jacobians computed by LIDORT to evaluate the impact of grid-scale perturbations to emissions of aerosol and aerosol precursors, $\sigma_{i,k}$, on direct radiative forcing, $J(\sigma_{\tau,i,k})$, where i and k are the spatial and species indices, respectively. We consider both the annual global radiative forcing and the annual regional radiative forcing within four different latitude bands (τ), which are: the Arctic (60N to 90N), the northern hemisphere mid-latitudes (28N to 60N), the Tropics (28S to 28N) and the southern hemisphere extra tropics (90S to 28S). The adjoint sensitivities are calculated in several steps as shown in Equation A.4 (evaluated from right to left),

$$\lambda_{\tau,i,k} = \left(\frac{\partial J(\sigma_{\tau,i,k})}{\partial \sigma_{i,k}}\right)^T = \left(\frac{\partial \mathbf{B}_{conc,i,k}}{\partial \sigma_{i,k}}\right)^T \left(\frac{\partial \mathbf{A}_{opt,i}}{\partial \mathbf{B}_{conc,i,k}}\right)^T \frac{\partial J(\sigma_{\tau,i,k})}{\partial \mathbf{A}_{opt,i}}. \tag{A.4}$$

where $\lambda_{\tau,i,k}$ is the radiative forcing sensitivity for a given region, τ, with respect emissions of species, k, within grid cell, i. $\mathbf{A}_{opt}$ is the array of optical parameters (aerosol optical depth, single-scattering albedo and phase function) in GEOS-Chem, which is used as an input for LIDORT, and $\mathbf{B}_{conc}$ is the array of aerosol mass concentrations within GEOS-Chem. In the first step, sensitivities of $J(\sigma_{\tau,i,k})$ with respect to aerosol optical parameters are calculated using LIDORT Jacobians and offline Mie calculations [39]. These derivatives are then used to force an adjoint calculation, which propagates sensitivity information backwards through the model for all components of the GEOS-Chem governing equations including aerosol thermodynamics, chemistry, deposition and transport.

In order to efficiently calculate adjoint sensitivities of annual radiative forcing, yearly values were approximated using the average of weekly simulations of the first week of each month. All simulations used a one year forward model spin-up using the RCP historical emissions [56].

A.4 Radiative forcing scaling

Calculations described thus far are only for direct radiative forcing and are based on a single model. However, as discussed in the introduction, there is a range of uncertainties related to direct radiative forcing and other aerosol properties and mechanisms. Therefore, following UNEP and WMO, 2011 [111], here we use total forcing estimates calculated across a suite of chemistry-climate models to develop several scaling factors that are applied to our direct radiative forcing calculations to account for three major effects: direct radiative forcing ($SF_{k,DRF}$), aerosol semi and indirect effects ($SF_{k,SI}$), and the forcing from snow-ice albedo changes due to BC deposition ($\lambda_{BC,i,ALB}$). The direct radiative forcing scaling factors ($SF_{k,DRF}$) are created from a comparison of eight to eleven (depending on species) different chemistry-climate models [75, 17] and the direct radiative forcing from GEOS-Chem. Many of these models include the radiative forcing for sulfate and nitrate [75], while GEOS-Chem estimates the direct radiative forcing due to emissions of SO_2, NO_x and NH_3, which lead to the formation of sulfate, nitrate and ammonium. Since separate RF values for ammonium-sulfate and ammonium-nitrate are not reported for the models used in Myhre et al., 2013 [75], here we assume that the direct radiative forcing from emissions of SO_2, NO_x, and NH_3 combine to match the direct radiative forcing estimates of sulfate and nitrate from Myhre et al., 2013 [75], giving a central estimate of $SF_{k,DRF}$ of 0.567. The values for the central estimate and upper and lower bounds for $SF_{k,DRF}$ of all aerosol species are shown in Table 1. Since sulfate acts chemically and physically similar to nitrate with respect to cloud interactions, the same $SF_{k,SI}$ is used for all secondary inorganic precursors, which is based on the effective radiative forcing aerosol-cloud interaction (ERF_{aci}) for sulfate from Boucher et al., 2013 [17] divided by the effective radiative forcing aerosol-radiation interaction (ERF_{ari}) for sulfate from Myhre et al., 2013 [75]. This scaling factor, $SF_{SIA,SI}$, is used for all secondary inorganic aerosol precursors (SIA, Table 1).

Both BC and OC are directly emitted aerosols, therefore $SF_{k,DRF}$ for these species is calculated using the ratio of estimated direct radiative forcing from GEOS-Chem to the direct radiative forcing values in Myhre et al., 2013 [75]. This direct radiaitive forcing scaling is needed to correct

for some of the aforementioned assumptions regarding mixing state and BC aging in the GEOS-Chem forward model. BC semi-direct effects ($\pm$ 0.4 W m^{-2}) are larger in magnitude than the BC ERF_{aci}; the latter are therefore assumed to be negligible. The BC semi-direct effects perturb the upper and lower bounds of the radiative forcing but not the central estimate. Unlike BC, OC has a large indirect component. Since the ERF_{aci} is not reported for OC [17], we infer a value from the difference between the modeled $ERF_{SIA,aci}$ and the modeled ERF_{aci} for all species [17]. This assumes that all of the ERF_{aci} comes from either OC or the secondary inorganic species, since the BC ERF_{aci} is negligible.

Lastly, we implement $\lambda_{BC,i,ALB}$ to account for the deposition of BC on snow and ice, which leads to a large change in radiative forcing through a decrease in surface albedo. The magnitude of this change ($RF_{BC,global,ALB}$) is approximately 0.15 $\pm$ 0.1 W m^{-2} [111, 75, 11]. Given the strong spatial dependency of this forcing mechanism, we spatially distribute $RF_{BC,global,ALB}$ using deposition sensitivities ($\lambda_{BC,i,dep}$) of BC onto snow and sea ice calculated with the GEOS-Chem adjoint model, where $J_{BC,dep}$ is the global deposition of BC onto snow and sea ice,

$$\lambda_{BC,i,dep} = \frac{\partial J_{BC,dep}}{\partial \sigma_{BC,i}}. \tag{A.5}$$

Figure A.2 shows the seasonal variation of grid cells which have snow or ice cover according to the GMAO datasets retrieved from the NASA Langley Research Center Atmospheric Science Data Center (https://eosweb.larc.nasa.gov/). These sensitivities are used to redistribute $RF_{BC,global,ALB}$ into a spatially resolved radiative forcing sensitivity ($\lambda_{BC,i,ALB}$) by converting the sensitivity of global deposition onto snow and ice with respect to emissions in each grid cell ($\lambda_{BC,i,dep}$) as shown in Equation A.6,

$$\lambda_{BC,i,ALB} = \lambda_{BC,i,dep} \frac{0.15 \text{ Wm}^{-2}}{J_{BC,dep}}. \tag{A.6}$$

Due to the strong seasonality in $\lambda_{BC,i,dep}$, these snow-ice albedo sensitivities are calculated for the first week of each month and averaged before being applied to Equation 1. Figure A.3 shows the resulting yearly average for the spatially resolved radiative forcing sensitivities ($\bar{\lambda}_{BC,i,ALB}$) in Wm^{-2} per kilogram BC emitted. This map shows not only the expected higher sensitivities near

the poles but also the higher impacts from emissions near higher altitude mountainous regions such as the Himalayas, Alps and Andes. The high sensitivities over central Europe, the western coast of South America and central Asia show that the radiative forcing per emission of BC in these regions is actually equal to or great than the direct radiative forcing sensitivities.

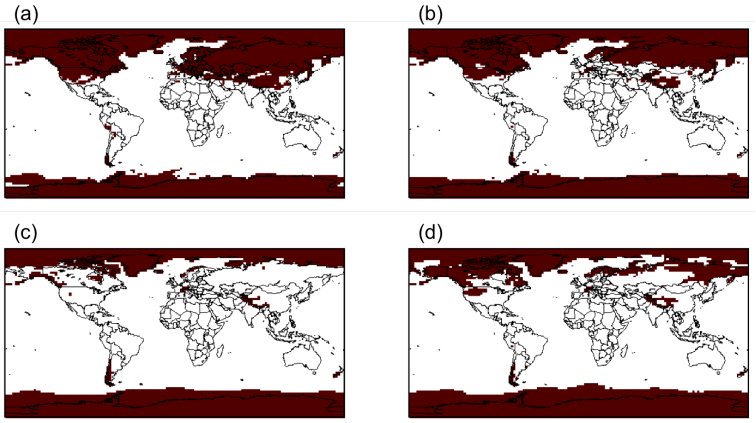

Figure A.2: Grid cells containing over 50 cm H_2O equivalent snow depth for a weekly-average noon GMAO estimated snow depth for different months (a) January 2009, (b) April 2009, (c) July 2009, (d) October 2009.

A.5 Results

Table A.1: Model estimates of contribution to total temperature change and emissions metrics for all countries with model inputs of annual emissions form solid-fuel cookstove use (Column 1) and Φ (Column 2), cooling impact from removal of annual cookstove emissions (Column 3), or efficiency in terms of cooling effect per emission (Column 4 and 5).

Country	Carbonaceous Aerosol Emissions [kg C]	Phi [BC/TC]	Temperature Change Contribution [K]	Cookstove Change Efficiency [K[kg C]$^{-1}$]	Fuel Switching Efficiency [K[kg C]$^{-1}$]
Afghanistan	1.314E+07	0.155	-3.070E-04	-2.337E-11	-2.034E-11
Albania	1.419E+06	0.139	-1.551E-05	-1.093E-11	-1.583E-11
Angola	1.904E+07	0.212	-6.973E-05	-3.663E-12	-1.113E-11
Armenia	2.525E+06	0.140	-8.422E-05	-3.335E-11	-3.611E-11
Azerbaijan	3.893E+07	0.143	-1.080E-03	-2.773E-11	-3.187E-11
Bangladesh	1.348E+08	0.213	-6.274E-04	-4.656E-12	-8.743E-12
Belize	1.033E+06	0.131	9.082E-06	8.795E-12	-6.937E-12
Benin	9.661E+06	0.217	-1.264E-04	-1.308E-11	-1.603E-11
Bhutan	7.131E+06	0.214	-8.379E-05	-1.175E-11	-9.010E-12
Bolivia	3.735E+06	0.158	1.167E-05	3.124E-12	-6.796E-12
Bosnia & Herzegovina	1.363E+06	0.141	-1.589E-05	-1.165E-11	-1.907E-11
Botswana	1.871E+06	0.211	-4.735E-07	-2.530E-13	-4.589E-12
Brazil	3.430E+07	0.085	3.594E-04	1.048E-11	-3.707E-12
Bulgaria	6.993E+06	0.140	-9.483E-05	-1.356E-11	-2.128E-11
Burkina Faso	2.680E+07	0.216	-3.729E-04	-1.391E-11	-1.657E-11
Burundi	5.312E+06	0.212	-6.491E-06	-1.222E-12	-1.066E-11
Cambodia	2.292E+07	0.214	-1.530E-06	-6.674E-14	-1.038E-11
Cameroon	3.443E+07	0.197	-2.853E-04	-8.284E-12	-1.444E-11
Cape Verde	1.472E+03	0.208	5.519E-09	3.749E-12	-1.030E-11
Central African Republic	7.539E+06	0.213	-3.488E-05	-4.627E-12	-1.176E-11
Chad	1.281E+07	0.219	-1.867E-04	-1.458E-11	-1.530E-11
Chile	6.527E+05	0.193	-4.018E-07	-6.156E-13	-3.751E-12

China	1.186E+09	0.236	-3.309E-02	-2.789E-11	-2.085E-11
Colombia	6.095E+06	0.134	1.173E-05	1.925E-12	-9.809E-12
Congo	1.078E+07	0.209	-8.091E-05	-7.509E-12	-1.404E-11
Congo, DRC	1.295E+08	0.207	-5.830E-04	-4.501E-12	-1.328E-11
Costa Rica	1.306E+06	0.140	1.274E-05	9.758E-12	-6.855E-12
Cote dIvory	2.282E+07	0.249	-3.399E-04	-1.490E-11	-1.423E-11
Croatia	7.039E+05	0.139	-9.771E-06	-1.388E-11	-2.331E-11
Cuba	6.843E+06	0.146	4.355E-05	6.363E-12	-5.895E-12
Djibouti	1.589E+06	0.219	-7.360E-06	-4.631E-12	-1.085E-11
Dominica	1.055E+02	0.031	1.433E-09	1.358E-11	-2.654E-12
Dominican Republic	1.375E+06	0.171	6.325E-06	4.602E-12	-5.489E-12
Ecuador	2.196E+05	0.195	-1.001E-06	-4.557E-12	-1.136E-11
El Salvador	7.951E+06	0.130	8.273E-05	1.040E-11	-5.663E-12
Equatorial Guinea	4.795E+05	0.202	-3.559E-06	-7.421E-12	-1.300E-11
Eritrea	1.004E+07	0.221	-6.995E-05	-6.967E-12	-1.076E-11
Estonia	6.012E+06	0.148	-5.514E-04	-9.173E-11	-7.888E-11
Ethiopia	1.839E+08	0.217	-3.794E-04	-2.064E-12	-1.034E-11
Fiji	1.669E+04	0.200	1.191E-07	7.136E-12	-6.055E-12
Gabon	3.202E+06	0.186	-1.959E-05	-6.117E-12	-1.357E-11
Georgia	1.473E+07	0.143	-5.691E-04	-3.864E-11	-3.872E-11
Ghana	2.288E+07	0.234	-3.203E-04	-1.400E-11	-1.523E-11
Guatemala	9.661E+06	0.130	9.539E-05	9.874E-12	-5.804E-12
Guinea	7.220E+06	0.236	-5.445E-05	-7.542E-12	-1.255E-11
Guinea-Bissau	1.575E+06	0.240	-1.272E-05	-8.078E-12	-1.331E-11
Guyana	4.893E+05	0.083	3.378E-06	6.905E-12	-6.611E-12
Haiti	7.541E+05	0.155	4.019E-06	5.330E-12	-5.964E-12
Honduras	1.967E+07	0.130	1.850E-04	9.408E-12	-6.230E-12

India	9.351E+08	0.217	-6.165E-03	-6.593E-12	-1.009E-11
Indonesia	9.797E+07	0.239	-3.646E-04	-3.721E-12	-1.095E-11
Jamaica	7.688E+04	0.200	2.720E-07	3.538E-12	-6.264E-12
Kazakhstan	1.140E+07	0.138	-1.339E-03	-1.175E-10	-8.652E-11
Kenya	1.070E+08	0.219	5.230E-05	4.889E-13	-7.737E-12
Kyrgyzstan	2.706E+07	0.143	-1.289E-03	-4.763E-11	-3.827E-11
Laos	2.469E+07	0.211	-4.621E-05	-1.872E-12	-1.014E-11
Latvia	1.358E+07	0.143	-8.570E-04	-6.311E-11	-6.203E-11
Lesotho	1.317E+06	0.211	6.627E-07	5.031E-13	-1.880E-12
Liberia	7.183E+06	0.222	-4.463E-05	-6.213E-12	-1.060E-11
Lithuania	1.638E+07	0.143	-8.199E-04	-5.005E-11	-5.295E-11
Macedonia	5.234E+06	0.142	-6.201E-05	-1.185E-11	-1.701E-11
Madagascar	1.748E+07	0.231	2.184E-05	1.250E-12	-4.325E-12
Malawi	1.064E+07	0.220	-2.035E-05	-1.912E-12	-7.141E-12
Mali	1.664E+07	0.219	-3.063E-04	-1.841E-11	-1.771E-11
Mauritania	3.650E+06	0.236	-4.948E-05	-1.356E-11	-1.604E-11
Mexico	4.485E+07	0.129	2.471E-04	5.511E-12	-1.045E-11
Moldova	1.006E+07	0.142	-2.564E-04	-2.549E-11	-3.362E-11
Mongolia	3.862E+06	0.227	-2.926E-04	-7.574E-11	-4.300E-11
Morocco	4.658E+05	0.492	-2.144E-05	-4.602E-11	-2.366E-11
Mozambique	4.696E+07	0.218	-2.957E-05	-6.297E-13	-5.652E-12
Myanmar	7.519E+07	0.219	-4.367E-04	-5.808E-12	-9.858E-12
Namibia	1.653E+06	0.209	4.531E-07	2.741E-13	-6.135E-12
Nepal	5.298E+07	0.209	-6.625E-04	-1.250E-11	-9.676E-12
Nicaragua	1.083E+07	0.129	9.990E-05	9.222E-12	-7.060E-12
Niger	1.671E+07	0.207	-3.742E-04	-2.239E-11	-1.967E-11
Nigeria	1.171E+08	0.189	-1.390E-03	-1.187E-11	-1.711E-11

North Korea	2.186E+07	0.220	-5.664E-04	-2.591E-11	-1.869E-11
Pakistan	5.767E+07	0.223	-9.109E-04	-1.580E-11	-1.246E-11
Panama	1.327E+06	0.130	1.301E-05	9.804E-12	-8.179E-12
Papua New Guinea	2.111E+06	0.202	2.862E-06	1.356E-12	-7.797E-12
Paraguay	1.323E+07	0.229	4.231E-05	3.198E-12	-3.436E-12
Peru	2.306E+06	0.324	-4.337E-05	-1.881E-11	-1.601E-11
Philippines	1.680E+07	0.214	7.272E-05	4.329E-12	-7.714E-12
Romania	3.674E+07	0.142	-6.186E-04	-1.684E-11	-2.578E-11
Rwanda	6.933E+06	0.211	-4.615E-06	-6.656E-13	-1.021E-11
Samoa	2.517E+02	0.171	1.864E-09	7.403E-12	-5.087E-12
Sao Tome & Principe	4.438E+01	0.150	1.782E-10	4.015E-12	-9.728E-12
Senegal	1.005E+07	0.245	-7.615E-05	-7.574E-12	-1.335E-11
Serbia & Montenegro	6.495E+06	0.140	-8.183E-05	-1.260E-11	-1.982E-11
Sierra Leone	3.290E+06	0.233	-1.341E-05	-4.076E-12	-1.025E-11
Slovenia	3.150E+05	0.146	-4.990E-06	-1.584E-11	-2.493E-11
Solomon Is.	3.859E+03	0.165	3.416E-08	8.852E-12	-5.620E-12
Somalia	1.423E+07	0.227	-8.898E-05	-6.252E-12	-1.150E-11
South Africa	1.125E+07	0.206	9.975E-06	8.863E-13	-2.969E-12
Sri Lanka	1.175E+07	0.200	6.486E-05	5.521E-12	-8.481E-12
Sudan	4.887E+07	0.232	-4.505E-04	-9.218E-12	-1.293E-11
Suriname	9.179E+05	0.139	5.500E-07	5.992E-13	-9.078E-12
Swaziland	1.001E+06	0.212	1.494E-06	1.493E-12	-3.280E-12
Tajikistan	4.065E+07	0.143	-1.246E-03	-3.066E-11	-2.538E-11
Tanzania	8.795E+07	0.217	-1.009E-04	-1.147E-12	-9.338E-12
Thailand	4.864E+07	0.235	-1.410E-04	-2.898E-12	-1.067E-11
Timor Leste	1.853E+05	0.211	6.347E-07	3.426E-12	-8.203E-12
Togo	5.045E+06	0.222	-6.400E-05	-1.269E-11	-1.551E-11

Turkey	8.105E+04	0.144	-2.410E-06	-2.974E-11	-4.073E-11
Uganda	5.840E+07	0.215	9.886E-05	1.693E-12	-9.014E-12
Ukraine	3.752E+07	0.139	-1.433E-03	-3.819E-11	-4.307E-11
Uzbekistan	3.344E+07	0.141	-1.737E-03	-5.194E-11	-4.025E-11
Vanuatu	4.909E+02	0.160	4.314E-09	8.788E-12	-6.033E-12
Vietnam	8.396E+07	0.227	-3.794E-04	-4.519E-12	-1.069E-11
Yemen	9.597E+04	0.224	-7.402E-07	-7.713E-12	-1.047E-11
Zambia	2.339E+07	0.215	-3.640E-05	-1.556E-12	-8.002E-12
Zimbabwe	1.951E+07	0.216	-9.418E-06	-4.826E-13	-5.274E-12

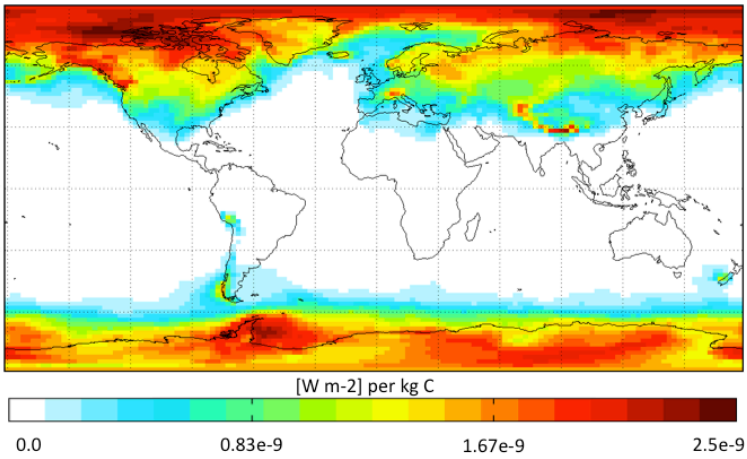

Figure A.3: Spatial distribution of BC radiative forcing sensitivities ($\lambda_{BC,i,ALB}$) for the albedo change from deposition onto snow and sea ice in the units of RF per kg of BC emitted in each grid cell.

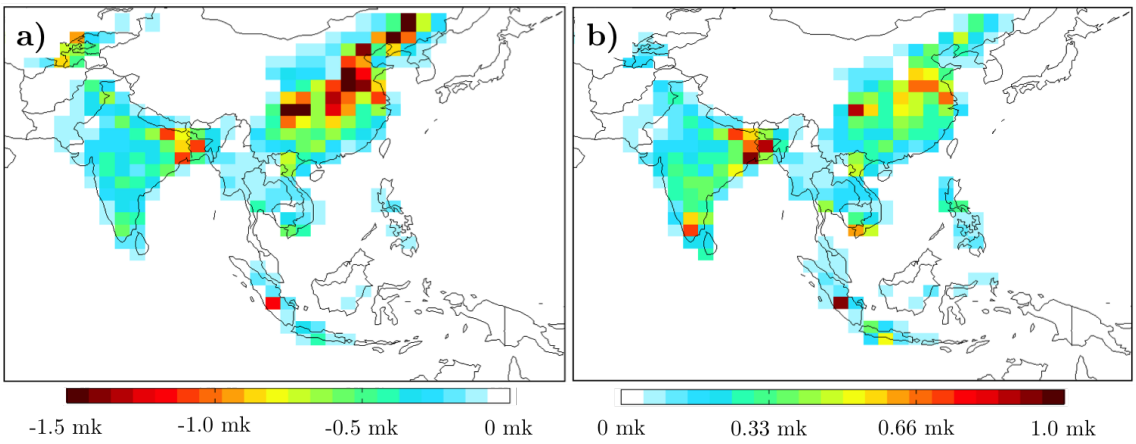

Figure A.4: Sample model calculation showing grid-scale contributions to surface temperature change of a 100% removal of biofuel emissions using ARTP calculations. (a) Contributions from removal of BC emissions. (b) Contributions from removal of OC emissions.

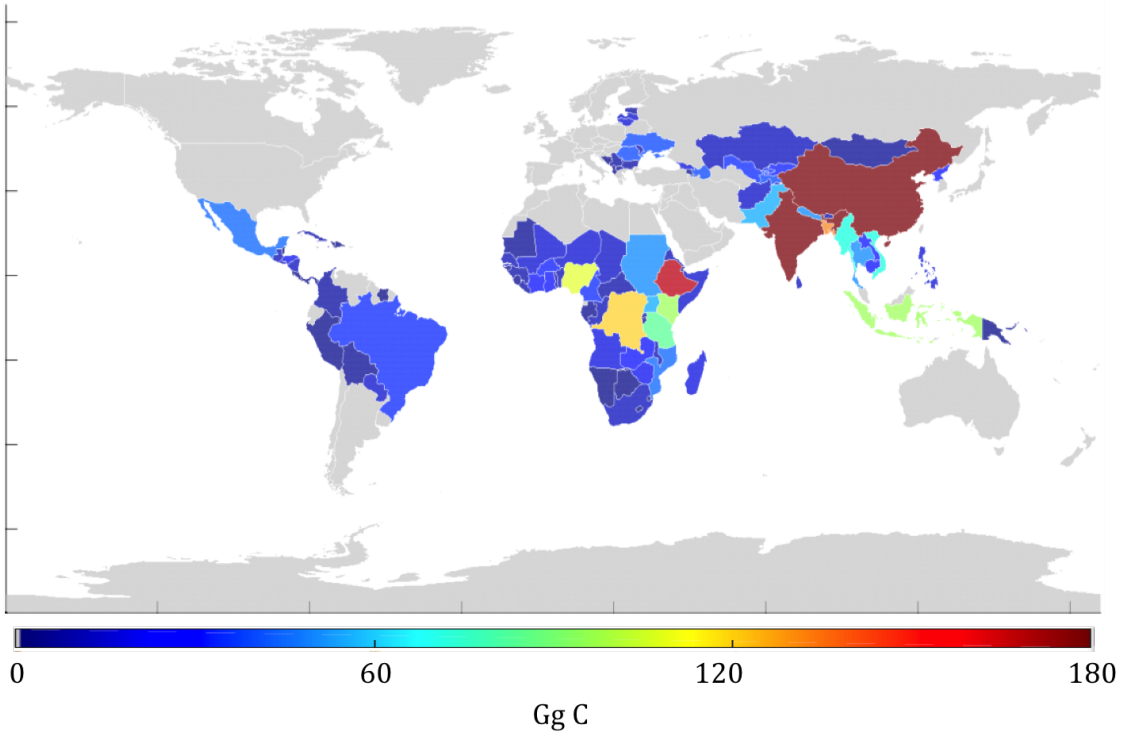

Figure A.5: Country-level total annual carbonaceous (BC + OC) aerosol emission due to cookstove use (total emissions for India = 878 Gg C per year and China = 1080 Gg C per year). Countries in grey have less than 5% total population using solid fuels.

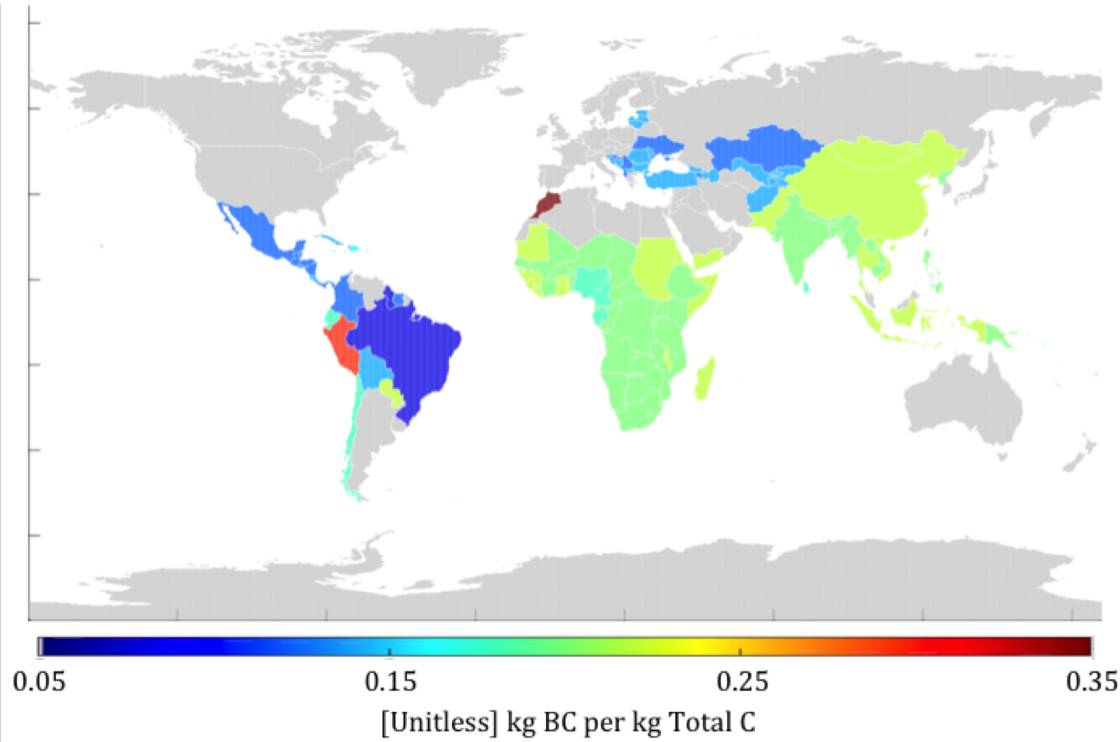

Figure A.6: Calculated Φ from cookstove emissions inventory [29, 14, 15] on a country-level basis. Lower Φ denotes smaller BC to TC ratio and higher Φ denotes larger BC to TC ratio. Countries in grey have less than 5% total population using solid fuels.

Appendix B

Supporting Information: Transient climate and ambient health impacts due to solid fuel cookstove use

B.1 Methods

This study evaluates the transient climate and ambient health impacts of a reduction in emissions of aerosols, aerosol precursors, and greenhouse gases (GHG) from solid fuel cooking. Results are calculated for a linear reduction in cookstove solid fuel use from year 2000 emissions to complete removal of emissions in 2020. These impacts are calculated using multiple GEOS-Chem adjoint model simulations corresponding to different timescales and impacts as described below.

B.1.1 GEOS-Chem

The model used for this work is GEOS-Chem [7], a global chemical transport model, run at the $2^\circ \times 2.5^\circ$ resolution . Simulations use assimilated meteorology from the Goddard Earth Observing System (GEOS5). Base anthropogenic emissions are the historical year 2000 RCP emissions from Lamarque et al., 2010 [56]. Natural aerosols and aerosol precursors emissions include volcanoes, ocean dimethyl sulfide, lightning NO_x [91, 74], soil emissions, and biogenic species (isoprene, terpenes) from MEGAN v2.1 [36].

In order to effectively model the formation and transport of aerosols, GEOS-Chem include heterogeneous chemistry [28], aerosol phase partitioning [9], and aerosol feedbacks on photolysis rates [69]. Both wet and dry deposition are included in the model [119, 42, 63], along with offline calculation of hygroscopic growth from the lognormal species-specific initial dry size distribution

[69]. When considering $PM_{2.5}$ aerosol is calculated at a 35% relative humidity fraction and spatially variable ratio of organic matter to organic carbon [80].

The adjoint of the GEOS-Chem model [40] is also used for calculating cost function specific sensitivities, in this case both regional radiative forcing (RF) [39, 55] and premature mortality due to exposure of ambient $PM_{2.5}$ [58]. Adjoint models allow for the efficient calculation of sensitivities with respect to gird-scale emissions that would take the equivalent of 10^6 forward model runs. The GEOS-Chem adjoint model has been verified compared to traditional finite difference techniques [40] and has been used as a tool in a number of previously published works.

B.1.2 Climate Impacts

B.1.2.1 Temperature Response

In this work, the climate response for a change in emissions is calculated by combining adjoint model estimates of regional aerosol radiative forcing, following Lacey and Henze, 2015 [55], with greenhouse gas radiative forcing parameterizations. While the base version of the forward GEOS-Chem model calculates aerosol mass concentration, the model used here combines these estimates of grid-cell aerosol mass with an offline Mie theory calculation and the LIDORT radiative transfer model [107] to estimate the change in upward radiative flux from a base pre-industrial atmosphere [39]. The adjoint model then considers an infinitesmal perturbation in the cost function, in this case radiative forcing, and tracks that perturbation backward in time through the model processes to calculate the grid-scale model sensitivities,

$$\lambda_{b,y,i,k} = \frac{\partial RF_b}{\partial E_{y,i,k}} \approx \frac{\Delta RF_b}{\Delta E_{y,i,k}}, \tag{B.1}$$

where RF is the regional radiative forcing for some base atmospheric condition, b, and $E_{y,i,k}$ is the species (k), year (y), and grid cell (i) specific emissions. These sensitivities take into account all of the model processes and are used to calculate the radiative forcing for an emissions perturbation

as:

$$RF_{b,y,k} = \sum_{i=1}^{n} \lambda_{b,y,i,k} \sigma_{y,i,k}, \tag{B.2}$$

where $\sigma_{y,i,k}$ is an annual emissions perturbation of species k. For this work, the base atmosphere is 1850 and the perturbed cases are both the present day case modeled around the year 2000 historical emissions [56] and a future case for the year 2050 anthropogenic emissions following the Representative Concentration Pathway (RCP) 4.5 [104, 73]. This paper also takes into account the latitudinal effects of radiative forcing following Lacey and Henze, 2015 [55], therefore calculating a weighted RF based on four different latitude bands through the use absolute regional temperature potentials (ARTP) [98, 96].

In order to include the impacts of GHGs, radiative forcing is calculated by first estimating the concentration response using impulse response functions (IRF), which calculate the response to an emissions pulse. The form of the impulse response function for CO_2 is:

$$IRF_{b,y,CO_2} = a_0 + \sum_{s=1}^{3} a_s exp\left(\frac{-(y-b)}{\tau_{s,CO_2}}\right), \tag{B.3}$$

where b is the base year, y is the year of interest, and τ_s and a_s are constants derived from model calculations in Joos et al., 2013 [48] and shown in Table B.1. Similarly, for non-CO_2 greenhouse gases species, specific impulse response functions from Aamaas et al., 2013 [1] are:

$$IRF_{b,y,k} = exp\left(\frac{-(y-b)}{\tau_k}\right), \tag{B.4}$$

where τ_k is the species' atmospheric lifetime [75] shown in Table B.2. These impulse response function are then used to estimate the concentration response to a perturbation in annual emissions ($\sigma_{k,t}$), yielding:

$$[C]_{b,y,k} = \beta_k \sum_{t=b}^{y} \sigma_{k,t} IRF_{b,y,k} + [C]_{b,k}, \tag{B.5}$$

where y is response year, t is the year of the emissions perturbation, and $[C]_{b,k}$ is a base year concentration of each species. β_k is the unit conversion from global annual emissions (in Gt) to ppm for CO_2 and ppb for CH_4 and N_2O.

Table B.1: CO_2 impulse response function coefficients from Joos et al., 2013 [48].

	0	1	2	3
a	0.2173	0.2240	0.2824	0.2763
τ	n/a	394.4	36.54	4.304

Table B.2: Species specific lifetimes from Myhre et al., 2013 [75].

	τ
CH_4	8.4
N_2O	114

The radiative impacts of this change in concentration are calculated following Aamaas et al., 2013 [1] to give the change in RF between two scenarios for a given year. For CO_2, this is purely a function of CO_2 concentrations (Equation B.6) while the CH_4 impacts are a function of both base and present year CH_4 and N_2O concentrations. The full equations are shown in Equation B.7 and Equation B.8 for each species, respectively.

$$RF_{b,y,CO_2} = 5.35 \ln \left(\frac{[C]_{b,y,CO_2}}{[C]_{b,CO_2}} \right) \tag{B.6}$$

$$\begin{aligned} RF_{b,y,CH_4} = {} & 0.036 \left(([C]_{b,y,CH_4})^{0.5} - ([C]_{b,CH_4})^{0.5} \right) - 0.47 \ln(1 + 2.01 \times 10^{-5} ([C]_{b,y,CH_4}[C]_{b,N_2O})^{0.75} \\ & - 5.31 \times 10^{-15} [C]_{b,y,CH_4} ([C]_{b,y,CH_4}[C]_{b,N_2O})^{1.52}) + 0.47 \ln(1 + 2.01 \times 10^{-5} ([C]_{b,CH_4}[C]_{b,N_2O})^{0.75} \\ & + 5.31 \times 10^{-15} [C]_{b,CH_4} ([C]_{b,CH_4}[C]_{b,N_2O})^{1.52}), \end{aligned} \tag{B.7}$$

$$RF_{b,y,N_2O} = 0.036\left(([C]_{b,y,N_2O})^{0.5} - ([C]_{b,N_2O})^{0.5}\right) - 0.47\ln(1 + 2.01\times10^{-5}([C]_{b,y,N_2O}[C]_{b,CH_4})^{0.75} - 5.31\times10^{-15}[C]_{b,CH_4}([C]_{b,y,N_2O}[C]_{b,CH_4})^{1.52}) + 0.47\ln(1 + 2.01\times10^{-5}([C]_{b,N_2O}[C]_{b,CH_4})^{0.75} + 5.31\times10^{-15}[C]_{b,CH_4}([C]_{b,N_2O}[C]_{b,CH_4})^{1.52}). \quad \text{(B.8)}$$

Given the transient RFs calculated in year y from the equations above, the transient climate response in subsequent years (y) are calculated as:

$$\Delta T_{b,y,k} = RF_{b,y,k}\gamma_{y'}. \quad \text{(B.9)}$$

$gamma_{y'}$ is the transient global mean climate sensitivity for temperature change in year y' calculated as (Boucher and Reddy, 2008):

$$\gamma_y = \gamma^{ss} - \left(\frac{0.631}{exp(y/8.4)} + \frac{0.429}{exp(y/409.5)}\right) \quad \text{(B.10)}$$

where γ^{ss} is the equilibrium global mean sensitivity, here estimated as 1.06 K (W m^{-2})$^{-1}$. The first exponential corresponds to the response of the surface and shallow seas while the second exponential represents the thermal inertia of the deep ocean.

B.1.3 Health Impacts

This work also considers the health impacts due to changes in the ambient concentrations of $PM_{2.5}$ caused by anthropogenic emissions from solid fuel cooking. As explained in Lee et al., 2015 [58], the GEOS-Chem adjoint model uses estimated aerosol mass concentrations, satellite-derived PM2.5 concentrations, and integrated exposure response functions to calculate sensitivities of premature deaths due to ambient $PM_{2.5}$ exposure with respect to grid-cell emissions. The model has been updated to include spatially variable organic matter to organic carbon ratios from Phillip et al., 2014 [80] instead of the constant value of 1.8 used in Lee et al., 2015 [58]. The model estimates population-weighted $PM_{2.5}$ using satellite-derived global estimates of surface $PM_{2.5}$ concentrations

for 2010 at the $0.1^\circ \times 0.1^\circ$ resolution [18, 116]. These datasets are used in two ways. First, they are used to redistribute aerosol mass concentrations within a modeled grid cell (model grid, $2^\circ \times 2.5^\circ$) to scales more appropriate for population based metrics (subgrid, $0.1^\circ \times 0.1^\circ$) as shown in Equation B.11,

$$[C]_{SAT,i} = \frac{1}{n_i} \sum_m [C]_{GC,i} \frac{sat_m}{SAT_i}, \tag{B.11}$$

where $[C]_{GC,i}$ is the model estimated $PM_{2.5}$ concentrations, n is the number of non-zero subgrid cells within the modeled grid cell i, sat_m is the satellite-derived PM2.5 in subgrid cell m, and SAT_i is the model grid average satellite derived $PM_{2.5}$ concentrations. Second, for present-day calculations, the satellite data is also used to correct for model bias by rescaling the modeled grid cell aerosol mass concentrations to the satellite-derived values at the $2^\circ \times 2.5^\circ$ scale, as shown in Equation B.12,

$$[\hat{C}]_{GC,i} = [C]_{GC,i} \frac{SAT_i}{[C]_{GC,i}}. \tag{B.12}$$

The satellite-corrected $PM_{2.5}$ concentrations are then used in the model integrated exposure response (IER) functions of Burnett et al., 2014 [19] to calculate the premature deaths (J_b) from exposure to ambient population-weighted $PM_{2.5}$ as,

$$J_b = \sum_{i=1}^{n} \sum_{k=1}^{m} P_{i,b} \sum_{h=1}^{l} M_{i,h} AF_{i,h,k}. \tag{B.13}$$

where M is the mortality rate for different diseases (k), AF is the disease-specific relative risk parameters for a change in $PM_{2.5}$ exposure, and $P_{i,b}$ is grid-cell (i) population in the model year (b). The factors for M are derived in Lozano et al., 2012 [64], and are functions of a region's mortality rate which make them difficult to predict for future cases since the uncertainties in health resource allocation and demographics are large. $P_{i,b}$ has been estimated for future cases by scaling the present day population citeInternational-Earth-Science-Information-Network—CIESIN—Columbia-University:2005aa to 2050 national scale population based on 2010 United Nations World

Population Prospects[1] . Finally, AF is derived from Burnett et al., 2014 [19] and represents the health impact due to different diseases from a change in exposure to population weighted $PM_{2.5}$.

The adjoint model is then used to estimate sensitivities for J_b with respect to all model inputs as:

$$\delta_{b,i,k} = \frac{\partial J_b}{\partial \sigma_{b,i,k}} \approx \frac{\Delta J_b}{\Delta \sigma_{b,i,k}}, \tag{B.14}$$

where $\sigma_{b,i,k}$ is the model resolution specieated emissions [58]. These sensitivities are calculated around the atmospheric conditions, emissions and population used in the model year (b). This change in global premature deaths for a given change in grid-cell emissions is then calculated as:

$$\Delta J_b \approx \delta_{b,i,k} \hat{\sigma}_{b,i,k}, \tag{B.15}$$

where $\hat{\sigma}_{b,i,k}$ is a gridded change in emissions of a species for a given change in anthropogenic activity under that model year. This first order approximation of the response of J_b to emissions perturbations for individual species in individual grid cells has been validated in Lee et al. (2015) using finite difference calculations of the actual response to 10% perturbations, which have a regression slope of 0.8, 0.95, 0.93 and 1.01 for NO_X, SO_2, NH_3 and BC, respectively.

In order to account for the difference between satellite reanalysis methods in the bounds of our health impacts we have compared the model results using Brauer et al., 2016 [18] as the central estimate while using the dataset from van Donkelaar et al., 2016 [116] as a bound for the health impacts. The upper and lower bounds are calculated by running the full model with each dataset independently, then using the maximum and minimum exposure estimates for each grid cell, along with the corresponding adjoint sensitivities to calculate the bounds of premature deaths from a given change in emissions. In general, the results using the dataset from van Donkelaar et al., 2016 [116] tend to estimate lower population-weighted $PM_{2.5}$ due to the differences in the sub-grid spatial distributions of surface $PM_{2.5}$, but in regions that this is not the case, these results are used as the upper bound instead.

[1] https://esa.un.org/unpd/wpp/